EUROPEAN ORGANIZATION FOR NUCLEAR RESEARCH

CERN-PH-EP/2006-001
hep-ex/0602042

April 12, 2006

Search for Neutral MSSM Higgs Bosons at LEP

ALEPH, DELPHI, L3 and OPAL Collaborations
The LEP Working Group for Higgs Boson Searches[1]

Abstract

The four LEP collaborations, ALEPH, DELPHI, L3 and OPAL, have searched for the neutral Higgs bosons which are predicted by the Minimal Supersymmetric Standard Model (MSSM). The data of the four collaborations are statistically combined and examined for their consistency with the background hypothesis and with a possible Higgs boson signal. The combined LEP data show no significant excess of events which would indicate the production of Higgs bosons. The search results are used to set upper bounds on the cross-sections of various Higgs-like event topologies. The results are interpreted within the MSSM in a number of "benchmark" models, including CP-conserving and CP-violating scenarios. These interpretations lead in all cases to large exclusions in the MSSM parameter space. Absolute limits are set on the parameter $\tan\beta$ and, in some scenarios, on the masses of neutral Higgs bosons.

Submitted to Eur. Phys. Journal C

[1] See Appendix C for the list of authors

1 Introduction

One of the outstanding questions in particle physics is that of electroweak symmetry breaking and the origin of mass. The leading candidate for an answer is the Higgs mechanism [1] whereby fundamental scalar Higgs fields acquire nonzero vacuum expectation values and spontaneously break the electroweak symmetry. Gauge bosons and fermions obtain their masses by interacting with the resulting vacuum Higgs fields. Associated with this description is the existence of massive scalar particles, the Higgs bosons.

The Standard Model [2] requires one complex Higgs field doublet and predicts a single neutral Higgs boson of unknown mass. After extensive searches at LEP, a lower bound of 114.4 GeV/c^2 has been established for the mass of the Standard Model Higgs boson, at the 95% confidence level (CL) [3].

Supersymmetric (SUSY) [4] extensions of the Standard Model are of interest since they provide a consistent framework for the unification of the gauge interactions at a high energy scale and for the stability of the electroweak scale. SUSY is also a basic ingredient of models such as Supergravity and Superstring which aim at a unified description of all fundamental forces, including the gravitational force. It is remarkable that the predictions of SUSY extensions of the Standard Model are found to be compatible with existing high-precision data [5].

In SUSY, each of the Standard Model fermions has a bosonic superpartner "sfermion", and each boson has a fermionic superpartner "gaugino" or "Higgsino". These additional particles, if they exist, have several virtues. Their presence modifies the renormalisation group evolution of the gauge couplings, improving the convergence of the couplings at a unique (GUT) energy. The new particles lead to a naturally light Higgs boson (close to the electroweak energy scale) since the divergent loop contributions of the Standard Model particles are almost completely compensated by corresponding contributions from the superpartners (the compensation would be perfect if SUSY were an exact symmetry). SUSY models also provide a perfect cold dark matter candidate, the neutralino, which arises from the mixing of the neutral gaugino and Higgsino fields.

The Minimal Supersymmetric Standard Model (MSSM) (reviewed, *e.g.*, in [6]) is the SUSY extension with minimal new particle content. It requires two Higgs field doublets and predicts the existence of three neutral and two charged Higgs bosons. The lightest of the neutral Higgs bosons is predicted to have a mass less than about 140 GeV/c^2 including radiative corrections [7]. This prediction provided a strong motivation for the searches at LEP energies.

Most of the experimental investigations carried out in the past at LEP and elsewhere were interpreted in MSSM scenarios where CP conservation in the Higgs sector was assumed. In such scenarios the neutral Higgs bosons are CP eigenstates. However, CP violation in the Higgs sector cannot be *a priori* excluded [8]. Scenarios with CP violation are theoretically appealing since they provide one of the ingredients needed to explain the observed cosmic matter-antimatter asymmetry. The observed size of CP violation in B and K meson systems is not sufficient to drive this asymmetry. In the MSSM, however, substantial CP violation can be induced by complex phases in the soft SUSY-breaking sector, through radiative corrections, especially from third-generation scalar quarks [9]. In such scenarios the three neutral Higgs mass eigenstates are mixtures of CP-even and CP-odd fields, with production and decay properties different from those in the CP-conserving scenarios. Hence, the experimental exclusions published so far for the CP-conserving MSSM scenarios may be weakened by CP-violating effects. There is currently one publication on searches interpreted in CP-violating scenarios [10].

In this paper we describe the results of a statistical combination based on the searches of the four LEP collaborations [10–13], which was carried out by the LEP Working Group for Higgs Boson Searches. These searches include all LEP2 data up to the highest energy, 209 GeV; in the case of Refs. [10, 12] they also include the LEP1 data collected at energies in the vicinity of 91 GeV (the Z boson resonance). The combined LEP data show no significant signal for Higgs boson production. The search results are used to set upper bounds on topological cross-sections for a number of Higgs-like final states. Furthermore, they are interpreted in a set of representative MSSM "benchmark" models, with and without CP-violating effects in the Higgs sector.

2 The MSSM framework

The LEP searches and their statistical combination presented in this paper are interpreted in a constrained MSSM model. At tree level, two parameters are sufficient (besides the known parameters of the Standard Model fermion and gauge sectors) to fully describe the Higgs sector. A convenient choice is one Higgs boson mass (m_{A} is chosen in CP-conserving scenarios and $m_{\mathrm{H}^\pm}$ in CP-violating scenarios), and the ratio $\tan\beta = v_2/v_1$ of the vacuum expectation values of the two Higgs fields (v_2 and v_1 refer to the fields which couple to the up- and down-type fermions). Additional parameters, M_{SUSY}, M_2, μ, A and $m_{\tilde{\mathrm{g}}}$, enter at the level of radiative corrections. M_{SUSY} is a soft SUSY-breaking mass parameter and represents a common mass for all scalar fermions (sfermions) at the electroweak scale. Similarly, M_2 represents a common SU(2) gaugino mass at the electroweak scale. The "Higgs mass parameter" μ is the strength of the supersymmetric Higgs mixing; $A = A_{\mathrm{t}} = A_{\mathrm{b}}$ is a common trilinear Higgs-squark coupling at the electroweak scale and $m_{\tilde{\mathrm{g}}}$ is the mass of the gluino (the superpartner of the gluons). Three of these parameters define the stop and sbottom mixing parameters $X_{\mathrm{t}} = A - \mu\cot\beta$ and $X_{\mathrm{b}} = A - \mu\tan\beta$. In CP-violating scenarios, the complex phases related to A and $m_{\tilde{\mathrm{g}}}$, $\arg(A)$ and $\arg(m_{\tilde{\mathrm{g}}})$, are supplementary parameters. In addition to all these MSSM parameters, the top quark mass also has a strong impact on the predictions through radiative corrections. In this paper, three fixed values are used in the calculations: $m_{\mathrm{t}} = 169.3$, 174.3 and 179.3 GeV/c^2. For the purposes of illustration, $m_{\mathrm{t}} = 174.3$ GeV/c^2 is used in producing the figures (unless explicitly specified otherwise), which is a previous world-average value [14] and which is within the current experimental range of 172.7$\pm$2.9 GeV/c^2 [15]. The influence of the top quark mass on the exclusion limits is discussed in Sections 5 and 6 along with the other results.

The combined LEP data are compared to the predictions of a number of MSSM "benchmark" models [16]. Within each of these models, the two tree-level parameters, $\tan\beta$ and

m_{A} (in the CP-conserving scenarios) or $m_{\mathrm{H}^{\pm}}$ (in the CP-violating scenarios) are scanned while the other parameters are set to fixed values. Each scan point thus represents a specific MSSM model. The ranges of the scanned parameters and the values of the fixed parameters are listed in Table 1 for the main scenarios studied. The first five models represent the main benchmarks for CP-conserving scenarios while the last model, labelled *CPX*, is a benchmark model for CP-violating scenarios. Some variants of these benchmark scenarios, which are also investigated, are presented in the text below.

Benchmark parameters						
	(1) m_{h}-*max*	(2) *no-mixing*	(3) *large-μ*	(4) *gluophobic*	(5) *small-α_{eff}*	(6) *CPX*
Parameters varied in the scan						
$\tan\beta$	0.4–40	0.4–40	0.7–50	0.4–40	0.4–40	0.6–40
m_{A} (GeV/c^2)	0.1–1000	0.1–1000	0.1–400	0.1–1000	0.1–1000	–
$m_{\mathrm{H}^{\pm}}$ (GeV/c^2)	–	–	–	–	–	4–1000
Fixed parameters						
M_{SUSY} (GeV)	1000	1000	400	350	800	500
M_2 (GeV)	200	200	400	300	500	200
μ (GeV)	-200	-200	1000	300	2000	2000
$m_{\tilde{\mathrm{g}}}$ (GeV/c^2)	800	800	200	500	500	1000
X_{t} (GeV)	$2\,M_{\mathrm{SUSY}}$	0	-300	-750	-1100	$A-\mu\cot\beta$
A (GeV)	$X_{\mathrm{t}}+\mu\cot\beta$	$X_{\mathrm{t}}+\mu\cot\beta$	$X_{\mathrm{t}}+\mu\cot\beta$	$X_{\mathrm{t}}+\mu\cot\beta$	$X_{\mathrm{t}}+\mu\cot\beta$	1000
arg(A)=arg($m_{\tilde{\mathrm{g}}}$)	-	-	-	-	-	90°

Table 1: *Parameters of the main benchmark scenarios investigated in this paper. The values of* $\tan\beta$ *and the mass parameters* m_{A} *(in the CP-conserving scenarios) or* $m_{\mathrm{H}^{\pm}}$ *(in the CP-violating scenarios) are scanned within the indicated ranges. For the definitions of* A *and* X_{t}*, the Feynman-diagrammatic on-shell renormalisation scheme is used in the CP-conserving scenarios and the* $\overline{\mathrm{MS}}$ *renormalisation scheme in the CP-violating scenarios.*

The scan range of $\tan\beta$ is limited by the following considerations. For values of $\tan\beta$ below the indicated lower bounds, the calculations of the observables in the Higgs sector (masses, cross-sections and decay branching ratios) become uncertain; for values above the upper bounds, the decay width of the Higgs bosons may become larger than the experimental mass resolution (typically a few GeV/c^2) and the modelling of the kinematic distributions of the signal becomes inaccurate[2]. The scan range of m_{A} is limited in most cases to less than 1000 GeV/c^2; at higher values the Higgs phenomenology is insensitive to the choice of m_{A}.

For a given scan point, the observables in the Higgs sector are calculated using two theoretical approaches, both including one- and two-loop corrections. The `FeynHiggs2.0` code [17] is based on a Feynman-diagrammatic approach and uses the *on-shell* renormalization scheme.

[2]The DELPHI Collaboration included the variation of the Higgs boson decay width with $\tan\beta$ in their simulation for $\tan\beta$ between 30 and 50. With increasing $\tan\beta$, DELPHI observed an increase of the mass resolutions and hence a loss in the signal detection efficiencies; but this was compensated by the increase of the cross-sections, such that DELPHI found no significant drop in the overall sensitivity.

The SUBHPOLE calculation and its CP-violating variant CPH [18] are based on a renormalization-group improved effective potential calculation [19] and use the $\overline{\mathrm{MS}}$ scheme[3].

In the CP-conserving case, the FeynHiggs calculation is retained for the presentation of the results since it yields slightly more conservative results (the theoretically allowed parameter space is wider) than SUBHPOLE does. Also, FeynHiggs is preferred on theoretical grounds since its radiative corrections are more detailed than those of SUBHPOLE.

In the CP-violating case, neither of the two calculations is preferred on theoretical grounds. While FeynHiggs contains more advanced one-loop corrections, the CPH code has a more precise phase dependence at the two-loop level. We opted therefore for a solution where, in each scan point, the CPH and FeynHiggs calculations are compared and the calculation yielding the weaker exclusion (more conservative) is retained. However, we also discuss in Section 6 the effect of using separately either one or the other of the two calculations. Rather large discrepancies between the two codes are found in calculating the partial width for the Higgs boson cascade decay $\Gamma(\mathcal{H}_2 \rightarrow \mathcal{H}_1\mathcal{H}_1)$ ($\mathcal{H}_1$ and $\mathcal{H}_2$ are the lightest and the second-lightest neutral MSSM Higgs bosons). Aiming at conservative exclusion limits, therefore, the CPH formula for this decay was also used within the FeynHiggs code.

All codes are implemented in a modified version of the HZHA program package [21], which takes into account initial-state radiation and the interference between identical final states from Higgsstrahlung and boson fusion processes.

2.1 CP-conserving scenarios

Assuming CP conservation, the spectrum of MSSM Higgs bosons consists of two CP-even neutral scalars, h and H (h is defined to be the lighter of the two), one CP-odd neutral scalar, A, and one pair of charged Higgs bosons, $\mathrm{H}^{\pm}$. The following ordering of masses is valid at tree level: $m_{\mathrm{h}}<(M_{\mathrm{Z}},\, m_{\mathrm{A}})<m_{\mathrm{H}}$ and $m_{\mathrm{W}^{\pm}}<m_{\mathrm{H}^{\pm}}$. This ordering may be substantially modified by radiative corrections [7] where the largest contribution arises from the incomplete cancellation between top and scalar top (stop) loops. The corrections affect mainly the neutral Higgs boson masses and decay branching ratios.

In $\mathrm{e^+e^-}$ collisions at LEP energies, the main production processes of h, H and A are the Higgsstrahlung processes $\mathrm{e^+e^-}\rightarrow$ hZ and HZ and the pair production processes $\mathrm{e^+e^-}\rightarrow$ hA and HA (in most of the MSSM parameter space only the hZ and hA processes are possible by kinematics). The fusion processes $\mathrm{e^+e^-}\rightarrow(\mathrm{WW}\rightarrow \mathrm{h})\nu_{\mathrm{e}}\bar{\nu}_{\mathrm{e}}$ and $\mathrm{e^+e^-}\rightarrow(\mathrm{ZZ}\rightarrow \mathrm{h})\mathrm{e^+e^-}$ play a marginal role at LEP energies but they are also taken into account in the derivation of the results.

The cross-sections for Higgsstrahlung and pair production can be expressed in terms of the Standard Model Higgs boson production cross-section $\sigma_{\mathrm{HZ}}^{\mathrm{SM}}$. The following expressions hold for

[3] New developments in this approach are implemented in the code CPsuperH [20].

the processes involving the lightest scalar boson h:

$$\sigma_{\mathrm{hZ}} = \sin^2(\beta-\alpha)\ \sigma^{\mathrm{SM}}_{\mathrm{HZ}} \tag{1}$$

$$\sigma_{\mathrm{hA}} = \cos^2(\beta-\alpha)\bar{\lambda}\ \sigma^{\mathrm{SM}}_{\mathrm{HZ}}. \tag{2}$$

Here α is the mixing angle which diagonalises the CP-even Higgs mass matrix (at lowest order it can be expressed in terms of m_{A}, M_{Z} and $\tan\beta$) and $\bar{\lambda}$ is a kinematic factor:

$$\bar{\lambda} = \lambda^{3/2}_{\mathrm{Ah}}/[\lambda^{1/2}_{\mathrm{Zh}}(12M^2_{\mathrm{Z}}/s+\lambda_{\mathrm{Zh}})] \tag{3}$$

with

$$\lambda_{ij} = [1-(m_i+m_j)^2/s][1-(m_i-m_j)^2/s], \tag{4}$$

where s is the square of the centre-of-mass energy. The cross-sections for the processes involving the heavy scalar boson H are obtained by interchanging the MSSM suppression factors $\sin^2(\beta-\alpha)$ and $\cos^2(\beta-\alpha)$ in Eqs. 1 and 2 and replacing the index h by H in Eqs. 1, 2 and 3. The Higgsstrahlung and pair production cross-sections are complementary, as seen from Eqs. 1 and 2. At LEP energies, the process $\mathrm{e^+e^-}\rightarrow$ hZ is typically more abundant at small $\tan\beta$ and $\mathrm{e^+e^-}\rightarrow$ hA at large $\tan\beta$, but the latter process can be suppressed also by the kinematic factor $\bar{\lambda}$.

The following decay features are relevant to the neutral MSSM Higgs bosons. The h boson decays mainly to fermion pairs, with only a small fraction of WW* and ZZ* decays, since its mass is below the threshold of the on-shell processes h$\rightarrow$ WW and h$\rightarrow$ ZZ. However, for particular choices of the parameters, the fermionic final states may be strongly suppressed. The A boson also decays predominantly to fermion pairs, independently of its mass, since its coupling to vector bosons is zero at leading order. For $\tan\beta$>1, decays of h and A to $\mathrm{b\bar{b}}$ and $\tau^+\tau^-$ pairs are preferred while the decays to $\mathrm{c\bar{c}}$ and gluon pairs are suppressed. Decays to $\mathrm{c\bar{c}}$ may become important for $\tan\beta$<1. The decay h$\rightarrow$ AA may be dominant if allowed by kinematics [22]. Higgs boson decays into SUSY particles, such as sfermions, charginos or invisible neutralinos, are suppressed due to the high values of the SUSY-breaking scale M_{SUSY} which have been chosen.

In the following we describe the CP-conserving benchmark scenarios [16] which are examined in this paper. The corresponding parameters are listed in Table 1.

2.1.1 The m_{h}-*max* scenario

In the m_{h}-*max* scenario the stop mixing parameter is set to a large value, $X_{\mathrm{t}} = 2M_{\mathrm{SUSY}}$. This model is designed to maximise the theoretical upper bound on m_{h} for a given $\tan\beta$ and fixed m_{t} and M_{SUSY} (uncertainties due to unknown higher-order corrections are ignored). This model thus provides the largest parameter space in the m_{h} direction and conservative exclusion limits for $\tan\beta$.

We also examine a variant of this scenario where the sign of μ is changed to positive, since, in the context of SUSY extensions of the Standard Model, a positive sign of μ is favoured by presently available results on $(g-2)_\mu$ [23, 24]. This variant is labelled m_{h}-*max* (a) below. Furthermore, we examine the case where, besides changing the sign of μ to positive, the sign of the mixing parameter X_{t} is changed to negative. This choice of parameters gives better agreement with measurements of the branching ratios and of the CP- and isospin-asymmetries for the process $\mathrm{b} \to \mathrm{s}\gamma$ [16, 25]. This variant is labelled m_{h}-*max* (b) below.

2.1.2 The *no-mixing* scenario

In the *no-mixing* scenario the stop mixing parameter X_{t} is set to zero, giving rise to a relatively restricted MSSM parameter space. Like in the m_{h}-*max* scenario, we also examine a variant of the *no-mixing* scenario where the sign of μ is changed to positive. At the same time, we raise M_{SUSY} to 2 TeV in order to enlarge the allowed parameter space [16]. In the case of this variant, which is labelled *no-mixing* (a) below, the scan in $\tan\beta$ is done only from 0.7 upward, due to numerical instabilities, at lower values, in the diagonalisation of the mass matrix.

2.1.3 Special scenarios

Some scenarios were designed to illustrate choices of the MSSM parameters for which the detection of Higgs bosons at LEP, at the Tevatron and at the LHC is expected to be difficult *a priori* due to the suppression of some main discovery channels [16].

- The *large-μ* scenario is constructed in such a way that, while the h boson is accessible by kinematics at LEP for all scan points, the decay $\mathrm{h} \to \mathrm{b\bar{b}}$, on which most of the searches at LEP and at the Tevatron are based, is typically strongly suppressed. For many of the scan points the decay $\mathrm{h} \to \tau^+\tau^-$ is also suppressed, such that the dominant decay modes are $\mathrm{h} \to \mathrm{c\bar{c}}$, gg and WW^*. The detection of Higgs bosons thus relies mainly on flavour- and decay-mode-independent searches. Moreover, for some of the scan points, the $\mathrm{e^+e^-} \to \mathrm{hZ}$ process is suppressed altogether by a small value of $\sin^2(\beta-\alpha)$. In such cases, however, the heavy neutral scalar H is within reach ($m_{\mathrm{H}} < 111$ GeV/c^2) and the cross-section for $\mathrm{e^+e^-} \to \mathrm{HZ}$, proportional to $\cos^2(\beta-\alpha)$, is large; the search may thus proceed *via* the heavy Higgs boson H.

- The *gluophobic* scenario is constructed in such a way that the Higgs boson coupling to gluons is suppressed due to a cancellation between the top and the stop loops at the hgg vertex. Since at the LHC the searches will rely heavily on producing the Higgs boson in gluon-gluon fusion, and since the mass determination will rely in part on the decays into gluon pairs, such a scenario may present experimental difficulties.

- In the *small-α_{eff}* scenario the couplings governing the decays $\mathrm{h} \to \mathrm{b\bar{b}}$ and $\mathrm{h} \to \tau^+\tau^-$ are suppressed with respect to their Standard Model values by a factor $-\sin\alpha_{\mathrm{eff}}/\cos\beta$ (α_{eff} is the effective mixing angle of the neutral CP-even Higgs sector including radiative corrections). This suppression is most prominent for $\tan\beta > 15$ and $170 < m_{\mathrm{A}} <$

350 GeV/c^2. (One should note that in most models which fall in this domain, all three neutral Higgs bosons are beyond the kinematic reach of LEP.)

2.2 CP-violating scenarios

In CP-violating MSSM scenarios the three neutral Higgs mass eigenstates $\mathcal{H}_i$ ($i = 1, 2, 3$) do not have well defined CP quantum numbers. Each of them can thus be produced by Higgsstrahlung ($e^+e^- \rightarrow \mathcal{H}_i Z$) via the CP-even field component and in pairs ($e^+e^- \rightarrow \mathcal{H}_i\mathcal{H}_j \quad (i \neq j)$). The relative rates depend on the choice of the parameters describing the CP-even/odd mixing.

Experimentally, the CP-violating scenarios are more challenging than the CP-conserving scenarios. For a wide range of model parameters, the coupling of the lightest Higgs boson $\mathcal{H}_1$ to the Z boson may be suppressed. Furthermore, the second- and third-lightest $\mathcal{H}_2$ and $\mathcal{H}_3$ bosons may both have masses close to or beyond the kinematic reach of LEP. Also, in CP-violating scenarios, the decays to the main "discovery channels", $\mathcal{H}_1 \rightarrow b\bar{b}$, $\mathcal{H}_2 \rightarrow b\bar{b}$ and $\mathcal{H}_2 \rightarrow \mathcal{H}_1\mathcal{H}_1 \rightarrow b\bar{b}b\bar{b}$ [4], may have lower branching ratios. One therefore anticipates less search sensitivity in the CP-violating scenarios than in the CP-conserving scenarios. An example illustrating this situation is given in Table 2.

Parameters	`FeynHiggs`	`CPH`
H^+ (GeV/c^2)	129.0	129.0
$\tan\beta$	5.0	5.0
$m_{\mathcal{H}_1}$ (GeV/c^2)	38.1	33.4
$m_{\mathcal{H}_2}$ (GeV/c^2)	105.4	102.4
$\sigma(\mathcal{H}_1 Z \rightarrow b\bar{b}Z)$ (pb)	0.0051	0.0019
$\sigma(\mathcal{H}_2 Z \rightarrow b\bar{b}Z)$ (pb)	0.0156	0.0197
$\sigma(\mathcal{H}_2 Z \rightarrow \mathcal{H}_1\mathcal{H}_1 Z \rightarrow b\bar{b}b\bar{b}Z)$ (pb)	0.0866	0.0978
$\sigma(\mathcal{H}_1\mathcal{H}_2 \rightarrow b\bar{b}b\bar{b})$ (pb)	0.0066	0.0094

Table 2: *A typical parameter set which is difficult to address by the present searches. The results of the two calculations,* `FeynHiggs` *and* `CPH`*, are given for a centre-of-mass energy of 206 GeV. The main input parameters are listed in the first two lines; all other input parameters correspond to the CPX benchmark scenario and are listed in the last column of Table 1. The output masses $m_{\mathcal{H}_1}$, $m_{\mathcal{H}_2}$ and the relevant topological cross-sections are listed below the second horizontal line.*

[4] Regarding the decay properties, the CP-violating scenarios maintain a certain similarity to the CP-conserving scenarios although the branching ratios are, in general, different. The lightest mass eigenstate $\mathcal{H}_1$ predominantly decays to $b\bar{b}$ if allowed by kinematics, with a small fraction decaying to $\tau^+\tau^-$ and $c\bar{c}$. The second-lightest Higgs boson $\mathcal{H}_2$ may decay to $\mathcal{H}_1\mathcal{H}_1$ when allowed by kinematics; otherwise it decays preferentially to $b\bar{b}$.

The cross-sections for Higgsstrahlung and pair production are given by [9]

$$\sigma_{\mathcal{H}_i\mathrm{Z}} = g^2_{\mathcal{H}_i\mathrm{ZZ}}\ \sigma^{\mathrm{SM}}_{\mathrm{HZ}} \tag{5}$$

$$\sigma_{\mathcal{H}_i\mathcal{H}_j} = g^2_{\mathcal{H}_i\mathcal{H}_j\mathrm{Z}}\ \bar{\lambda}\ \sigma^{\mathrm{SM}}_{\mathrm{HZ}} \tag{6}$$

(in the expression for $\bar{\lambda}$, Eq. 3, the indices h and A have to be replaced by $\mathcal{H}_i$ and $\mathcal{H}_j$). The couplings

$$g_{\mathcal{H}_i\mathrm{ZZ}} = \cos\beta\mathcal{O}_{1i} + \sin\beta\mathcal{O}_{2i} \tag{7}$$

$$g_{\mathcal{H}_i\mathcal{H}_j\mathrm{Z}} = \mathcal{O}_{3i}(\cos\beta\mathcal{O}_{2j} - \sin\beta\mathcal{O}_{1j}) - \mathcal{O}_{3j}(\cos\beta\mathcal{O}_{2i} - \sin\beta\mathcal{O}_{1i}) \tag{8}$$

obey the complementarity relation

$$\sum_{i=1}^{3} g^2_{\mathcal{H}_i\mathrm{ZZ}} = 1 \tag{9}$$

$$g_{\mathcal{H}_k\mathrm{ZZ}} = \varepsilon_{ijk}g_{\mathcal{H}_i\mathcal{H}_j\mathrm{Z}} \tag{10}$$

where ε_{ijk} is the usual Levi-Civita symbol.

In CP-violating scenarios, the orthogonal matrix $\mathcal{O}_{ij}$ $(i,j = 1,2,3)$ relating the weak CP eigenstates to the mass eigenstates has non-vanishing off-diagonal elements. These elements, giving rise to CP-even/odd mixing, are proportional to

$$\frac{m_t^4\ \mathrm{Im}(\mu A)}{v^2\ M^2_{\mathrm{SUSY}}} \tag{11}$$

with $v = \sqrt{v_1^2 + v_2^2}$. Substantial deviations from the CP-conserving scenarios are thus expected for small M_{SUSY} and large $\mathrm{Im}(\mu A)$, which are obtained if the CP-violating phase $\arg(A)$ takes values close to 90°. Furthermore, the effects from CP violation strongly depend on the precise value of the top quark mass [15].

The parameters of the benchmark model *CPX* have been chosen [18] to maximise the phenomenological differences with respect to the CP-conserving scenarios. Constraints from measurements of the electron and neutron electric dipole moments [26] were also taken into account. The basic set of parameters is listed in the last column of Table 1. Note that the scan of $m_{\mathrm{H}^\pm}$ started at 4 GeV/c^2 but values less than about 100 GeV/c^2 give unphysical results and are thus considered as theoretically inaccessible.

The parameters which follow have been varied one-by-one while all the other parameters were kept at their standard *CPX* value.

- Top quark mass: m_{t} = 169.3, 174.3, and 179.3 GeV/c^2, embracing the current experimental value, $m_{\mathrm{t}} = 172.7 \pm$ 2.9 GeV/c^2 [15].
- The CP-violating phases: $\arg(A) = \arg(m_{\tilde{\mathrm{g}}}) = 0°,\ 30°,\ 60°,\ 90°$ (*CPX* value), 135° and 180° (the values 0° and 180° correspond to CP-conserving limits).
- The Higgs mass parameter: μ = 0.5, 1.0, 2.0 (*CPX* value) and 4.0 TeV.

- The SUSY-breaking scale: $M_{\mathrm{SUSY}} = 0.5$ TeV (*CPX* value) and 1.0 TeV. The proposal of the *CPX* scenario [18] predicts a weak dependence on M_{SUSY} if the relations $|A| = |m_{\tilde{g}}| = \mu/2 = 2M_{\mathrm{SUSY}}$ are preserved. This behaviour is examined by studying a model where M_{SUSY} is increased from 0.5 TeV to 1 TeV and the values of A, $m_{\tilde{g}}$ and μ are scaled to 2000 GeV, 2000 GeV and 4000 GeV, respectively.

3 Experimental searches

The searches carried out by the four LEP collaborations are based on e^+e^- collision data which span a large range of centre-of-mass energies, from 91 GeV to 209 GeV. The searches include the Higgsstrahlung and pair production processes, ensuring, by their complementarity, a high sensitivity over the accessible MSSM parameter space. It is important to note that the kinematic properties of the signal processes are to a large extent independent of the CP composition of the Higgs bosons. This implies that the same topological searches can be applied to study the CP-conserving and CP-violating scenarios. For Higgsstrahlung this is natural since only the CP-even components of the Higgs fields couple to the Z boson. In pair production involving CP-even and CP-odd field components, the similarity of the kinematic properties (*e.g.*, angular distributions) arises from the scalar nature of the Higgs bosons. Small differences may occur from spin-spin correlations between final-state particles but these were found to have no noticeable effect on the signal detection efficiencies. We therefore adopt in the following a common notation for the CP-conserving and CP-violating processes in which $\mathcal{H}_i$ $(i = 1, 2, 3)$ designate three generic neutral Higgs bosons of increasing mass, with undefined CP properties; in the CP-conserving limit ($\arg(A) = \arg(m_{\tilde{g}}) = 0°$), these become the CP eigenstates h, A, H (the correspondence depends on the mass hierarchy).

In each of the four LEP experiments, the data analysis is done in several steps. A preselection is applied to reduce some of the largest backgrounds, in particular, from two-photon processes. The remaining background, mainly from production of fermion pairs and WW or ZZ (possibly accompanied by photon or gluon radiation), is further reduced by more selective cuts or by applying multivariate techniques such as likelihood analyses and neural networks. The identification of b-quarks in the decay of the Higgs bosons plays an important role in the discrimination between signal and background, as does the kinematic reconstruction of the Higgs boson masses. The detailed implementation of these analyses, as well as the data samples used by the four collaborations, are described in the individual publications. A full catalog of the searches provided by the four LEP collaborations for this combination, with corresponding references to the detailed descriptions, is given in Appendix A.

3.1 Search topologies

Searches have been carried out for the two main signal processes, the Higgsstrahlung process $e^+e^- \to \mathcal{H}_1 Z$ (which also apply in some cases to $e^+e^- \to \mathcal{H}_2 Z$) and the pair production process

$e^+e^- \to \mathcal{H}_2\mathcal{H}_1$.

(a) Considering first the Higgsstrahlung process $e^+e^- \to \mathcal{H}_1 Z$, the principal signal topologies are those used in the search for the Standard Model Higgs boson at LEP [3], namely:

- the four-jet topology, $(\mathcal{H}_1 \to b\bar{b})(Z \to q\bar{q})$, in which the invariant mass of two jets is close to the Z boson mass M_Z while the other two jets contain b-flavour;
- the missing energy topology, $(\mathcal{H}_1 \to b\bar{b}, \tau^+\tau^-)(Z \to \nu\bar{\nu})$, in which the event consists of two b-jets or identified tau decays and substantial missing momentum and missing mass, compatible with M_Z;
- the leptonic final states, $(\mathcal{H}_1 \to b\bar{b})(Z \to e^+e^-, \mu^+\mu^-)$, in which the invariant mass of the two leptons is close to M_Z;
- the final states with tau-leptons, $(\mathcal{H}_1 \to \tau^+\tau^-)(Z \to q\bar{q})$ and $(\mathcal{H}_1 \to b\bar{b}, \tau^+\tau^-)(Z \to \tau^+\tau^-)$, in which either the $\tau^+\tau^-$ or the $q\bar{q}$ pair has an invariant mass close to M_Z.

Most of these signatures are relevant for Higgs boson masses above the $b\bar{b}$ threshold and rely on the identification of b-quarks in the final state. Searches for lighter Higgs bosons, listed in Appendix A, use signatures which are described in the specific publications. In some regions of the MSSM parameter space, the $\mathcal{H}_1 \to b\bar{b}$ decay may be suppressed while decays into other quark flavours or gluon pairs are favoured. The above searches are therefore complemented or replaced[5] by flavour-independent searches for $(\mathcal{H}_1 \to q\bar{q})Z$ in which there is no requirement on the quark-flavour of the jets. Finally, the searches for Higgsstrahlung also include the Higgs cascade decay $e^+e^- \to \mathcal{H}_2 Z \to (\mathcal{H}_1\ \mathcal{H}_1)Z$, giving rise to a new class of event topologies. These processes may play an important role in those regions of the parameter space where they are allowed by kinematics.

(b) In the case of the pair production process, $e^+e^- \to \mathcal{H}_2\mathcal{H}_1$, the principal signal topologies at LEP are:

- the four-b final state $(\mathcal{H}_2 \to b\bar{b})(\mathcal{H}_1 \to b\bar{b})$;
- the mixed final states $(\mathcal{H}_2 \to \tau^+\tau^-)(\mathcal{H}_1 \to b\bar{b})$ and $(\mathcal{H}_2 \to b\bar{b})(\mathcal{H}_1 \to \tau^+\tau^-)$;
- the four-tau final state $(\mathcal{H}_2 \to \tau^+\tau^-)(\mathcal{H}_1 \to \tau^+\tau^-)$.

The Higgs cascade decay, $e^+e^- \to \mathcal{H}_2\mathcal{H}_1 \to (\mathcal{H}_1\mathcal{H}_1)\mathcal{H}_1$, gives rise to event topologies ranging from six b-jets to six tau-leptons. Most of these searches are relevant for Higgs boson masses above the $\tau^+\tau^-$ threshold. Similarly to the Higgsstrahlung case, the above searches for pair production are complemented or replaced, whenever more efficient, by flavour-independent searches.

[5] The replacement is necessary whenever the overlap in terms of selected events is important, in order to avoid double-counting.

3.2 Additional experimental constraints

If the combination of the above searches is not sufficiently sensitive for excluding a given model point, additional constraints are applied; these are listed below.

- Constraint from the measured decay width of the Z boson, Γ_{Z}, and its possible deviation, $\Delta\Gamma_{\mathrm{Z}}$, from the Standard Model prediction. The model point is regarded as excluded if the following relation between the relevant cross-sections is found to be true:

$$\sum_i \sigma_{\mathcal{H}_i\mathrm{Z}}(m_{\mathrm{Z}}) + \sum_{i,j} \sigma_{\mathcal{H}_i\mathcal{H}_j}(m_{\mathrm{Z}}) > \frac{\Delta\Gamma_{\mathrm{Z}}}{\Gamma_{\mathrm{Z}}} \cdot \sigma_{\mathrm{Z}}^{\mathrm{tot}}(m_{\mathrm{Z}}), \quad (12)$$

  where $\Delta\Gamma_{\mathrm{Z}} = 2.0$ MeV [27] stands for the 95% CL upper bound on the possible additional decay width of the Z boson, beyond the Standard Model prediction, and $\sigma_{\mathrm{Z}}^{\mathrm{tot}}$ is the Z pole cross-section.

- Constraint from a decay mode independent search for $\mathrm{e}^+\mathrm{e}^- \rightarrow \mathcal{H}_1\mathrm{Z}$ [28]. The model point is regarded as excluded if the condition

$$\sigma_{\mathcal{H}_i\mathrm{Z}} > k(m_{\mathcal{H}_i}) \cdot \sigma_{\mathrm{HZ}}^{\mathrm{SM}} \quad (13)$$

  is fulfilled, where $k(m_{\mathcal{H}_i})$ is a mass-dependent factor which scales the Standard Model Higgs production cross-section to the value that is excluded at the 95% CL.

- Constraint from a search for light Higgs bosons produced by the Yukawa process[6]. The model point is regarded as excluded if the predicted Yukawa enhancement factor $\xi(m_{\mathcal{H}_1})$, defined in [29], is excluded by this search. To be conservative, the weaker of the two enhancement factors, for CP-even and CP-odd couplings, is used.

These additional constraints are particularly useful at small $m_{\mathcal{H}_1}$ and $m_{\mathcal{H}_2}$, below the $\mathrm{b}\bar{\mathrm{b}}$ threshold.

3.3 Statistical combination of search channels

The statistical method by which the topological searches are combined is described in Refs. [3, 30].

After selection, the combined data configuration (distribution of all selected events in several discriminating variables) is compared in a frequentist approach to a large number of simulated configurations generated separately for two hypotheses: the background (b) hypothesis and the signal-plus-background ($s+b$) hypothesis. The ratio

$$Q = \mathcal{L}_{s+b}/\mathcal{L}_b \quad (14)$$

[6]Note that, in the case of DELPHI, the Yukawa channels are not used as external constraints but are combined with the other search channels.

of the corresponding likelihoods is used as the test statistic. The predicted, normalised, distributions of Q (probability density functions) are integrated to obtain the p-values [31] $1 - CL_b = 1 - \mathcal{P}_b(Q \leq Q_{\mathrm{observed}})$ and $CL_{s+b} = \mathcal{P}_{s+b}(Q \leq Q_{\mathrm{observed}})$; these measure the compatibility of the observed data configuration with the two hypotheses. Here $\mathcal{P}_b$ and $\mathcal{P}_{s+b}$ are the probabilities for a single experiment to obtain a value of Q smaller than or equal to the observed value, given the background or the signal-plus-background hypothesis. More details can be found in Ref. [3].

Systematic errors are incorporated in the calculation of the likelihoods by randomly varying the signal and background estimates in each channel[7] according to Gaussian error distributions and widths corresponding to the systematic errors. For a given source of uncertainty, correlations are addressed by applying these random variations simultaneously to all those channels for which the source of uncertainty is relevant. Errors which are correlated among the experiments arise mainly from using the same Monte Carlo generators and cross-section calculations for the signal and background processes. The uncorrelated errors arise mainly from the limited statistics of the simulated background event samples.

In a purely frequentist approach, the exclusion limit is computed from the confidence CL_{s+b} for the signal-plus-background hypothesis: a signal is regarded as excluded at the 95% CL, for example, if an observation is made such that CL_{s+b} is lower than 0.05. However, this procedure may lead to the undesired situation in which a large downward fluctuation of the background would exclude a signal hypothesis for which the experiment has no sensitivity since the expected signal rate is too small. This problem is avoided by using the ratio

$$CL_s = CL_{s+b}/CL_b \tag{15}$$

instead of CL_{s+b}. We adopt this quantity for setting exclusion limits and consider a given model to be excluded at the 95% CL if the corresponding value of CL_s is less than 0.05. Since CL_b is a positive number less than one, CL_s is always larger than CL_{s+b} and the limits obtained in this way are therefore conservative.

3.4 Comparisons of the data with the expected background

The distribution of the p-value $1 - CL_b$ over the parameter space covered by the searches provides a convenient way of studying the agreement between the data and the expected background and of discussing the statistical significance of any local excess in the data. While a purely background-like behaviour[8] would yield p-values close to 0.5, much smaller values are expected in the case of a signal-like excess. For example, a local excess of three or five standard deviations would give rise to a p-value $1 - CL_b$ of 2.7×10^{-3} or 5.7×10^{-7}, respectively.

[7] The word "channel" designates any subset of the data in which a search has been carried out. These subsets may correspond to specific final-state topologies, to data sets collected at different centre-of-mass energies or to the subsets of data collected by different experiments.

[8] Single, background-like, experiments have values of $1 - CL_b$ uniformly distributed between zero and one.

One has to be careful, however, when interpreting these numbers as probabilities for local excesses occurring over the extended domains covered by the searches. For example, the probability for a fluctuation of three standard deviations to occur *anywhere* in the parameter space is much larger than the number 2.7×10^{-3} just quoted. A multiplication factor has to be applied to the probability $1 - CL_b$ which reflects the number of independent "bins" of the parameter space; this factor can be estimated from the total size of the parameter space and the experimental resolutions. For example, the searches for the Higgsstrahlung process $e^+e^- \to \mathcal{H}_1 Z$, covering the range $0 < m_{\mathcal{H}_1} < 120$ GeV/c^2 with a mass resolution $\Delta m_{\mathcal{H}_1}$ of about 3 GeV/c^2, would yield about twenty fairly independent mass-bins of width $2\Delta m_{\mathcal{H}_1}$; hence, a multiplication factor of about twenty. Much bigger multiplication factors are expected in the searches for the pair production process $e^+e^- \to \mathcal{H}_2\mathcal{H}_1$ with two independent search parameters (masses).

These simple considerations do not take into account, for example, possible correlations from resolution tails extending over several adjacent bins or correlations between different searches sharing candidate events. A more elaborate evaluation of the multiplication factor has therefore been performed. A large number of background experiments was simulated, covering the whole parameter space, using realistic resolution functions and taking correlations into account. From these random experiments, the probability to obtain $1 - CL_b$ smaller than a given value, *anywhere* in the parameter space of a given scenario, has been determined (the m_h-*max* scenario was taken for this study). A scale factor of at least 60 was obtained in this manner. According to this estimate, the probability of observing a background fluctuation of three standard deviations *anywhere* in the parameter space of a given scenario (e.g., m_h-*max*) can be 16% or more. Also, to observe two fluctuations with two standard deviations turns out to be more likely than to observe only one.

Figure 1 shows the distribution of the p-value $1-CL_b$, determined from the present combined searches, for the CP-conserving benchmark scenario m_h-*max* and the CP-violating scenario *CPX*. Over the largest part of the parameter space, the local excesses are smaller than two standard deviations. In the m_h-*max* scenario, the lowest value, $1 - CL_b = 1.3 \times 10^{-2}$, lies within the vertical band at m_h around 100 GeV/c^2 and corresponds to 2.5 standard deviations. This excess, and a less significant excess at about 115 GeV/c^2, come from the Higgsstrahlung search; both are discussed in Ref. [3] in the context of the search for the Standard Model Higgs boson. In the *CPX* scenario, one observes two small regions at $m_{\mathcal{H}_1} \approx$ 35-40 GeV/c^2, $m_{\mathcal{H}_2} \approx 105$ GeV/c^2 and $\tan\beta \approx 10$, where the significance exceeds three standard deviations; they arise from the search for the pair production process.

The exact position and size of these fluctuations may vary from one scenario to the other. In Tables 3 and 4 we list the parameters of the most significant excesses for all CP-conserving and CP-violating benchmark scenarios considered in this paper. The largest fluctuation of all has a significance of 3.5 standard deviations; its probability is estimated as 3.6% at least, when the scale factor of 60 or more is applied.

From these studies one can conclude that there is a reasonable agreement between the data and the simulated background, with no compelling evidence for a Higgs boson signal, and that the excesses observed are compatible with random fluctuations of the background.

Benchmark	$m_{\rm h}$	$m_{\rm H}$	$m_{\rm A}$	$m_{\rm H^\pm}$	$\tan\beta$	$1-CL_b$	σ (st.dev.)
$m_{\rm h}$-*max*	99	253	169	184	0.7	1.3×10^{-2}	2.5
$m_{\rm h}$-*max (a)*	99	277	156	171	0.6	1.4×10^{-2}	2.5
$m_{\rm h}$-*max (b)*	99	345	310	319	0.9	1.6×10^{-2}	2.4
no-mixing	99	165	152	171	3.7	1.4×10^{-2}	2.5
no-mixing (a)	99	134	114	138	5.4	1.1×10^{-2}	2.5
large-μ	59	108	67	104	3.1	1.0×10^{-2}	2.6
gluophobic	56	124	69	105	4.1	5.5×10^{-3}	2.8
small-α_{eff}	60	121	75	109	5.5	2.4×10^{-3}	3.0

Table 3: *The most significant excesses with respect to the predicted background, for each of the CP-conserving benchmark scenarios. Columns 2 to 6 show the mass parameters (in* GeV/c^2*) and* $\tan\beta$ *at which the excess occurs. Column 7 gives the corresponding p-values* $1-CL_b$. *In the last column, the significances of the excesses, in standard deviations, are listed.*

4 Limits on topological cross-sections

In this section we present upper bounds on the cross-sections for the most important final-state topologies expected from the Higgsstrahlung process $e^+e^-\to \mathcal{H}_1 Z$ and the pair production process $e^+e^-\to \mathcal{H}_2\mathcal{H}_1$. These can be used to test a wide range of specific models.

We define the scaling factor

$$S_{95} = \sigma_{\rm max}/\sigma_{\rm ref}, \tag{16}$$

where $\sigma_{\rm max}$ is the largest cross-section compatible with the data, at the 95% CL, and $\sigma_{\rm ref}$ is a reference cross-section. For the topologies motivated by Higgsstrahlung, $\sigma_{\rm ref}$ is taken to be the Standard Model Higgs production cross-section; for final states motivated by the pair production process, $\sigma_{\rm ref}$ is taken to be the MSSM Higgs production cross-section of Eq. 2 with the MSSM suppression factor set to 1. Numerical values for the cross-section limits are listed in Appendix B.

Figure 2 shows the upper bound S_{95} for final states motivated by the Higgsstrahlung process $e^+e^-\to \mathcal{H}_1 Z$ (the figure is reproduced from Ref. [3]). In part (a), the Higgs boson is assumed to decay into fermions and bosons with branching ratios as given by the Standard Model. Contributions from the fusion processes WW$\to \mathcal{H}_1$ and ZZ$\to \mathcal{H}_1$, according to the Standard Model, corrected for initial-state radiation, are assumed to scale with energy like the Higgsstrahlung process. In part (b) it is assumed that the Higgs boson decays exclusively to $b\bar{b}$ and in part (c)

	$m_{\mathcal{H}_1}$	$m_{\mathcal{H}_2}$	$m_{\mathcal{H}_3}$	$m_{\mathrm{H}^\pm}$	$\tan\beta$	$1-CL_b$ (CPH)	$1-CL_b$ (FeynH.)	σ (st.dev.)
CPX scenario	35-40	105	120	120	10	1×10^{-3}	2×10^{-3}	3.1
m_t = 169 GeV/c^2	40	100	125	120	10-15	8×10^{-4}	9×10^{-4}	3.3
m_t = 179 GeV/c^2	95	125	145	155	3	4×10^{-3}	4×10^{-3}	2.9
m_t = 183 GeV/c^2	95	130	150	155	3	4×10^{-3}	4×10^{-3}	2.9
$\arg(A)=\arg(m_{\tilde{\mathrm{g}}})=0°$	40	95	125	115	12	8×10^{-4}	1×10^{-3}	3.1
$\arg(A)=\arg(m_{\tilde{\mathrm{g}}})=30°$	45	100	125	110	10-20	1×10^{-3}	1×10^{-3}	3.1
$\arg(A)=\arg(m_{\tilde{\mathrm{g}}})=60°$	45	95	130	115	5-20	5×10^{-4}	6×10^{-4}	3.5
$\arg(A)=\arg(m_{\tilde{\mathrm{g}}})=135°$	40	105	120	110	>20	2×10^{-3}	3×10^{-3}	3.0
$\arg(A)=\arg(m_{\tilde{\mathrm{g}}})=180°$	95	130	170	170	6	4×10^{-3}	4×10^{-3}	2.9
μ = 500 GeV	95	100	125	130	1	4×10^{-3}	4×10^{-3}	2.9
μ = 1000 GeV	95	110	125	135	2	5×10^{-3}	5×10^{-3}	2.8
μ = 4000 GeV	95	180	330	300	4	5×10^{-3}	5×10^{-3}	2.8
M_SUSY=1 TeV	95	105	145	130	2	4×10^{-3}	4×10^{-3}	2.9
M_SUSY=1 TeV, scaled	40	105	120	130	10	2×10^{-3}	2×10^{-3}	3.1

Table 4: *The most significant excesses with respect to the predicted background in the CP-violating benchmark scenario CPX and its variants. The first column indicates either the CPX scenario or the parameter value which differs from the standard CPX set listed in the last column of Table 1. Columns 2 to 6 show the mass parameters (in* GeV/c^2*) and* $\tan\beta$ *at which the excesses occur (the more conservative of the* `CPH` *and* `FeynHiggs` *calculations is used). Columns 7 and 8 give the corresponding p-values,* $1-CL_b$*, using in turn the* `CPH` *and* `FeynHiggs` *codes (note the overall agreement of the two calculations in this respect). In the last column, the significances of the excesses, in standard deviations, are listed.*

exclusively to $\tau^+\tau^-$. Besides representing bounds on topological cross-sections, this figure also illustrates the overall agreement between the data and the expected background from Standard Model processes. The largest deviations observed barely exceed two standard deviations.

Figure 3 shows contours of S_{95} for the cascade process $\mathrm{e^+e^-}\to\mathcal{H}_2\mathrm{Z}\to(\mathcal{H}_1\mathcal{H}_1)\mathrm{Z}$, projected onto the ($m_{\mathcal{H}_2}$, $m_{\mathcal{H}_1}$) plane, assuming that the $\mathcal{H}_2$ boson decays exclusively to $\mathcal{H}_1\mathcal{H}_1$. In part (a) it is assumed that the $\mathcal{H}_1$ boson decays exclusively to $\mathrm{b\bar{b}}$ and in part (b) exclusively to $\tau^+\tau^-$. In part (c), as an example, an equal mixture of $\mathcal{H}_1\to\mathrm{b\bar{b}}$ and $\mathcal{H}_1\to\tau^+\tau^-$ is assumed, which implies 25% $\mathrm{b\bar{b}b\bar{b}Z}$, 25% $\tau^+\tau^-\tau^+\tau^-\mathrm{Z}$ and 50% $\mathrm{b\bar{b}}\tau^+\tau^-\mathrm{Z}$ final states. The sensitivity of the $\mathrm{b\bar{b}b\bar{b}Z}$ channel starts at the $\mathrm{b\bar{b}}$ threshold and extends almost to the kinematic limit. In the $\tau^+\tau^-\tau^+\tau^-\mathrm{Z}$ channel the sensitivity is altogether weaker (the discontinuities reveal the limited and inhomogeneous mass coverage of the four experiments in this channel).

Figure 4 shows S_{95} for final states motivated by the pair-production process $\mathrm{e^+e^-}\to\mathcal{H}_2\mathcal{H}_1$, for the particular case where the masses $m_{\mathcal{H}_2}$ and $m_{\mathcal{H}_1}$ are approximately equal. Such is the case, for example, in the CP-conserving MSSM scenario m_h-*max* for $\tan\beta$ larger than about 10 and small $m_{\mathcal{H}_2}$ ($\equiv m_{\mathrm{A}}$). In part (a), the $\mathcal{H}_2$ and $\mathcal{H}_1$ decay branching ratios correspond to the m_{h}-*max* benchmark scenario with $\tan\beta = 10$ (see the caption for the exact values); in part (b), both $\mathcal{H}_2$ and $\mathcal{H}_1$ are assumed to decay exclusively to $\mathrm{b\bar{b}}$; in part (c), one Higgs boson is assumed to decay exclusively to $\mathrm{b\bar{b}}$ while the other exclusively to $\tau^+\tau^-$; in part (d), $\mathcal{H}_2$ and $\mathcal{H}_1$ are both assumed to decay exclusively to $\tau^+\tau^-$. At low masses, the exclusion limits are completed using the constraint from the measured decay width of the Z boson (see Section 3.2). This figure also illustrates the overall agreement between the data and the expected background from Standard Model processes since the largest deviations are within two standard deviations.

Figure 5 shows contours of S_{95} for final states motivated by the process $\mathrm{e^+e^-} \to \mathcal{H}_2\mathcal{H}_1$, projected onto the ($m_{\mathcal{H}_2}$, $m_{\mathcal{H}_1}$) plane. In part (a), both Higgs bosons are assumed to decay exclusively to $\mathrm{b\bar{b}}$ and in part (b) exclusively to $\tau^+\tau^-$. In parts (c) / (d), the $\mathcal{H}_2$ / $\mathcal{H}_1$ boson is assumed to decay exclusively to $\mathrm{b\bar{b}}$ while the other boson is assumed to decay exclusively to $\tau^+\tau^-$.

Figure 6 shows contours of S_{95} for the cascade process $\mathrm{e^+e^-} \to \mathcal{H}_2\mathcal{H}_1 \to (\mathcal{H}_1\mathcal{H}_1)\mathcal{H}_1$, projected onto the ($m_{\mathcal{H}_2}$, $m_{\mathcal{H}_1}$) plane, assuming that the $\mathcal{H}_2$ boson decays exclusively to $\mathcal{H}_1\mathcal{H}_1$. In part (a), the $\mathcal{H}_1$ boson is assumed to decay exclusively to $\mathrm{b\bar{b}}$ and in part (b) exclusively to $\tau^+\tau^-$. In part (c), as an example, an equal mixture of $\mathcal{H}_1 \to \mathrm{b\bar{b}}$ and $\mathcal{H}_1 \to \tau^+\tau^-$ is assumed, which implies 12.5% $\mathrm{b\bar{b}b\bar{b}b\bar{b}}$, 37.5% $\mathrm{b\bar{b}b\bar{b}}\tau^+\tau^-$, 37.5% $\mathrm{bb}\tau^+\tau^-\tau^+\tau^-$ and 12.5% $\tau^+\tau^-\tau^+\tau^-\tau^+\tau^-$ final states.

A word of caution is in place concerning the correlations which exist between some of the above cross-section limits which arise from overlapping candidates in the corresponding selections. Such correlations are present, for example, between b-tagged and flavour-independent searches of a given experiment or between searches addressing direct decays (e.g., $\mathcal{H}_1\mathrm{Z} \to \mathrm{b\bar{b}b\bar{b}}$) and cascade decays (e.g., $(\mathcal{H}_2 \to \mathcal{H}_1\mathcal{H}_1)\mathrm{Z} \to \mathrm{b\bar{b}b\bar{b}b\bar{b}}$); they may be a source of problems if several of the cross-section limits are used in conjunction to test a given model. Note, however, that these correlations are properly taken into account in the model interpretations which follow.

5 Results interpreted in CP-conserving MSSM scenarios

In this section, the search results are interpreted in the CP-conserving benchmark scenarios presented in Section 2.1. The exclusion limits, which are shown in the figures below at the 95% CL and the 99.7% CL, are obtained from the values of CL_s (see Eq. 15), for an assumed top quark mass of $m_{\mathrm{t}} = 174.3$ GeV/c^2. The exclusion limits are presented in four projections of the MSSM parameter space. The limits expected on the basis of Monte Carlo simulations with no signal, at the 95% CL, are also indicated. The exact mass bounds and exclusions for $\tan\beta$ are listed in Table 5, for three values of m_{t}.

The exclusions for the m_{h}-*max* benchmark scenario are shown in Figure 7. In the region with $\tan\beta$ less than about five, the exclusion is provided mainly by the Higgsstrahlung process, giving a lower bound of about 114 GeV/c^2 for m_{h}. At high $\tan\beta$, the pair production process is most useful, providing limits in the vicinity of 93 GeV/c^2 for both $m_{\rm h}$ and $m_{\rm A}$. For $m_{\rm h}$ in the vicinity of 100 GeV/c^2, one observes a deviation between the expected and the experimental exclusions. This deviation, which is also present in other CP-conserving scenarios, is due to the excess in the Higgsstrahlung channel which was discussed in Ref. [3] and gives rise to the vertical bands in Figures 1 (a) and (b). Note that the mass bounds obtained are largely insensitive to the top quark mass.

The data also exclude certain domains of $\tan\beta$. This is best illustrated in the ($m_{\rm h}$, $\tan\beta$) projection (plot (b)) where the upper boundary of the parameter space along $m_{\rm h}$ is indicated for three values of $m_{\rm t}$; the intersections of these boundaries with the experimental exclusions define the regions of $\tan\beta$ which are excluded. The exclusion in $\tan\beta$, as a function of the assumed top quark mass, is summarised in Figure 8.

One should be aware that the upper boundary of the parameter space along $m_{\rm h}$ also depends moderately on the choice of $M_{\rm SUSY}$. For example, changing $M_{\rm SUSY}$ from 1 TeV to 2 TeV would broaden the parameter space by about 2 GeV/c^2 along $m_{\rm h}$, with corresponding effects on the exclusions in $\tan\beta$. This observation holds for all CP-conserving scenarios which follow.

Figures 9 and 10 show the same set of plots for the two variants, (a) and (b), of the $m_{\rm h}$-*max* scenario introduced in Section 2.1.1. The change of the sign of the Higgs mass parameter μ or of the mixing parameter $X_{\rm t}$ barely affect the mass limits; differences occur, however, in the exclusions of $\tan\beta$ (see Table 5). Note, in Figure 9, the small domains at $m_{\rm h}$ between 60 and 75 GeV/c^2, small $m_{\rm A}$ and $\tan\beta$<0.9 which are excluded at the 95% CL but not at the 99.7% CL.

The exclusions for the CP-conserving *no-mixing* benchmark scenario are shown in Figure 11. In this scenario, the theoretical boundaries of the parameter space are more restricted than in the $m_{\rm h}$-*max* scenario. As a consequence, large domains of $\tan\beta$ are excluded for all the top quark masses considered. Note the relatively strong variation of the exclusion limits with $m_{\rm t}$ in this scenario (see Table 5), which is caused by the proximity of the experimental lower bound of $m_{\rm h}$ from the Higgsstrahlung searches and the theoretical upper bound of $m_{\rm h}$.

An interesting feature of this scenario is that, for $m_{\rm h}$ larger than about 100 GeV/c^2 and large $\tan\beta$, the heavy scalar boson H is within kinematic reach. Moreover, the cross-section for the process $\rm e^+e^-\rightarrow$ HZ is increasing with $\tan\beta$, resulting in an improved search sensitivity; this explains the nearly circular shape of the expected limit in Figure 11 (b).

Note the small domain at $m_{\rm h}$ between 75 and 80 GeV/c^2, small $m_{\rm A}$ and $\tan\beta < 0.7$, barely perceptible in the plots, which is not excluded in this scenario at 95% CL (this domain is excluded for $m_{\rm t}$ = 169.3 GeV/c^2). The branching ratio for $\rm h\rightarrow b\bar{b}$ is small and the decay $\rm h\rightarrow AA$ is dominant in this region. The A boson, with mass below the $\tau^+\tau^-$ threshold, may decay to final states which are not sufficiently covered by the present searches. For this reason, the mass limits given in Table 5 for this scenario and for $m_{\rm t}$ larger than 169.3 GeV/c^2 are valid only for $\tan\beta \geq 0.7$. Conversely, for $m_{\rm t}$ larger than 169.3 GeV/c^2, the quoted exclusion of $\tan\beta$ is valid only for $m_{\rm A}$ larger than about 3 GeV/c^2.

Figure 12 shows the exclusion plots for the (a) variant of the *no-mixing* scenario introduced in Section 2.1.2. The change of sign of the Higgs mass parameter μ and the increase of the weak SUSY-breaking scale from 1 TeV to 2 TeV affect only the theoretical bounds of the parameter space but barely change the mass limits, except for m_{t}=169.3 GeV/c^2. There are moderate changes though in the exclusions of $\tan\beta$. In the hatched domain ($\tan\beta$<0.7), the contributions from top and stop quark loops to the radiative corrections are large and uncertain; hence, no exclusions can be claimed there.

The exclusions for the *large-μ* benchmark scenario are shown in Figure 13. As mentioned in Section 2.3, this scenario was constructed to test the sensitivity of LEP to MSSM scenarios which may be *a priori* difficult to handle experimentally since the Higgs boson decays to $\mathrm{b\bar{b}}$ are largely suppressed. It turns out that the flavour-independent and decay-mode-independent searches are sufficiently powerful to exclude all such situations at 95% CL, for top quark masses up to 174.3 GeV/c^2. There remains a thin strip at $\tan\beta$ larger than about 10 and running from m_{A} of about 100 to about 200 GeV/c^2, which is excluded at the 95% CL but not at 99.7% CL because the suppression of the $\mathrm{b\bar{b}}$ channel is particularly strong in that region. This strip is found to grow with increasing m_{t} and becomes gradually non-excluded at the 95% CL. Other small, weakly excluded, regions are located at $m_{\mathrm{h}} \approx 60$ GeV/c^2 and small m_{A}, and along the $m_{\mathrm{h}} \approx m_{\mathrm{A}}$ "diagonal" of plot (a).

Similar plots are shown in Figures 14 and 15 for the *gluophobic* and *small-α_{eff}* scenarios defined in Section 2.1.3. These scenarios were designed to test situations which can be problematic at the Tevatron and LHC colliders. In both cases, large domains of the parameter space are excluded by the LEP searches.

6 Results interpreted in CP-violating MSSM scenarios

In this section, the search results are interpreted in the CP-violating benchmark scenario *CPX* presented in Section 2.2, and in some variants of *CPX* where the basic model parameters are varied one-by-one. Note that in these scenarios $m_{\mathcal{H}_3}$ is always larger than 120 GeV/c^2, except where the CP-violating phases $\arg(A) = \arg(m_{\tilde{g}})$ are put to 0° or 180°.

The experimental exclusions for the *CPX* benchmark scenario are shown in Figure 16, in four projections. For large $m_{\mathcal{H}_2}$, the $\mathcal{H}_1$ is almost completely CP-even; in this case the limit on $m_{\mathcal{H}_1}$ is close to 114 GeV/c^2, the limit obtained for the Standard Model Higgs boson [3]. For example, for $m_{\mathcal{H}_2}$ larger than 133 GeV/c^2, one can quote a lower bound of 113 GeV/c^2 for $m_{\mathcal{H}_1}$. Large CP-odd admixtures to $\mathcal{H}_1$ occur, however, for smaller $m_{\mathcal{H}_2}$, giving rise to domains at lower $m_{\mathcal{H}_1}$ which are not excluded.

The exclusion is particularly weak for $\tan\beta$ between about 3.5 and 10. Here, the signal is spread over several channels arising from the Higgsstrahlung and pair-production processes, including the $\mathcal{H}_2 \rightarrow \mathcal{H}_1\mathcal{H}_1$ cascade decays, which give rise to complex final states with six jets. The parameter set of Table 2 is a typical example of this situation. This is illustrated in Figure 17 where the main final-state cross-sections are plotted as a function of $\tan\beta$ (the FeynHiggs calculation is used). In general, these signal contributions cannot be added up statistically because of a large overlap in the selected events; hence, a relatively low overall detection efficiency is expected. Moreover, one of the experiments presents a local excess of about two standard deviations in this domain of $\tan\beta$ and for $m_{\mathcal{H}_1}$ of about 45 GeV/c^2 [10], which lowers the exclusion power below the expectation. Nonetheless, the region defined by $m_{\mathcal{H}_1} < 114$ GeV/c^2 and $\tan\beta < 3.0$ is excluded by the data (see Figure 16 (b)) and a 95% CL lower bound of 2.9 can be set on $\tan\beta$ in this scenario. The two distinct domains in Figure 16 (b), at moderate $\tan\beta$, with $m_{\mathcal{H}_1}$<15 GeV/c^2 and 30 GeV/c^2<$m_{\mathcal{H}_1}$<55 GeV/c^2, which are not excluded at the 95% CL, are found to be excluded, respectively, at the 50% CL and 66% CL.

Figure 18 illustrates the exclusions in the ($m_{\mathcal{H}_1}, \tan\beta$) projection, using the CPH calculation (part (a)) and the FeynHiggs calculation (part (b)). Differences occur mainly at large $\tan\beta$ where the FeynHiggs calculation predicts a larger Higgsstrahlung cross-section and hence a better search sensitivity than the CPH calculation. The two distinct domains at moderate $\tan\beta$, with $m_{\mathcal{H}_1}$<15 GeV/c^2 and 30 GeV/c^2<$m_{\mathcal{H}_1}$<55 GeV/c^2, which are not excluded at the 95% CL, are found to be excluded, respectively, at the 55% CL and 77% CL using the CPH calculation, and at the 50% CL and 66% CL, respectively, using the FeynHiggs calculation. A third domain appears in part (b) at higher $m_{\mathcal{H}_1}$ (where the CPH calculation indicates no exclusion power at all); this domain is excluded at the 42% CL using FeynHiggs.

As explained in Section 2, neither of the two approaches, CPH or FeynHiggs, are preferred on theoretical grounds. For this reason, part (c) of this figure was obtained by choosing in each scan point of the parameter space the more conservative of the two approaches, *i.e.*, the one for which the less significant exclusion is observed. The same procedure was adopted in Figure 16 and in all the figures which follow.

The significant impact of the top mass on the CP-violating effects, indicated by Eq. 11, is illustrated in Figure 19 where the ($m_{\mathcal{H}_1}$, $\tan\beta$) projection is shown for three values of m_{t}. With increasing m_{t}, one observes a reduction of the exclusion power, especially in the region of $\tan\beta$ between 3.5 and 10. No lower bound on $m_{\mathcal{H}_1}$ can be quoted in this domain. In plot (a) (for $m_{\mathrm{t}} = 169.3$ GeV/c^2), the two domains with $m_{\mathcal{H}_1} < 15$ GeV/c^2 and 30 GeV/c^2 $< m_{\mathcal{H}_1} < 55$ GeV/c^2 are excluded at the 60% CL and 88% CL, respectively. (The levels of exclusion for the two domains which appear in plot (b) (for $m_{\mathrm{t}} = 174.3$ GeV/c^2), have been quoted above, in the discussion of Figure 16.)

Figure 20 illustrates the exclusion in the ($m_{\mathcal{H}_1}$, $\tan\beta$) plane as a function of the CP-violating phases, $\arg(A) = \arg(m_{\tilde{g}})$, which are varied together. For phase angles close to 0°, the experimental exclusions are similar to those in the CP-conserving scenarios (see, for example, Figure 7 but note the differences in the allowed parameter space). Sizable differences are observed for larger phase angles, especially for $\arg(A) = \arg(m_{\tilde{g}}) = 90°$ (the *CPX* value). At $\arg(A) = \arg(m_{\tilde{g}}) = 180°$ (another CP-conserving scenario), the allowed parameter space is excluded almost completely. Note however that in the hatched region, with $\tan\beta$ greater than about 12, the calculation of the bottom-Yukawa coupling has large theoretical uncertainties; hence no exclusion can be claimed in this domain.

In Figure 21, the value of the Higgs mass parameter μ is varied from 500 GeV through 1000 GeV and 2000 GeV (the *CPX* value) to 4000 GeV. At small values, the CP-violating effects are small (see Eq. 11) and the exclusion power is strong (as in the CP-conserving case). For μ larger than 2000 GeV and large $\tan\beta$, the `FeynHiggs` and `CPH` calculations both provide bottom-Yukawa coupling in the non-perturbative regime, giving rise to negative values for the square of $m_{\mathcal{H}_1}$ and to other unphysical results. For $\mu \leq 2000$ GeV this regime sets in only at $\tan\beta$ larger than 40 whereas for $\mu = 4000$ GeV this situation already occurs at $\tan\beta$ abowe 20. Hence, in Figure 21 (d), the hatched domain should not be considered as being integrally part of the allowed parameter space.

Figure 22 illustrates the dependence on the soft SUSY-breaking scale parameter, M_{SUSY}, which is increased from the *CPX* value of 500 GeV in part (a) to 1000 GeV in part (b). This decreases the CP-violating effects (see Eq. 11) and leads to a larger exclusion. The "scaling" behaviour mentioned in Section 2.3, namely the relative insensitivity of the exclusions to changes in M_{SUSY} as long as the relations $|A_{\mathrm{t,b}}| = |m_{\tilde{\mathrm{g}}}| = \mu/2 = 2M_{\mathrm{SUSY}}$ are preserved, is qualitatively confirmed by comparing parts (a) and (c) of the figure.

7 Summary

The searches for neutral MSSM Higgs bosons described in this paper are based on the data collected by the four LEP collaborations, ALEPH, DELPHI, L3 and OPAL, which were statistically combined by the LEP Working Group for Higgs Boson Searches. The data samples include those collected during the LEP 2 phase at $\mathrm{e^+e^-}$ centre-of-mass energies up to 209 GeV; two experiments also provided LEP 1 data, at energies in the vicinity of the Z boson resonance. The searches address a large number of final-state topologies arising from the Higgsstrahlung process $\mathrm{e^+e^-} \rightarrow \mathcal{H}_1\mathrm{Z}$ and from the pair production process $\mathrm{e^+e^-} \rightarrow \mathcal{H}_2\mathcal{H}_1$. The combined LEP data do not reveal any excess of events which would indicate the production of Higgs bosons. The differences with respect to the background predictions are compatible with statistical fluctuations of the background.

From these results, upper bounds are derived for the cross-sections of a number of Higgs-like event topologies. These upper bounds cover a wide range of Higgs boson masses and are typically well below the cross-sections predicted within the MSSM framework; these limits can be used to constrain a large number of theoretical models.

The combined search results are used to test several MSSM scenarios which include CP-conserving and CP-violating benchmark models. These models are motivated mainly by physics arguments but some of them are constructed to test specific situations where the detection of Higgs bosons at the Tevatron and LHC colliders might present experimental difficulties. It is found that in all these scenarios the searches conducted at LEP exclude sizeable domains of the theoretically allowed parameter space.

In the CP-conserving case, lower bounds can be set on the masses of neutral Higgs bosons and the value of $\tan\beta$ can be restricted. Taking, for example, the CP-conserving scenario m_{h}-*max* and a top quark mass of 174.3 GeV/c^2, values of m_{h} and m_{A} less than 92.8 GeV/c^2 and 93.4 GeV/c^2, respectively, are excluded at the 95% CL. In the same scenario, values of $\tan\beta$ between 0.7 and 2.0 are excluded, but this range depends considerably on the assumed top quark mass and may also depend on M_{SUSY}.

In the CP-violating benchmark scenario *CPX* and the variants which have been studied, the combined LEP data show large domains which are not excluded, down to the lowest mass values; hence, no absolute limits can be set for the Higgs boson masses. The excluded domains vary considerably with the precise value of the top quark mass and the MSSM model parameters. For example, in the *CPX* scenario with standard parameters and $m_{\mathrm{t}} = 174.3$ GeV/c^2, $\tan\beta$ can be restricted to values larger than 2.9 at the 95% CL.

Acknowledgements

We congratulate the LEP Accelerator Division for the successful running of LEP over twelve years, up to the highest energies. We also would like to express our thanks to the engineers and technicians in all our institutions for their contributions to the excellent performance of the four LEP experiments.

Benchmark scenario	m_{t} (GeV/c^2)	m_{h} (GeV/c^2)	m_{A} (GeV/c^2)	Exclusions of $\tan\beta$
m_{h}-*max*	169.3	92.9 (94.8)	93.4 (95.1)	0.6–2.6 (0.6–2.7)
	174.3	92.8 (94.9)	93.4 (95.2)	0.7–2.0 (0.7–2.1)
	179.3	92.9 (94.8)	93.4 (95.2)	0.9–1.5 (0.9–1.6)
m_{h}-*max* (a)	169.3	92.7 (94.9)	93.1 (95.1)	0.7–2.1 (0.7–2.2)
	174.3	92.7 (94.8)	93.1 (95.1)	0.7–2.1 (0.7–2.2)
	179.3	92.6 (94.8)	93.1 (95.1)	0.9–1.6 (0.8–1.7)
m_{h}-*max* (b)	169.3	92.8 (94.8)	93.2 (95.2)	0.5–3.3 (0.5-3.5)
	174.3	92.6 (94.9)	93.4 (95.1)	0.6–2.5 (0.6–2.7)
	179.3	92.6 (94.8)	93.4 (95.1)	0.7–2.0 (0.7–2.1)
no-mixing	169.3	excl. (excl.)	excl. (excl.)	excl. (excl.)
	174.3	93.6 (96.0)	93.6 (96.4)	0.4–10.2 (0.4–19.4)
	179.3	93.3 (95.0)	93.4 (95.0)	0.4–5.5 (0.4–6.5)
no-mixing (a)	169.3	93.2 (95.2)	93.4 (95.4)	0.7–7.1 (0.7–9.3)
	174.3	92.8 (94.9)	93.1 (95.1)	0.7–4.6 (0.7–5.1)
	179.3	92.8 (94.9)	93.1 (95.0)	0.7–3.5 (0.7–3.8)
large-μ	169.3	excl. (excl.)	excl. (excl.)	excl. (excl.)
	174.3	excl. (excl.)	excl. (excl.)	excl. (excl.)
	179.3	109.2 (109.2)	225.0 (225.0)	0.7–43 (0.7–43)
gluophobic	169.3	90.6 (93.2)	95.7 (98.2)	0.4–10.3 (0.4–21.5)
	174.3	90.5 (92.3)	96.3 (98.0)	0.4–5.4 (0.4–6.4)
	179.3	90.0 (91.8)	96.5 (98.2)	0.4–3.9 (0.4–4.2)
small-α_{eff}	169.3	88.2 (90.0)	98.2 (99.6)	0.4–6.1 (0.4–7.4)
	174.3	87.3 (89.0)	98.8 (100.0)	0.4–4.2 (0.4–4.5)
	179.3	86.6 (88.0)	99.8 (100.7)	0.5–3.2 (0.5–3.4)

Table 5: *Lower mass bounds and exclusions in* $\tan\beta$*, at 95% CL, obtained in the case of the CP-conserving MSSM benchmark scenarios, for three values of the top quark mass. In each case, the observed limit is followed, between parentheses, by the value expected on the basis of Monte Carlo simulations with no signal. The* no-mixing *scenario is entirely excluded for* $m_{\mathrm{t}} = 169.3\,\mathrm{GeV}/c^2$ *or smaller. In the* no-mixing *scenario and for* m_{t} *larger than* $169.3\,\mathrm{GeV}/c^2$*, the quoted mass limits are only valid for* $\tan\beta \geq 0.7$ *and the exclusion in* $\tan\beta$ *is only valid for* m_{A} *larger than about* $3\,\mathrm{GeV}/c^2$*. The* large-μ *scenario is entirely excluded for* $m_{\mathrm{t}} = 174.3\,\mathrm{GeV}/c^2$ *or smaller.*

References

[1] P.W. Higgs, Phys. Lett. **12** (1964) 132; Phys. Rev. Lett. **13** (1964) 508; Phys. Rev. **145** (1966) 1156;
F. Englert and R. Brout, Phys. Rev. Lett. **13** (1964) 321;
G.S. Guralnik, C.R. Hagen and T.W.B. Kibble, Phys. Rev. Lett. **13** (1964) 585.

[2] S. Weinberg, Phys. Rev. Lett. **19** (1967) 1264;
A. Salam, *Elementary Particle Theory*, ed. N. Svartholm (Almquist and Wiksells, Stockholm, 1968), 367.

[3] ALEPH, DELPHI, L3 and OPAL Collaborations, The LEP Working Group for Higgs Boson Searches, Phys. Lett. **B565** (2003) 61.

[4] J. Wess and B. Zumino, Nucl. Phys. **B70** (1974) 39; Phys. Lett. **B49** (1974) 52;
P. Fayet, Phys. Lett. **B69** (1977) 489; Phys. Lett. **B84** (1979) 421; Phys. Lett. **86B** (1979) 272.

[5] W. de Boer and Ch. Sander, Phys. Lett. **B585** (2004) 276;
J. R. Ellis, S. Heinemeyer, K. Olive and G. Weiglein, JHEP **0502** (2005) 13;
S. Heinemeyer, W. Hollik and G. Weiglein, hep-ph/0412214.

[6] H.E. Haber and G.L. Kane, Phys. Rep. **C117** (1985) 75;
J.F. Gunion, H.E. Haber, G.L. Kane and S. Dawson, *The Higgs Hunter's Guide* (Addison-Wesley) 1990;
H.E. Haber, *Supersymmetry*, Phys. Rev. **D66** (2002) 010001-895;
A. Djouadi, *The Anatomy of Electro-Weak Symmetry Breaking, Tome II: The Higgs boson in the Minimal Supersymmetric Model*, hep-ph/0503173.

[7] Y. Okada, M. Yamaguchi and T. Yanagida, Theor. Phys. **85** (1991)1;
H. Haber and R. Hempfling, Phys. Rev. Lett. **66** (1991) 1815;
J. Ellis, G. Ridolfi and F. Zwirner, Phys. Lett. **B257** (1991) 83;
R. Barbieri and M. Frigeni, Phys. Lett. **B258** (1991) 395;
M. Carena, M. Quiros and C.E.M. Wagner, Nucl. Phys. **B461** (1996) 407;
H. Haber, R. Hempfling and A. Hoang, Z. Phys. **C75** (1997) 539;
S. Heinemeyer, W. Hollik and G. Weiglein, Eur. Phys. J. **C9** (1999) 343; Phys. Rev. **D58** (1998) 091701; Phys. Lett. **B440** (1998) 296; JHEP 0006 (2000) 009;
J. R. Espinosa and R.-J. Zhang, Nucl. Phys. **B586** (2000) 3;
A. Brignole, G. Degrassi, P. Slavich and F. Zwirner, Nucl. Phys. **B631** (2002) 195;
G. Degrassi, S. Heinemeyer, W. Hollik, P. Slavich and G. Weiglein, Eur. Phys. J. **C28** (2003) 133.

[8] A. D. Sakharov, JETP Lett. **5** (1967) 24;
A. Pilaftsis, Phys. Rev. **D 58** (1998) 096010; Phys. Lett. **B 435** (1998) 88.

[9] D. Demir, Phys. Rev. **D 60** (1999) 055006;
A. Pilaftsis and C. Wagner, Nucl. Phys. **B 553** (1999) 3;

S. Choi, M. Drees and J. Lee, Phys. Lett. **B 481** (2000) 57;
M. Carena, J. Ellis, A. Pilaftsis and C. Wagner, Nucl. Phys. **B 586** (2000) 92;
M. Carena et al., Nucl. Phys. **B599** (2001) 158;
S. Heinemeyer, Eur. Phys. J. **C 22** (2001) 521;
T. Ibrahim and P. Nath, Phys. Rev. **D 63** (2001) 035009; Phys. Rev. **D 66** (2002) 015005;
M. Frank, S. Heinemeyer, W. Hollik and G. Weiglein, *Supersymmetry and unification of fundamental interactions*, hep-ph/0212037, Proceedings, SUSY02, DESY, Hamburg (Germany), July 2002, vol.2, p.637.

[10] OPAL Collaboration, G. Abbiendi et al., Eur. Phys. J. **C37** (2004) 49.

[11] ALEPH Collaboration, Phys. Lett. **B526** (2002) 191.

[12] DELPHI Collaboration, J. Abdallah et al., Eur. Phys. J. **C32** (2004) 145;
DELPHI 2005-020-CONF-740, *Final results from DELPHI on neutral Higgs bosons in MSSM benchmark scenarios*, paper in preparation.

[13] L3 Collaboration, P. Achard et al., Phys. Lett. **B 545** (2002) 30.

[14] D. E. Groom et al., Eur. Phys. J. **C15** (2000) 1.

[15] The CDF and D0 Collaborations, and the Tevatron Electroweak Working Group, *Combination of the CDF and D0 Results on the Top-Quark Mass*, hep-ex/0507091 (July 2005).

[16] M. Carena, S. Heinemeyer, C.E.M. Wagner and G. Weiglein, hep-ph/9912223; Eur. Phys. J. **C26** (2003) 601.

[17] S. Heinemeyer, W. Hollik and G. Weiglein, Comp. Phys. Comm. **124** (2000) 76;
S. Heinemeyer, hep-ph/0407244;
M. Frank, T. Hahn, S. Heinemeyer, W. Hollik, H. Rzehak and G. Weiglein, in preparation.
The code is accessible via `http://www.feynhiggs.de` .

[18] M. Carena, J. R. Ellis, A. Pilaftsis and C. E. Wagner, Phys. Lett. **B495** (2000) 155; Nucl. Phys. **B586** (2000) 92.

[19] M. Carena, M. Quirós and C.E.M. Wagner, Nucl. Phys. **B461** (1996) 407;
M. Carena, S. Mrenna and C. Wagner, Phys. Rev. **D60** (1999) 075010;
M. Carena, H. E. Haber, S. Heinemeyer, W. Hollik, C. E. M. Wagner and G. Weiglein, Nucl. Phys. **B580** (2000) 29;
J. R. Espinosa and R.-J. Zhang, JHEP 0003 (2000) 026.

[20] J. S. Lee, A. Pilaftsis, M. Carena, S. Y. Choi, M. Drees, J. R. Ellis and C. E. M. Wagner, Comp. Phys. Comm. **156** (2004) 283.

[21] P. Janot, *Physics at LEP2*, Ed. G. Altarelli, T. Sjöstrand and F. Zwirner, CERN 96-01 Vol. 2, p. 309.

[22] S. Heinemeyer and W. Hollik, Nucl. Phys. **B474** (1996) 32.

[23] G. W. Bennett *et al.*, Phys. Rev. Lett. **92** (2004) 161802;
M. Davier and W. Marciano, Ann. Rev. Nucl. Part. Sci. **54** (2004) 115.

[24] T. Moroi, Phys. Rev. **D53** (1996) 6565; [Erratum: Phys. Rev. **D56** (1997) 4424].

[25] ALEPH Collaboration, R. Barate et al., , Phys. Lett. **B429** (1998) 169;
CLEO Collaboration, T. E. Coan et al., Phys. Rev. Lett. **84** (2000) 5283;
CLEO Collaboration, S. Chen et al., Phys. Rev. Lett. **87** (2001) 251807;
BELLE Collaboration, K. Abe et al., Phys. Lett. **B511** (2001) 151;
BABAR Collaboration, B. Aubert et al., Phys. Rev. Lett. **88** (2002) 101815;
BABAR Collaboration, B. Aubert et al., hep-ex/0407003, submitted to Phys. Rev. Lett. (2004);
BELLE Collaboration, M. Nakao et al., Phys. Rev. **D69** (2004) 112001;
A. L. Kagan and M. Neubert, Phys. Rev. **D58** (1998) 094012; Phys. Lett. **B539** (2002) 227.

[26] E. D. Commins, S. B. Ross, D. DeMille and B. C. Regan, Phys. Rev. A **50** (1994) 2960;
P. G. Harris *et al.*, Phys. Rev. Lett. **82** (1999) 904.

[27] The ALEPH, DELPHI, L3, OPAL and SLD Collaborations, the LEP Electroweak Working Group, the SLD Electroweak and Heavy Flavour Groups, *Precision Electroweak Measurements on the Z Resonance*, CERN-PH-EP/2005-041, hep-ex/0509008, to be published in Phys. Reports.

[28] OPAL Collaboration, G. Abbiendi *et al.*, Eur. Phys. J **C 27** (2003) 311.

[29] OPAL Collaboration, G. Abbiendi *et al.*, Eur. Phys. J. C **23** (2002) 397.

[30] T. Junk, Nucl. Instr. Meth. Phys. Res. **A434** (1999) 435;
A. Read, in *1st Workshop on Confidence Limits*, CERN-2000-005;
P. Bock, *Computation of confidence levels for exclusion or discovery of a signal with the method of fractional event counting*, hep-ex/0405072 (2004).

[31] K. Hagiwara et al., Phys. Rev. **D66**, 010001-1 (2002), Review No. 31 on *Statistics*, p. 229.

[32] ALEPH Collaboration, Eur. Phys. J. **C17** (2000) 223.

[33] ALEPH Collaboration, Phys. Lett. **B499** (2001) 53.

[34] ALEPH Collaboration, Phys. Lett. **B495** (2000) 1.

[35] ALEPH Collaboration, Phys. Lett. **B544** (2002) 25.

[36] DELPHI Collaboration, P. Abreu et al., Z. Phys. **C51** (1991) 25.

[37] DELPHI Collaboration, P. Abreu et al., Nucl. Phys. **B342** (1990) 1.

[38] DELPHI Collaboration, P. Abreu et al., Nucl. Phys. **B373** (1992) 3.

[39] DELPHI Collaboration, P. Abreu et al., Nucl. Phys. **B421** (1994) 3.

[40] DELPHI Collaboration, P. Abreu et al., Eur. Phys. J. **C2** (1998) 1.

[41] DELPHI Collaboration, P. Abreu et al., Eur. Phys. J. **C10** (1999) 563.

[42] DELPHI Collaboration, P. Abreu et al., Eur. Phys. J. **C17** (2000) 187; [Addendum: Eur. Phys. J. **C17** (2000) 529].

[43] DELPHI Collaboration, J. Abdallah et al., Eur. Phys. J. **C32** (2004) 145.

[44] DELPHI Collaboration, J. Abdallah et al., Eur. Phys. J. **C23** (2002) 409.

[45] DELPHI Collaboration, J. Abdallah et al., Eur.Phys.J. **C44** (2005) 147.

[46] DELPHI 92-80 Dallas PHYS 191, *Neutral Higgs Bosons in a Two Doublet Model*, contribution to the 1992 ICHEP conference; quoted by G.Wormser, in proc. of the XXVI ICHEP conference (Dallas, August 1992), Vol. 2, pages 1309-14, ref. 4.

[47] DELPHI 2003-045-CONF-665, *DELPHI results on neutral Higgs bosons in MSSM benchmark scenarios*, contribution to the 2003 summer conferences.

[48] S. Dagoret, PhD Thesis, Université de Paris-Sud, Centre d'Orsay, LAL-preprint 91-12 (May 1991).

[49] DELPHI Collaboration, P. Abreu et al., Phys. Lett **B245** (1990) 276.

[50] DELPHI Collaboration, J. Abdallah et al., Eur. Phys. J. **C38** (2004) 1.

[51] DELPHI Collaboration, P. Abreu et al., Z. Phys. **C67** (1995) 69.

[52] L3 Collaboration, M. Acciarri *et al.*, Phys. Lett. **B461** (1999) 376.

[53] L3 Collaboration, M. Acciarri *et al.*, Phys. Lett. **B508** (2001) 225.

[54] L3 Collaboration, P. Achard *et al.*, Phys. Lett. **B517** (2001) 319.

[55] L3 Collaboration, P. Achard *et al.*, Phys. Lett. **B583** (2004) 14.

[56] L3 Collaboration, P. Achard *et al.*, Phys. Lett. **B545** (2002) 30.

[57] L3 Collaboration, M. Acciarri *et al.*, Phys. Lett. **B471** (1999) 321.

[58] L3 Collaboration, M. Acciarri *et al.*, Phys. Lett. **B503** (2001) 21.

[59] OPAL Collaboration, K. Ackerstaff *et. al.*, Eur. Phys. J. **C1** (1998) 425.

[60] OPAL Collaboration, K. Ackerstaff *et. al.*, Eur. Phys. J. **C5** (1998) 19.

[61] OPAL Collaboration, G. Abbiendi *et. al.*, Eur. Phys. J. **C7** (1999) 407.

[62] OPAL Collaboration, G. Abbiendi *et. al.*, Eur. Phys. J. **C12** (2000) 567.

[63] OPAL Collaboration, G.Abbiendi *et al.*, Eur. Phys. J. **C26** (2003) 479.

[64] OPAL Collaboration, G. Alexander *et. al.*, Z. Phys. **C73** (1997) 189.

[65] OPAL Collaboration, R. Akers *et. al.*, Z. Phys. **C64** (1994) 1.

[66] OPAL Collaboration, G. Abbiendi *et. al.*, Eur. Phys. J. **C18** (2001) 425.

[67] OPAL Collaboration, G. Abbiendi *et al.*, Phys. Lett. **B594** (2004) 11.

[68] OPAL Collaboration, G.Abbiendi *et al.*, Eur. Phys. J. **C27** (2003) 483.

[69] OPAL Collaboration, G. Abbiendi *et al.*, Eur. Phys. J. **C40** (2005) 317.

Appendix A: Catalog of searches

The searches of the four LEP collaborations which contribute to this combined analysis are listed in Tables 6 to 13. The list is structured into two tables per experiment, one for the Higgsstrahlung process $e^+e^- \rightarrow \mathcal{H}_1 Z$ and one for the pair production process $e^+e^- \rightarrow \mathcal{H}_2\mathcal{H}_1$. In each of these tables, the upper part contains the final states of the direct process and the lower part contains, where it applies, those of the cascade process $\mathcal{H}_2 \rightarrow \mathcal{H}_1\mathcal{H}_1$.

The final-state topologies are listed in the first column. In the notation adopted, $\mathcal{H}_1$ represents the lightest and $\mathcal{H}_2$ the second-lightest neutral Higgs boson. In the CP-conserving case, $\mathcal{H}_1$ is identified with the CP-even eigenstate h and $\mathcal{H}_2$ is identified with the CP-odd eigenstate A, except in the case of the cascade process $\mathcal{H}_2 \rightarrow \mathcal{H}_1\mathcal{H}_1$ which is identified with $h \rightarrow AA$.

The symbol q indicates an arbitrary quark flavour, u, d, s, c or b. "Hadrons" include quarks and gluons. In the missing energy channel, in addition to the $\mathcal{H}_1 Z \rightarrow \mathcal{H}_1 \nu\bar{\nu}$ process, the W fusion process $\mathcal{H}_1 \nu_e \bar{\nu}_e$ (including interference) is also considered; similarly, in the leptonic channel, in addition to the $\mathcal{H}_1 Z \rightarrow \mathcal{H}_1 \ell^+\ell^-$ process, the Z fusion process $\mathcal{H}_1 e^+e^-$ (including interference) is also considered.

The contributions based on LEP1 data (from two experiments only) can be identified by their value "91" in the second column which indicates the e^+e^- collision energy, $\sqrt{s}$ (GeV); the LEP1 data used in this combination represent an integrated luminosity $\mathcal{L}$ of about 125 pb^{-1}. The LEP2 data span an energy range between 133 GeV and 209 GeV; they represent an integrated luminosity of about 2400 pb^{-1}. The integrated luminosities for the individual searches are listed in the third column.

Responding to the increasing data samples and e^+e^- energies, the searches were gradually upgraded or replaced so as to become more efficient in detecting Higgs bosons of higher masses. The mass ranges where the searches are relevant are listed in the next column(s). In the last column, references are given to the publications where the details of the searches can be found.

	$\sqrt{s}$ (GeV)	$\mathcal{L}$ (pb^{-1})	Mass range (GeV/c^2)	Ref.
$\mathcal{H}_1\mathrm{Z}\to$ (...) (...)			$m_{\mathcal{H}1}$	
$(\mathrm{bb})(\mathrm{q\bar{q}})$, $(\mathrm{bb}, \mathrm{c\bar{c}}, \tau\tau, \mathrm{gg})(\nu\bar{\nu})$	189	176.2	75 – 110	[32]
(any)$(\mathrm{e^+e^-},\ \mu^+\mu^-)$	189	176.2	75 – 110	[32]
$(\mathrm{b\bar{b}})(\tau^+\tau^-), (\tau^+\tau^-)(\mathrm{q\bar{q}})$	189	176.2	65 – 110	[32]
$(\mathrm{b\bar{b}})(\mathrm{q\bar{q}}, \nu\bar{\nu})$	192 – 202	236.7	60 – 120	[33]
$(\mathrm{b\bar{b}}, \tau^+\tau^-, \mathrm{c\bar{c}}, \mathrm{gg})(\mathrm{e^+e^-}, \mu^+\mu^-)$	192 – 202	236.7	60 – 120	[33]
$(\mathrm{b\bar{b}}, \tau^+\tau^-, \mathrm{c\bar{c}}, \mathrm{gg})(\tau^+\tau^-), (\tau^+\tau^-)(\mathrm{q\bar{q}})$	192 – 202	236.7	60 – 120	[33]
$(\mathrm{b\bar{b}})(\mathrm{q\bar{q}})$	199 – 209	217.2	75 – 120	[11,34]
$(\mathrm{b\bar{b}}, \tau^+\tau^-, \mathrm{c\bar{c}}, \mathrm{gg}, \mathrm{WW})(\tau^+\tau^-, \nu\bar{\nu})$	199 – 209	217.2	75 – 120	[11,34]
$(\mathrm{b\bar{b}}, \tau^+\tau^-, \mathrm{c\bar{c}}, \mathrm{gg})(\mathrm{e^+e^-}, \mu^+\mu^-)$	199 – 209	217.2	70 – 120	[11,34]
$(\mathrm{b\bar{b}}, \mathrm{c\bar{c}}, \mathrm{s\bar{s}}, \mathrm{gg})(\mathrm{q\bar{q}})$	189	176.2	40 – 100	[35]
$(\mathrm{b\bar{b}}, \mathrm{c\bar{c}}, \mathrm{s\bar{s}}, \mathrm{gg})(\nu\bar{\nu})$	189	176.2	60 – 100	[35]
$(\mathrm{b\bar{b}}, \mathrm{c\bar{c}}, \mathrm{s\bar{s}}, \mathrm{gg})(\mathrm{e^+e^-}, \mu^+\mu^-)$	189	176.2	60 – 115	[32,35]
$(\tau^+\tau^-)(\mathrm{q\bar{q}})$	189	176.2	65 – 110	[32]
$(\mathrm{b\bar{b}}, \mathrm{c\bar{c}}, \mathrm{s\bar{s}}, \mathrm{gg})(\mathrm{q\bar{q}})$	192 – 202	236.7	40 – 110	[35]
$(\mathrm{b\bar{b}}, \mathrm{c\bar{c}}, \mathrm{s\bar{s}}, \mathrm{gg})(\nu\bar{\nu})$	192 – 202	236.7	60 – 116	[35]
$(\mathrm{b\bar{b}}, \mathrm{c\bar{c}}, \mathrm{s\bar{s}}, \mathrm{gg})(\mathrm{e^+e^-}, \mu^+\mu^-)$	192 – 202	236.7	60 – 115	[33,35]
$(\tau^+\tau^-)(\mathrm{q\bar{q}})$	192 – 202	236.7	60 – 120	[33]
$(\mathrm{b\bar{b}}, \mathrm{c\bar{c}}, \mathrm{s\bar{s}}, \mathrm{gg})(\mathrm{q\bar{q}})$	199 – 209	217.2	40 – 115	[35]
$(\mathrm{b\bar{b}}, \mathrm{c\bar{c}}, \mathrm{s\bar{s}}, \mathrm{gg})(\nu\bar{\nu})$	199 – 209	217.2	75 – 120	[35]
$(\mathrm{b\bar{b}}, \mathrm{c\bar{c}}, \mathrm{s\bar{s}}, \mathrm{gg})(\mathrm{e^+e^-}, \mu^+\mu^-)$	199 – 209	217.2	70 – 120	[11,34,35]
$(\tau^+\tau^-)(\mathrm{q\bar{q}})$	199 – 209	217.2	60 – 120	[11,34]

Table 6: *Summary of the ALEPH searches for the Higgsstrahlung process* $\mathrm{e^+e^-}\to \mathcal{H}_1\mathrm{Z}$. *The top part of the table lists the searches originally developed for the Standard Model Higgs boson. The bottom part lists flavour-independent searches where the decays of the Higgs boson into a quark pair of any flavour, a gluon pair or a tau pair were considered; the signal efficiencies were evaluated for all indicated hadronic decays of the Higgs boson. In the cases of the* $(\tau^+\tau^-)(\mathrm{q\bar{q}})$ *and leptonic channels listed in the flavour-independent part, the event selections of the Standard Model Higgs boson searches were used.*

	$\sqrt{s}$ (GeV)	$\mathcal{L}$ (pb^{-1})	Mass range (GeV/c^2)	Ref.
$\mathcal{H}_2\mathcal{H}_1 \to$ (...)(...)			$(m_{\mathcal{H}_2} + m_{\mathcal{H}_1})/2$	
$(\mathrm{b\bar{b}})(\mathrm{b\bar{b}})$, $(\tau^+\tau^-)(\mathrm{b\bar{b}})$, $(\mathrm{b\bar{b}})(\tau^+\tau^-)$	189	176.2	65 – 95	[32]
$(\mathrm{b\bar{b}})(\mathrm{b\bar{b}})$, $(\mathrm{b\bar{b}}, \tau^+\tau^-, \mathrm{c\bar{c}}, \mathrm{gg})(\tau^+\tau^-)$, $(\tau^+\tau^-)(\mathrm{b\bar{b}}, \tau^+\tau^-, \mathrm{c\bar{c}}, \mathrm{gg})$	192 – 202	236.7	60 – $\sqrt{s}/2$	[33]
$(\mathrm{b\bar{b}})(\mathrm{b\bar{b}})$, $(\mathrm{b\bar{b}}, \tau^+\tau^-, \mathrm{c\bar{c}}, \mathrm{gg})(\tau^+\tau^-)$, $(\tau^+\tau^-)(\mathrm{b\bar{b}}, \tau^+\tau^-, \mathrm{c\bar{c}}, \mathrm{gg})$	199 – 209	217.2	75 – $\sqrt{s}/2$	[11,34]

Table 7: *Summary of the ALEPH searches for the pair production process* $\mathrm{e^+e^-} \to \mathcal{H}_2\mathcal{H}_1$. *The searches are restricted to* $|m_{\mathcal{H}_2} - m_{\mathcal{H}_1}|$ *less than about 20* GeV/c^2.

	$\sqrt{s}$ (GeV)	$\mathcal{L}$ (pb^{-1})	Mass ranges (GeV/c^2)		Ref.
$e^+e^- \to \mathcal{H}_1 Z \to$ (...)(...)			$m_{\mathcal{H}_1}$		
(any)(e^+e^-, $\mu^+\mu^-$), (V^0)(any)	91	2.5	< 0.21		[36]
(2 prongs)($q\bar{q}$)	91	0.5	$0.21 - 2$		[37]
(jet)(e^+e^-, $\mu^+\mu^-$)	91	0.5	$1 - 20$		[37]
(jet jet)($\ell^+\ell^-$, $\nu\bar{\nu}$)	91	3.6	$12 - 50$		[38]
(jet jet)(e^+e^-, $\mu^+\mu^-$, $\nu\bar{\nu}$)	91	33.4	$35 - 70$		[39]
($b\bar{b}$)(any), ($\tau^+\tau^-$)($q\bar{q}$)	161,172	19.9	$40 - 80$		[40]
($b\bar{b}$)(any), ($\tau^+\tau^-$)($q\bar{q}$)	183	52.0	$45 - 95$		[41]
($b\bar{b}$)(any), ($\tau^+\tau^-$)(qq)	189	158.0	$65 - 100$		[42]
($b\bar{b}$)(any)	192-209	452.4	$12 - 120$		[43,44]
($\tau^+\tau^-$)(qq)	192-209	452.4	$45 - 120$		[43,44]
($q\bar{q}$, gg)($q\bar{q}$, $\nu\bar{\nu}$, e^+e^-, $\mu^+\mu^-$)	189-209	610.4	$4 - 116$		[45]
$e^+e^- \to \mathcal{H}_2 Z \to (\mathcal{H}_1\mathcal{H}_1)Z \to$ (...)(...)			$m_{\mathcal{H}_2}$	$m_{\mathcal{H}_1}$	
(any)($q\bar{q}$)	91	16.2	$12 - 70$	< 0.21	[46]
(V^0V^0)(any but $\tau^+\tau^-$)	91	9.7	$0.5 - 55$	< 0.21	[46]
($\gamma\gamma$)(any)	91	12.5	$0.5 - 60$	< 0.21	[46]
(4 prongs)(any)	91	12.9	$0.5 - 60$	$0.21 - 10$	[46]
(hadrons)($\nu\bar{\nu}$)	91	15.1	$1 - 60$	$0.21 - 30$	[46]
($\tau^+\tau^-\tau^+\tau^-$)($\nu\bar{\nu}$)	91	15.1	$9 - 73$	$3.5 - 12$	[46]
(any)($q\bar{q}$, $\nu\bar{\nu}$)	161,172	20.0	$40 - 70$	$20 - 35$	[40]
($b\bar{b}b\bar{b}$)($q\bar{q}$)	183	54.0	$45 - 85$	$12 - 40$	[41]
($b\bar{b}b\bar{b}$, $b\bar{b}c\bar{c}$, $c\bar{c}c\bar{c}$)($q\bar{q}$)	192-208	452.4	$30 - 105$	$12 - 50$	[43,44]
($c\bar{c}c\bar{c}$)($q\bar{q}$)	192-208	452.4	$10 - 105$	$4 - 12$	[47]

Table 8: *List of the DELPHI searches for the Higgsstrahlung processes* $e^+e^- \to \mathcal{H}_1 Z$ *and* $\mathcal{H}_2 Z$.

	$\sqrt{s}$ (GeV)	$\mathcal{L}$ (pb^{-1})	Mass ranges (GeV/c^2)		Ref.
$e^+e^- \to \mathcal{H}_2\mathcal{H}_1 \to$ (...)(...)			$m_{\mathcal{H}_2}$	$m_{\mathcal{H}_1}$	
4 prongs	91	5.3	$0.2-10$	$0.2-10$	[39]
$(\tau^+\tau^-)$(hadrons)	91	0.5	$4-35$	$4-35$	[48]
$(\tau^+\tau^-)$(jet jet)	91	3.6	$25-42$	$25-42$	[49]
$(b\bar{b})(b\bar{b})$, $(b\bar{b})(c\bar{c})$	91	33.4	$15-46$	$15-46$	[38]
$\tau^+\tau^- b\bar{b}$	91	79.4	$4-70$	$4-70$	[47]
$b\bar{b}b\bar{b}$	91	79.4	$12-40$	$20-70$	[50]
$b\bar{b}b\bar{b}$	133	6.0	$40-68$	$35-73$	[51]
$b\bar{b}b\bar{b}$, $\tau^+\tau^- b\bar{b}$	161,172	20.0	$40-70$	$35-75$	[40]
$b\bar{b}b\bar{b}$, $\tau^+\tau^- b\bar{b}$	183	54.0	$50-80$	$25-105$	[41]
$b\bar{b}b\bar{b}$, $\tau^+\tau^- b\bar{b}$	189	158.0	$65-90$	$40-115$	[42]
$\tau^+\tau^- b\bar{b}$	192-208	452.4	$50-100$	$60-150$	[43, 44]
$b\bar{b}b\bar{b}$	192-208	452.4	$12-100$	$40-190$	[43, 44]
$\tau^+\tau^-\tau^+\tau^-$	189-208	570.9	$4-90$	$4-170$	[50]
$b\bar{b}b\bar{b}$	189-208	610.2	$12-70$	$30-170$	[50]
quarks or gluons	189-208	610.4	$4-170$	$4-170$	[45]
$e^+e^- \to \mathcal{H}_2\mathcal{H}_1 \to (\mathcal{H}_1\mathcal{H}_1)\mathcal{H}_1 \to$ (...)(...)			$m_{\mathcal{H}_2}$	$m_{\mathcal{H}_1}$	
$(\gamma\gamma)(\gamma\gamma)$	91	12.5	$0.5-60$	< 0.21	[46]
(4 prongs)(2 prongs)	91	12.9	$0.5-60$	$0.21-10$	[46]
(hadrons)(hadrons)	91	15.1	$1-60$	$0.21-30$	[46]
$(\tau^+\tau^-\tau^+\tau^-)(\tau^+\tau^-)$	91	15.1	$9-60$	$3.5-12$	[46]
(any)(any)	161,172	20.0	$40-70$	$20-35$	[40]

Table 9: *List of the DELPHI searches for the pair production process* $e^+e^- \to \mathcal{H}_2\mathcal{H}_1$.

	$\sqrt{s}$ (GeV)	$\mathcal{L}$ (pb^{-1})	Mass ranges (GeV/c^2)		Ref.
$e^+e^- \to \mathcal{H}_1 Z \to$ (...)(...)			$m_{\mathcal{H}_1}$		
$(b\bar{b})$(any),$(\tau^+\tau^-)(q\bar{q})$	189	176.4	60 – 100		[52]
$(b\bar{b})$(any),$(\tau^+\tau^-)(q\bar{q})$	192 – 202	233.2	60 – 110		[53]
$(b\bar{b})$(any),$(\tau^+\tau^-)(q\bar{q})$	203 – 209	217.3	60 – 120		[54]
$(b\bar{b}$, $c\bar{c}$, gg)(any)	189	176.4	60 – 100		[55]
$(b\bar{b}$, $c\bar{c}$, gg)(any)	192 – 202	233.2	60 – 110		[55]
$(b\bar{b}$, $c\bar{c}$, gg)(any)	204 – 209	214.5	60 – 120		[55]
$e^+e^- \to \mathcal{H}_2 Z \to (\mathcal{H}_1\mathcal{H}_1)Z \to$ (...)(...)			$m_{\mathcal{H}_2}$	$m_{\mathcal{H}_1}$	
$(\mathcal{H}_1 \to$ bb,cc,gg$)(q\bar{q})$	189 – 209	626.9	30 – 85	10 – 42	[56]

Table 10: *List of the L3 searches for the Higgsstrahlung processes* $e^+e^- \to \mathcal{H}_1 Z$ *and* $\mathcal{H}_2 Z$.

	$\sqrt{s}$ (GeV)	$\mathcal{L}$ (pb^{-1})	Mass ranges (GeV/c^2)		Ref.
$e^+e^- \to \mathcal{H}_2\mathcal{H}_1 \to$ (...)(...)			$m_{\mathcal{H}_2}$	$m_{\mathcal{H}_1}$	
$(b\bar{b})(b\bar{b})$, $(b\bar{b})(\tau^+\tau^-)$, $(\tau^+\tau^-)(b\bar{b})$	189	176.4	50 – 95	50 – 95	[57]
$(b\bar{b})(b\bar{b})$, $(b\bar{b})(\tau^+\tau^-)$, $(\tau^+\tau^-)(b\bar{b})$	192 – 202	233.2	50 – 105	50 – 105	[58]
$(b\bar{b})(b\bar{b})$, $(b\bar{b})(\tau^+\tau^-)$, $(\tau^+\tau^-)(b\bar{b})$	204 – 209	216.6	50 – 110	50 – 110	[56]

Table 11: *List of the L3 searches for the pair production process* $e^+e^- \to \mathcal{H}_2\mathcal{H}_1$.

	$\sqrt{s}$ (GeV)	$\mathcal{L}$ (pb^{-1})	Mass ranges (GeV/c^2)		Ref.
$\mathcal{H}_1$Z$\to$ (...) (...)			$m_{\mathcal{H}_1}$		
(b$\bar{\text{b}}$)(q$\bar{\text{q}}$)	161–172	20.4	$40-80$		[59,60]
(b$\bar{\text{b}}$)(q$\bar{\text{q}}$)	183	54.1	$40-95$		[61]
(b$\bar{\text{b}}$)(q$\bar{\text{q}}$)	189	172.1	$40-100$		[62]
(b$\bar{\text{b}}$)(q$\bar{\text{q}}$)	192–209	421.2	$80-120$		[63]
(b$\bar{\text{b}}$)($\nu\bar{\nu}$)	161–172	20.4	$50-70$		[59,60]
(b$\bar{\text{b}}$)($\nu\bar{\nu}$)	183	53.9	$50-95$		[61]
(b$\bar{\text{b}}$)($\nu\bar{\nu}$)	189	171.4	$50-100$		[62]
(b$\bar{\text{b}}$)($\nu\bar{\nu}$)	192–209	419.9	$30-120$		[63]
(b$\bar{\text{b}}$)($\tau^+\tau^-$), ($\tau^+\tau^-$)(q$\bar{\text{q}}$)	161–172	20.4	$30-95$		[59,60]
(b$\bar{\text{b}}$)($\tau^+\tau^-$), ($\tau^+\tau^-$)(q$\bar{\text{q}}$)	183	53.7	$30-100$		[61]
(b$\bar{\text{b}}$)($\tau^+\tau^-$), ($\tau^+\tau^-$)(q$\bar{\text{q}}$)	189	168.7	$30-100$		[62]
(b$\bar{\text{b}}$)($\tau^+\tau^-$), ($\tau^+\tau^-$)(q$\bar{\text{q}}$)	192–209	417.4	$80-120$		[63]
(b$\bar{\text{b}}$)(e$^+$e$^-$), (b$\bar{\text{b}}$)($\mu^+\mu^-$)	183	55.9	$60-100$		[61]
(b$\bar{\text{b}}$)(e$^+$e$^-$), (b$\bar{\text{b}}$)($\mu^+\mu^-$)	189	170.0	$70-100$		[62]
(b$\bar{\text{b}}$)(e$^+$e$^-$), (b$\bar{\text{b}}$)($\mu^+\mu^-$)	192–209	418.3	$40-120$		[63]
(q$\bar{\text{q}}$, gg)($\tau^+\tau^-$, $\nu\bar{\nu}$), ($\tau^+\tau^-$)(q$\bar{\text{q}}$)	91	46.3	$0-70$		[64,65]
(q$\bar{\text{q}}$, gg)(e$^+$e$^-$, $\mu^+\mu^-$)	91	46.3	$20-70$		[64,65]
(any)(e$^+$e$^-$, $\mu^+\mu^-$)	161–172	20.4	$35-80$		[59,60]
(q$\bar{\text{q}}$, gg)(q$\bar{\text{q}}$)	189	174.1	$60-100$		[66]
(q$\bar{\text{q}}$, gg)(q$\bar{\text{q}}$)	192–209	424.2	$60-120$		[67]
(q$\bar{\text{q}}$, gg)($\nu\bar{\nu}$)	189	171.8	$30-100$		[66]
(q$\bar{\text{q}}$, gg)($\nu\bar{\nu}$)	192–209	414.5	$30-110$		[67]
(q$\bar{\text{q}}$, gg)($\tau^+\tau^-$), ($\tau^+\tau^-$)(q$\bar{\text{q}}$)	189	168.7	$30-100$		[66]
(q$\bar{\text{q}}$, gg)($\tau^+\tau^-$), ($\tau^+\tau^-$)(q$\bar{\text{q}}$)	192–209	418.9	$60-115$		[67]
(q$\bar{\text{q}}$, gg)(e$^+$e$^-$, $\mu^+\mu^-$)	189	170.0	$70-100$		[66]
(q$\bar{\text{q}}$, gg)(e$^+$e$^-$, $\mu^+\mu^-$)	192–209	422.0	$60-120$		[67]
e$^+$e$^-\to$ $\mathcal{H}_2$Z$\to$ ($\mathcal{H}_1\mathcal{H}_1$)Z$\to$ (...)(...)			$m_{\mathcal{H}_2}$	$m_{\mathcal{H}_1}$	
(q$\bar{\text{q}}$q$\bar{\text{q}}$)($\nu\bar{\nu}$)	91	46.3	$10-75$	$0-35$	[64,65]
(b$\bar{\text{b}}$b$\bar{\text{b}}$)(q$\bar{\text{q}}$)	183	54.1	$40-80$	$10.5-38$	[61]
(b$\bar{\text{b}}$b$\bar{\text{b}}$)(q$\bar{\text{q}}$)	189	172.1	$40-100$	$10.5-48$	[62]
(b$\bar{\text{b}}$b$\bar{\text{b}}$)(q$\bar{\text{q}}$)	192–209	421.2	$80-120$	$12-m_{\mathcal{H}_2}/2$	[10]
(b$\bar{\text{b}}$b$\bar{\text{b}}$)($\nu\bar{\nu}$)	183	53.9	$50-95$	$10.5-m_{\mathcal{H}_2}/2$	[61]
(q$\bar{\text{q}}$q$\bar{\text{q}}$)($\nu\bar{\nu}$)	189	171.4	$50-100$	$10.5-m_{\mathcal{H}_2}/2$	[62]
(b$\bar{\text{b}}$b$\bar{\text{b}}$)($\nu\bar{\nu}$)	199–209	207.2	$100-110$	$12-m_{\mathcal{H}_2}/2$	[10]
(b$\bar{\text{b}}$b$\bar{\text{b}}$)($\tau^+\tau^-$)	183	53.7	$30-100$	$10.5-m_{\mathcal{H}_2}/2$	[61]
(b$\bar{\text{b}}$b$\bar{\text{b}}$)($\tau^+\tau^-$)	189	168.7	$30-100$	$10.5-m_{\mathcal{H}_2}/2$	[62]
(c$\bar{\text{c}}$c$\bar{\text{c}}$, gggg, c$\bar{\text{c}}$gg, c$\bar{\text{c}}\tau^+\tau^-$, gg$\tau^+\tau^-$, $\tau^+\tau^-\tau^+\tau^-$)($\nu\bar{\nu}$, e$^+$e$^-$, $\mu^+\mu^-$)	189–209	598.5	$45-86$	$2-11$	[68]

Table 12: *List of the OPAL searches for the Higgsstrahlung processes* e$^+$e$^-\to$ $\mathcal{H}_1$Z *and* $\mathcal{H}_2$Z.

	$\sqrt{s}$ (GeV)	$\mathcal{L}$ (pb^{-1})	Mass ranges (GeV/c^2)		Ref.
$\mathcal{H}_2\mathcal{H}_1\to$ (...) (...)			$m_{\mathcal{H}_2}$	$m_{\mathcal{H}_1}$	Ref.
$(\mathrm{b\bar{b}})(\mathrm{b\bar{b}})$	130–136	5.2	Σ : $80-130$	Δ : $0-50$	[60]
$(\mathrm{b\bar{b}})(\mathrm{b\bar{b}})$	161	10.0	Σ : $80-130$	Δ : $0-60$	[59, 60]
$(\mathrm{b\bar{b}})(\mathrm{b\bar{b}})$	172	10.4	Σ : $80-130$	Δ : $0-60$	[59, 60]
$(\mathrm{b\bar{b}})(\mathrm{b\bar{b}})$	183	54.1	Σ : $80-150$	Δ : $0-60$	[61]
$(\mathrm{b\bar{b}})(\mathrm{b\bar{b}})$	189	172.1	Σ : $80-180$	Δ : $0-70$	[62]
$(\mathrm{b\bar{b}})(\mathrm{b\bar{b}})$	192	28.9	Σ : $83-183$	Δ : $0-70$	[10]
$(\mathrm{b\bar{b}})(\mathrm{b\bar{b}})$	196	74.8	Σ : $80-187$	Δ : $0-70$	[10]
$(\mathrm{b\bar{b}})(\mathrm{b\bar{b}})$	200	77.2	Σ : $80-191$	Δ : $0-70$	[10]
$(\mathrm{b\bar{b}})(\mathrm{b\bar{b}})$	202	36.1	Σ : $80-193$	Δ : $0-70$	[10]
$(\mathrm{b\bar{b}})(\mathrm{b\bar{b}})$	199–209	207.3	Σ : $120-190$	Δ : $0-70$	[10]
$(\mathrm{b\bar{b}})(\mathrm{b\bar{b}})$	199–209	207.3	Σ : $100-140$	Δ : $60-100$	[10]
$(\mathrm{b\bar{b}})(\tau^+\tau^-)$, $(\tau^+\tau^-)(\mathrm{b\bar{b}})$	161	10.0	$40-160$	$52-160$	[59, 60]
$(\mathrm{b\bar{b}})(\tau^+\tau^-)$, $(\tau^+\tau^-)(\mathrm{b\bar{b}})$	172	10.4	$37-160$	$28-160$	[59, 60]
$(\mathrm{b\bar{b}})(\tau^+\tau^-)$, $(\tau^+\tau^-)(\mathrm{b\bar{b}})$	183	53.7	Σ : $70-170$	Δ : $0-70$	[61]
$(\mathrm{b\bar{b}})(\tau^+\tau^-)$, $(\tau^+\tau^-)(\mathrm{b\bar{b}})$	189	168.7	Σ : $70-190$	Δ : $0-90$	[62]
$(\mathrm{b\bar{b}})(\tau^+\tau^-)$, $(\tau^+\tau^-)(\mathrm{b\bar{b}})$	192	28.7	Σ : $10-174$	Δ : $0-182$	[10]
$(\mathrm{b\bar{b}})(\tau^+\tau^-)$, $(\tau^+\tau^-)(\mathrm{b\bar{b}})$	196	74.7	Σ : $10-182$	Δ : $0-191$	[10]
$(\mathrm{b\bar{b}})(\tau^+\tau^-)$, $(\tau^+\tau^-)(\mathrm{b\bar{b}})$	200	74.8	Σ : $10-182$	Δ : $0-191$	[10]
$(\mathrm{b\bar{b}})(\tau^+\tau^-)$, $(\tau^+\tau^-)(\mathrm{b\bar{b}})$	202	35.4	Σ : $10-174$	Δ : $0-182$	[10]
$(\mathrm{b\bar{b}})(\tau^+\tau^-)$, $(\tau^+\tau^-)(\mathrm{b\bar{b}})$	199–209	203.6	Σ : $70-190$	Δ : $0-90$	[10]
$(\mathrm{q\bar{q}})(\tau^+\tau^-)$, $(\tau^+\tau^-)(\mathrm{q\bar{q}})$	91	46.3	$12-75$	$10-78$	[64, 65]
$(\mathrm{q\bar{q}})(\mathrm{q\bar{q}})$, $(\mathrm{q\bar{q}})(\mathrm{gg})$, $(\mathrm{gg})(\mathrm{q\bar{q}})$, $(\mathrm{gg})(\mathrm{gg})$	192–209	424.0	Σ : $60-175$	Δ : $0-113$	[69]
$\mathrm{e^+e^-}\to\mathcal{H}_2\mathcal{H}_1\to$ $(\mathcal{H}_1\mathcal{H}_1)\mathcal{H}_1\to$ (...)(...)			$m_{\mathcal{H}_2}$	$m_{\mathcal{H}_1}$	
$(\mathrm{b\bar{b}b\bar{b}})(\mathrm{b\bar{b}})$	91	27.6	$40-70$	$5-35$	[64, 65]
$(\mathrm{b\bar{b}b\bar{b}})(\mathrm{b\bar{b}})$	130–136	5.2	$55-65$	>27.5	[60]
$(\mathrm{b\bar{b}b\bar{b}})(\mathrm{b\bar{b}})$	161	10.0	$55-65$	>20.0	[59, 60]
$(\mathrm{b\bar{b}b\bar{b}})(\mathrm{b\bar{b}})$	172	10.4	$55-65$	$25-35$	[59, 60]
$(\mathrm{b\bar{b}b\bar{b}})(\mathrm{b\bar{b}})$	183	54.1	$30-80$	$12-40$	[61]
$(\mathrm{b\bar{b}b\bar{b}})(\mathrm{b\bar{b}})$	189	172.1	$24-80$	$12-40$	[62]
$(\mathrm{b\bar{b}b\bar{b}})(\mathrm{b\bar{b}})$	199–209	207.3	Σ : $90-200$	Δ : $40-160$	[10]
6τ, $4\tau2\mathrm{q}$, $2\tau4\mathrm{q}$	91	46.3	$30-75$	$4-30$	[64, 65]

Table 13: *List of the OPAL searches for the pair production process* $\mathrm{e^+e^-}\to\mathcal{H}_2\mathcal{H}_1$. *The symbols* Σ *and* Δ *stand for the mass sum* $m_{\mathcal{H}_2}+m_{\mathcal{H}_1}$ *and mass difference* $|m_{\mathcal{H}_2}-m_{\mathcal{H}_1}|$.

Appendix B: Limits on topological cross-sections

The tables presented below summarise the 95% CL upper bounds, as a function of the Higgs boson masses, of the scaling factor S_{95} defined in the text (see Eq. 16). Tables 14, 15 and 16 refer to final-state topologies arising from the Higgsstrahlung processes $e^+e^- \rightarrow \mathcal{H}_1 Z$ and $e^+e^- \rightarrow (\mathcal{H}_2 \rightarrow \mathcal{H}_1\mathcal{H}_1)Z$; Tables 18 to 21 refer to those arising from the pair production processes $e^+e^- \rightarrow \mathcal{H}_2\mathcal{H}_1$ and $e^+e^- \rightarrow (\mathcal{H}_2 \rightarrow \mathcal{H}_1\mathcal{H}_1)\mathcal{H}_1$. The corresponding figures, showing the same results, are mentioned in the table captions.

$m_{\mathcal{H}_1}$ (GeV/c^2)	(a)	(b)	(c)	$m_{\mathcal{H}_1}$ (GeV/c^2)	(a)	(b)	(c)
12	0.0204	0.0154	0.0925	66	0.0236	0.0218	0.0287
14	0.0176	0.0143	0.0899	68	0.0236	0.0218	0.0287
16	0.0158	0.0134	0.0923	70	0.0271	0.0246	0.0287
18	0.0150	0.0131	0.0933	72	0.0291	0.0274	0.0271
20	0.0156	0.0139	0.1060	74	0.0320	0.0301	0.0297
22	0.0177	0.0156	0.1080	76	0.0421	0.0380	0.0351
24	0.0194	0.0174	0.1110	78	0.0469	0.0424	0.0350
26	0.0207	0.0186	0.1140	80	0.0435	0.0410	0.0316
28	0.0223	0.0195	0.1110	82	0.0467	0.0475	0.0281
30	0.0203	0.0181	0.0893	84	0.0539	0.0585	0.0222
32	0.0193	0.0173	0.0796	86	0.0762	0.0816	0.0257
34	0.0191	0.0172	0.0682	88	0.112	0.118	0.0296
36	0.0241	0.0187	0.0653	90	0.153	0.152	0.0331
38	0.0299	0.0235	0.0634	92	0.179	0.175	0.0354
40	0.0333	0.0267	0.0615	94	0.229	0.214	0.0491
42	0.0367	0.0297	0.0599	96	0.239	0.220	0.0570
44	0.0378	0.0310	0.0594	98	0.256	0.233	0.0565
46	0.0387	0.0328	0.0572	100	0.244	0.216	0.0582
48	0.0391	0.0337	0.0575	102	0.237	0.216	0.0588
50	0.0363	0.0316	0.0445	104	0.255	0.227	0.0704
52	0.0386	0.0344	0.0454	106	0.263	0.223	0.0896
54	0.0387	0.0349	0.0464	108	0.266	0.227	0.110
56	0.0384	0.0360	0.0403	110	0.297	0.244	0.144
58	0.0390	0.0367	0.0427	112	0.435	0.343	0.212
60	0.0398	0.0365	0.0456	114	0.824	0.640	0.410
62	0.0293	0.0264	0.0444	116	1.41	1.79	1.79
64	0.0278	0.0258	0.0394				

Table 14: *The 95% CL upper bound, S_{95}, obtained for the normalised cross-section (see text) of the Higgsstrahlung process* $e^+e^- \to \mathcal{H}_1 Z$*, as a function of the Higgs boson mass. The numbers listed in this table correspond to the observed limit (full line) in Figure 2, which is reproduced from Ref. [3]. In the columns labelled (a) the Higgs boson is assumed to decay as in the Standard Model; in columns (b) it is assumed to decay exclusively to* $b\bar{b}$ *and in columns (c) exclusively to* $\tau^+\tau^-$.

$m_{\mathcal{H}_2}(\mathrm{GeV}/c^2)$	$m_{\mathcal{H}_1}(\mathrm{GeV}/c^2)$									
	10	15	20	25	30	35	40	45	50	55
20	0.020									
25	0.026									
30	0.037	0.046								
35	0.048	0.042								
40	0.053	0.056	0.051							
45	0.066	0.059	0.046							
50	0.087	0.058	0.048	0.049						
55	0.11	0.055	0.050	0.050						
60	0.29	0.103	0.094	0.094	0.053					
65	0.30	0.099	0.091	0.088	0.084					
70	0.25	0.098	0.097	0.095	0.083	0.059				
75	0.34	0.11	0.10	0.11	0.10	0.096				
80	0.39	0.13	0.14	0.14	0.13	0.12	0.13			
85	0.52	0.20	0.20	0.20	0.21	0.19	0.18			
90	≥ 1	0.23	0.23	0.23	0.27	0.26	0.24	0.28		
95	≥ 1	0.29	0.27	0.29	0.31	0.29	0.28	0.30		
100	≥ 1	0.30	0.29	0.31	0.30	0.27	0.28	0.29	0.29	
105	≥ 1	0.27	0.32	0.36	0.40	0.36	0.31	0.35	0.35	
110	≥ 1	0.44	0.54	0.55	0.96	0.97	≥ 1	≥ 1	0.89	≥ 1

Table 15: *The 95% CL upper bound, S_{95}, obtained for the normalised cross-section (see text) of the Higgsstrahlung cascade process* $e^+e^- \to (\mathcal{H}_2 \to \mathcal{H}_1\mathcal{H}_1)Z \to (b\bar{b}b\bar{b})Z$*, as a function of the Higgs boson masses $m_{\mathcal{H}_1}$ and $m_{\mathcal{H}_2}$. The numbers correspond to the contours shown in Figure 3 (a).*

	5	10	15	20	25	30	35	40	45
10	0.26								
15	0.033								
20	0.048	0.32							
25	0.070	0.076							
30	0.10	0.11	0.38						
35	0.18	0.19	0.51						
40	0.22	0.22	0.40	0.39					
45	0.30	0.31	0.49	0.49					
50	0.18	0.38	0.66	0.66	0.63				
55	0.18	0.37	0.68	0.69	0.68				
60	0.20	0.38	0.95	0.96	0.96	0.94			
65	0.20	0.38	≥ 1	≥ 1	≥ 1	≥ 1			
70	0.21	0.43	≥ 1	≥ 1	≥ 1	≥ 1	≥ 1		
75	0.19	0.46	≥ 1	≥ 1	≥ 1	≥ 1	≥ 1		
80	0.20	0.44	0.83	0.83	0.83	0.83	0.84	0.84	
85	0.25	0.56	≥ 1	≥ 1	≥ 1	≥ 1	≥ 1	≥ 1	

Table 16: *The 95% CL upper bound, S_{95}, obtained for the normalised cross-section (see text) of the Higgsstrahlung cascade process* $\mathrm{e^+e^-} \rightarrow (\mathcal{H}_2 \rightarrow \mathcal{H}_1\mathcal{H}_1)\mathrm{Z} \rightarrow (\tau^+\tau^-\tau^+\tau^-)\mathrm{Z}$, *as a function of the Higgs boson masses $m_{\mathcal{H}_1}$ and $m_{\mathcal{H}_2}$. The numbers correspond to the contours shown in Figure 3 (b).*

$m_{\mathcal{H}_1}+m_{\mathcal{H}_2}$ (GeV/c^2)	(a)	(b)	(c)	(d)	$m_{\mathcal{H}_1}+m_{\mathcal{H}_2}$ (GeV/c^2)	(a)	(b)	(c)	(d)
0	0.0237	0.0237	0.0237	0.0237	105	0.0243	0.0213	0.0354	0.0300
5	0.0238	0.0238	0.0238	0.0238	110	0.0297	0.0250	0.0418	0.0313
10	0.0242	0.0242	0.0242	0.0242	115	0.0472	0.0387	0.0484	0.0332
15	0.0248	0.0248	0.0248	0.0248	120	0.0682	0.0599	0.0409	0.0348
20	0.0255	0.0255	0.0255	0.0255	125	0.0676	0.0542	0.0493	0.0387
25	0.0266	0.0266	0.0266	0.0042	130	0.0688	0.0541	0.0524	0.0429
30	0.0054	0.0054	0.0018	0.0043	135	0.0618	0.0478	0.0571	0.0604
35	0.0044	0.0041	0.0018	0.0043	140	0.0669	0.0524	0.0660	0.0665
40	0.0029	0.0026	0.0021	0.0048	145	0.0600	0.0540	0.0506	0.0739
45	0.0033	0.0030	0.0021	0.0051	150	0.0798	0.0726	0.0591	0.0847
50	0.0036	0.0034	0.0017	0.0055	155	0.0967	0.0895	0.0696	0.0995
55	0.0043	0.0042	0.0016	0.0067	160	0.136	0.125	0.0847	0.118
60	0.0055	0.0057	0.0016	0.0083	165	0.179	0.122	0.175	0.144
65	0.0073	0.0070	0.0010	0.0097	170	0.323	0.237	0.234	0.188
70	0.0097	0.0106	0.0021	0.0117	175	0.352	0.294	0.245	0.269
75	0.0142	0.0163	0.0029	0.0134	180	0.765	0.596	0.408	0.391
80	0.0203	0.0227	0.0043	0.0165	185	0.838	0.702	0.582	0.700
85	0.0357	0.0383	0.0101	0.0198	190	1.04	0.855	0.764	1.07
90	0.0527	0.0522	0.0292	0.0247	195	1.93	1.81	1.10	2.88
95	0.0520	0.0493	0.0400	0.0266	200	6.97	6.47	3.49	5.29
100	0.0298	0.0257	0.0370	0.0283					

Table 17: *The 95% CL upper bound, S_{95}, obtained for the normalised cross-section (see text) of the pair production process* $e^+e^- \rightarrow \mathcal{H}_2\mathcal{H}_1$, *as a function of the Higgs boson mass sum* $m_{\mathcal{H}_1} + m_{\mathcal{H}_2}$. *The bounds are given for the particular case where* $m_{\mathcal{H}_2}$ *and* $m_{\mathcal{H}_1}$ *are approximately equal. This occurs, for example, in the CP-conserving MSSM scenario* m_h*-max for* $\tan\beta$ *greater than 10 and small* $m_{\mathcal{H}_2} (\equiv m_\mathrm{A})$. *The numbers listed in this table correspond to the four plots in Figure 4 (see the corresponding labels). For* $m_{\mathcal{H}_1} + m_{\mathcal{H}_2}$ *less than 30* GeV/c^2, *the bounds are derived from the measured decay width of the Z boson, see Section 3.2. Columns labelled (a): the Higgs boson decay branching ratios correspond to the* m_h*-max benchmark scenario with* $\tan\beta$*=10, giving 94% for* $\mathcal{H}_1 \rightarrow \mathrm{b\bar{b}}$, *6% for* $\mathcal{H}_1 \rightarrow \tau^+\tau^-$, *92% for* $\mathcal{H}_2 \rightarrow \mathrm{b\bar{b}}$ *and 8% for* $\mathcal{H}_2 \rightarrow \tau^+\tau^-$; *columns (b): both Higgs bosons are assumed to decay exclusively to* $\mathrm{b\bar{b}}$; *columns (c): one Higgs boson is assumed to decay exclusively to* $\mathrm{b\bar{b}}$ *only and the other exclusively to* $\tau^+\tau^-$; *columns (d): both Higgs bosons are assumed to decay exclusively to* $\tau^+\tau^-$.

$m_{\mathcal{H}_2}(\mathrm{GeV}/c^2)$	$m_{\mathcal{H}_1}(\mathrm{GeV}/c^2)$								
	10	15	20	25	30	35	40	45	50
15	≥ 1	0.012							
20	≥ 1	0.013	0.010						
25	≥ 1	0.017	0.013	0.011					
30	≥ 1	0.015	0.013	0.012	0.020	0.023			
40	≥ 1	0.016	0.018	0.022	0.028	0.039	0.043		
45	≥ 1	0.029	0.029	0.026	0.037	0.048	0.067	0.041	
50	≥ 1	0.035	0.026	0.042	0.044	0.069	0.043	0.035	0.028
55	≥ 1	0.063	0.056	0.076	0.071	0.058	0.050	0.038	0.030
60	≥ 1	0.075	0.084	0.098	0.051	0.051	0.050	0.044	0.039
65	≥ 1	0.14	0.13	0.10	0.065	0.064	0.070	0.068	0.069
70	≥ 1	0.20	0.16	0.11	0.072	0.074	0.066	0.072	0.071
75	≥ 1	0.23	0.13	0.14	0.076	0.075	0.083	0.066	0.093
80	≥ 1	0.26	0.19	0.12	0.078	0.089	0.072	0.064	0.093
85	≥ 1	0.26	0.17	0.13	0.095	0.080	0.070	0.071	0.10
90	≥ 1	0.18	0.13	0.11	0.073	0.070	0.076	0.081	0.13
95	≥ 1	0.20	0.13	0.095	0.073	0.078	0.081	0.11	0.15
100	≥ 1	0.21	0.12	0.092	0.085	0.091	0.12	0.16	0.18
105	≥ 1	0.16	0.13	0.12	0.11	0.13	0.18	0.20	0.20
110	0.297	0.16	0.14	0.15	0.14	0.17	0.20	0.20	0.19
115	0.338	0.22	0.20	0.20	0.18	0.20	0.21	0.21	0.23
120	0.355	0.28	0.25	0.23	0.22	0.22	0.23	0.27	0.36
125	0.409	0.29	0.26	0.25	0.22	0.25	0.29	0.40	0.51
130	0.494	0.35	0.32	0.32	0.24	0.32	0.46	0.57	0.72
135	0.617	0.44	0.42	0.42	0.36	0.51	0.67	0.84	0.98
140	0.696	0.57	0.53	0.66	0.62	0.83	0.97	≥ 1	≥ 1
145	0.811	0.73	0.80	≥ 1	0.94	≥ 1	≥ 1	≥ 1	≥ 1
	65	70	75	80	85	90	95	100	105
65	0.067								
70	0.082	0.078							
75	0.10	0.10	0.098						
80	0.11	0.11	0.14	0.14					
85	0.12	0.14	0.16	0.15	0.21				
90	0.17	0.16	0.17	0.25	0.24	0.41			
95	0.19	0.21	0.30	0.35	0.44	0.51	0.64		
100	0.21	0.31	0.39	0.42	0.43	0.74	≥ 1	≥ 1	
105	0.32	0.42	0.55	0.53	0.90	≥ 1	≥ 1	≥ 1	≥ 1
110	0.47	0.55	0.63	≥ 1	≥ 1	≥ 1	≥ 1	≥ 1	≥ 1
115	0.56	0.65	≥ 1	≥ 1	≥ 1	≥ 1	≥ 1	≥ 1	≥ 1
120	0.64	≥ 1	≥ 1	≥ 1	≥ 1	≥ 1	≥ 1	≥ 1	≥ 1
125	≥ 1	≥ 1	≥ 1	≥ 1	≥ 1	≥ 1	≥ 1	≥ 1	≥ 1

Table 18: *The 95% CL upper bound, S_{95}, obtained for the normalised cross-section (see text) of the pair production process* $e^+e^- \rightarrow \mathcal{H}_2\mathcal{H}_1 \rightarrow b\bar{b}b\bar{b}$, *as a function of the Higgs boson masses $m_{\mathcal{H}_1}$ and $m_{\mathcal{H}_2}$. The numbers correspond to the contours shown in Figure 5 (a).*

$m_{\mathcal{H}_2}(\mathrm{GeV}/c^2)$	$m_{\mathcal{H}_1}(\mathrm{GeV}/c^2)$									
	5	10	15	20	25	30	35	40	45	50
5	0.00041									
10	0.00047	0.00035								
15	0.0036	0.0032	0.0032							
20	0.0033	0.0035	0.0037	0.0040						
25	0.0037	0.0039	0.0043	0.0043	0.0046					
30	0.0052	0.0058	0.0045	0.0047	0.0055	0.0060				
35	0.0060	0.0058	0.0056	0.0065	0.0070	0.0081	0.0084			
40	0.0063	0.0064	0.0071	0.0070	0.0078	0.0092	0.011	0.0099		
45	0.0079	0.0068	0.0066	0.0083	0.0088	0.011	0.011	0.012	0.016	
50	0.0096	0.011	0.0086	0.0089	0.011	0.011	0.015	0.018	0.017	0.018
60	0.013	0.012	0.011	0.014	0.017	0.019	0.022	0.022	0.024	0.024
65	0.015	0.015	0.015	0.016	0.019	0.022	0.023	0.023	0.024	0.026
70	0.019	0.017	0.017	0.021	0.021	0.022	0.023	0.024	0.025	0.033
75	0.023	0.023	0.021	0.023	0.024	0.024	0.025	0.028	0.031	0.035
80	0.028	0.026	0.024	0.025	0.025	0.026	0.030	0.032	0.036	0.041
85	0.032	0.029	0.028	0.027	0.030	0.031	0.032	0.035	0.040	0.043
90	0.033	0.031	0.028	0.030	0.031	0.032	0.035	0.041	0.045	0.049
95	0.037	0.034	0.031	0.034	0.036	0.037	0.041	0.047	0.050	0.054
100	0.040	0.036	0.036	0.037	0.038	0.044	0.048	0.053	0.059	0.062
105	0.045	0.040	0.042	0.043	0.047	0.052	0.055	0.065	0.068	0.072
110	0.051	0.044	0.050	0.053	0.054	0.057	0.062	0.076	0.081	0.085
115	0.055	0.050	0.060	0.065	0.064	0.069	0.074	0.083	0.089	0.105
120	0.067	0.060	0.071	0.075	0.077	0.083	0.085	0.093	0.12	0.145
125	0.075	0.071	0.086	0.084	0.089	0.097	0.109	0.12	0.17	0.198
130	0.085	0.088	0.10	0.10	0.11	0.13	0.14	0.16	0.20	0.317
135	0.11	0.11	0.13	0.15	0.16	0.16	0.19	0.23	0.31	0.436
140	0.14	0.13	0.18	0.19	0.21	0.23	0.26	0.30	0.50	≥ 1
145	0.18	0.18	0.25	0.26	0.28	0.33	0.42	0.59	≥ 1	≥ 1
150	0.25	0.26	0.35	0.37	0.42	0.51	0.69	≥ 1	≥ 1	≥ 1
	55	60	65	70	75	80	85	90	95	100
55	0.021									
60	0.025	0.028								
65	0.030	0.033	0.036							
70	0.033	0.039	0.039	0.042						
75	0.038	0.040	0.044	0.048	0.049					
80	0.043	0.049	0.047	0.051	0.057	0.064				
85	0.048	0.050	0.055	0.061	0.071	0.075	0.097			
90	0.053	0.059	0.065	0.077	0.080	0.10	0.14	0.21		
95	0.059	0.067	0.076	0.080	0.10	0.14	0.21	0.38	0.70	
100	0.069	0.077	0.086	0.11	0.15	0.21	0.39	0.71	≥ 1	≥ 1
105	0.083	0.096	0.11	0.15	0.22	0.39	0.73	≥ 1	≥ 1	≥ 1
110	0.11	0.13	0.16	0.21	0.39	0.76	≥ 1	≥ 1	≥ 1	≥ 1
115	0.14	0.20	0.27	0.36	0.79	≥ 1	≥ 1	≥ 1	≥ 1	≥ 1
120	0.19	0.28	0.49	0.83	≥ 1	≥ 1	≥ 1	≥ 1	≥ 1	≥ 1
125	0.26	0.53	0.65	≥ 1	≥ 1	≥ 1	≥ 1	≥ 1	≥ 1	≥ 1
130	0.46	0.85	≥ 1	≥ 1	≥ 1	≥ 1	≥ 1	≥ 1	≥ 1	≥ 1
135	0.89	≥ 1	≥ 1	≥ 1	≥ 1	≥ 1	≥ 1	≥ 1	≥ 1	≥ 1

Table 19: *The 95% CL upper bound, S_{95}, obtained for the normalised cross-section (see text) of the pair production process* $e^+e^- \to \mathcal{H}_2\mathcal{H}_1 \to \tau^+\tau^-\tau^+\tau^-$*, as a function of the Higgs boson masses $m_{\mathcal{H}_1}$ and $m_{\mathcal{H}_2}$. The numbers correspond to the contours shown in Figure 5 (b).*

$m_{\mathcal{H}_2}(\mathrm{GeV}/c^2)$	$m_{\mathcal{H}_1}(\mathrm{GeV}/c^2)$										
	10	15	20	25	30	35	40	45	50	55	60
20	≥ 1										
25	0.096										
30	0.11	0.17									
35	0.13	0.075									
40	0.028	0.034	0.19								
45	0.15	0.047	0.034								
50	0.063	0.063	0.029	0.039							
55	0.074	0.087	0.042	0.055							
60	0.11	0.12	0.099	0.086	0.12						
65	0.25	0.17	0.13	0.14	0.13						
70	≥ 1	0.15	0.14	0.13	0.12	0.13					
75	0.72	0.17	0.16	0.14	0.13	0.13					
80	0.99	0.18	0.14	0.11	0.11	0.12	0.13				
85	≥ 1	0.19	0.15	0.13	0.14	0.14	0.16				
90	≥ 1	0.19	0.15	0.15	0.15	0.16	0.15	0.17			
95	≥ 1	0.20	0.17	0.17	0.16	0.15	0.17	0.20			
100	≥ 1	0.22	0.20	0.19	0.18	0.18	0.20	0.23	0.30		
105	≥ 1	0.26	0.22	0.21	0.23	0.24	0.27	0.32	0.38		
110	≥ 1	0.30	0.26	0.27	0.28	0.31	0.36	0.40	0.43	0.55	
115	≥ 1	0.35	0.32	0.33	0.33	0.38	0.43	0.47	0.54	0.70	
120	≥ 1	0.43	0.39	0.39	0.42	0.46	0.50	0.58	0.71	0.93	≥ 1
125	≥ 1	0.53	0.49	0.48	0.51	0.56	0.63	0.77	0.99	≥ 1	≥ 1
130	≥ 1	0.66	0.59	0.62	0.64	0.72	0.86	≥ 1	≥ 1	≥ 1	≥ 1
135	≥ 1	0.82	0.66	0.75	0.84	0.98	≥ 1	≥ 1	≥ 1	≥ 1	≥ 1
140	≥ 1	≥ 1	0.90	0.96	0.98	≥ 1	≥ 1	≥ 1	≥ 1	≥ 1	≥ 1

Table 20: *The 95% CL upper bound, S_{95}, obtained for the normalised cross-section (see text) of the pair production cascade process* $e^+e^- \to$ *(*$\mathcal{H}_2 \to \mathcal{H}_1\mathcal{H}_1$*)*$\mathcal{H}_1 \to$ (b$\bar{\mathrm{b}}$b$\bar{\mathrm{b}}$)b$\bar{\mathrm{b}}$, *as a function of the Higgs boson masses* $m_{\mathcal{H}_1}$ *and* $m_{\mathcal{H}_2}$*. The numbers correspond to the contours shown in Figure 6 (a).*

$m_{\mathcal{H}_2}(\mathrm{GeV}/c^2)$	$m_{\mathcal{H}_1}(\mathrm{GeV}/c^2)$			
	5	10	15	20
10	0.0006			
15	0.0016			
20	0.0017	0.011		
25	0.0018	0.0019		
30	0.0021	0.0021	0.013	
35	0.0024	0.0025	0.017	
40	0.0009	0.0016	≥ 1	≥ 1
45	0.0010	0.0019	≥ 1	≥ 1
50	0.0013	0.0023	≥ 1	≥ 1
55	0.0017	0.0029	≥ 1	≥ 1
60	0.0024	0.0043	≥ 1	≥ 1
65	0.0058	0.014	≥ 1	≥ 1

Table 21: *The 95% CL upper bound, S_{95}, obtained for the normalised cross-section (see text) of the pair production cascade process* $\mathrm{e^+e^-} \rightarrow (\mathcal{H}_2 \rightarrow \mathcal{H}_1\mathcal{H}_1)\mathcal{H}_1 \rightarrow (\tau^+\tau^-\tau^+\tau^-)\tau^+\tau^-$, *as a function of the Higgs boson masses $m_{\mathcal{H}_1}$ and $m_{\mathcal{H}_2}$. The numbers correspond to the contours shown in Figure 6 (b).*

Appendix C: List of authors

The ALEPH, DELPHI, L3 and OPAL Collaborations have provided the inputs for the combined results presented in this paper. The LEP Working Group for Higgs Boson Searches has performed the combinations. The Working Group consists of members of the four collaborations and of theorists among whom S. Heinemeyer[9], A. Pilaftsis[10] and G. Weiglein[11] are authors of this paper. The lists of authors from the collaborations follow.

[9]Departamento de Fisica Teorica, Facultad de Ciencias, Universidad de Zaragoza, 50009 Zaragoza, Spain; CERN TH division, Dept. of Physics, 1211 Geneva 23, Switzerland

[10]Department of Physics and Astronomy, University of Manchester, Manchester M13 9PL, UK

[11]Institute for Particle Physics Phenomenology, University of Durham, Durham DH1 3LE, UK

Appendix C1: The ALEPH Collaboration

S. Schael[1], R. Barate[2], R. Brunelière[2], I. De Bonis[2], D. Decamp[2], C. Goy[2], S. Jézéquel[2], J.-P. Lees[2], F. Martin[2], E. Merle[2], M.-N. Minard[2], B. Pietrzyk[2], B. Trocmé[2] S. Bravo[3], M. P. Casado[3], M. Chmeissani[3], J. M. Crespo[3], E. Fernandez[3], M. Fernandez-Bosman[3], Ll. Garrido,[3,j] M. Martinez[3], A. Pacheco[3], H. Ruiz[3], A. Colaleo[4], D. Creanza[4], N. De Filippis[4], M. de Palma[4], G. Iaselli[4], G. Maggi[4], M. Maggi[4], S. Nuzzo[4], A. Ranieri[4], G. Raso,[4,o] F. Ruggieri[4], G. Selvaggi[4], L. Silvestris[4], P. Tempesta[4], A. Tricomi[4,c], G. Zito[4], X. Huang[5], J. Lin[5], Q. Ouyang[5], T. Wang[5], Y. Xie[5], R. Xu[5], S. Xue[5], J. Zhang[5], L. Zhang[5], W. Zhao[5], D. Abbaneo[6], T. Barklow,[6,q] O. Buchmüller,[6,q] M. Cattaneo[6], B. Clerbaux[6,n] H. Drevermann[6], R. W. Forty[6], M. Frank[6], F. Gianotti[6], J. B. Hansen[6], J. Harvey[6], D. E. Hutchcroft[6,u], P. Janot[6], B. Jost[6], M. Kado[6,b] P. Mato[6], A. Moutoussi[6], F. Ranjard[6], L. Rolandi[6], D. Schlatter[6], F. Teubert[6], A. Valassi[6], I. Videau[6], F. Badaud[7], S. Dessagne[7], A. Falvard[7,l] D. Fayolle[7], P. Gay[7], J. Jousset[7], B. Michel[7], S. Monteil[7], D. Pallin[7], J. M. Pascolo[7], P. Perret[7], J. D. Hansen[8], J. R. Hansen[8], P. H. Hansen[8], A. C. Kraan[8], B. S. Nilsson[8], A. Kyriakis[9], C. Markou[9], E. Simopoulou[9], A. Vayaki[9], K. Zachariadou[9], A. Blondel[10,g], J.-C. Brient[10], F. Machefert[10], A. Rougé[10], H. Videau[10] V. Ciulli[11], E. Focardi[11], G. Parrini[11], A. Antonelli[12], M. Antonelli[12], G. Bencivenni[12], F. Bossi[12], G. Capon[12], F. Cerutti[12], V. Chiarella[12], G. Mannocchi[12], P. Laurelli[12], G. Mannocchi[12,e] G. P. Murtas[12], L. Passalacqua[12], J. Kennedy[13], J. G. Lynch[13], P. Negus[13], V. O'Shea[13], A. S. Thompson[13], S. Wasserbaech[14], R. Cavanaugh[15,d], S. Dhamotharan[15,m], C. Geweniger[15], P. Hanke[15], V. Hepp[15], E. E. Kluge[15], A. Putzer[15], H. Stenzel[15], K. Tittel[15], M. Wunsch[15,k] R. Beuselinck[16], W. Cameron[16], G. Davies[16], P. J. Dornan[16], M. Girone,[16,a] N. Marinelli[16], J. Nowell[16], S. A. Rutherford[1]6, J. K. Sedgbeer[16], J. C. Thompson[16,i], R. White[16], V. M. Ghete[17], P. Girtler[17], E. Kneringer[17], D. Kuhn[17], G. Rudolph[17], E. Bouhova-Thacker[18], C. K. Bowdery[18], D. P. Clarke[18], G. Ellis[18], A. J. Finch[18], F. Foster[18], G. Hughes[18], R. W. L. Jones[18], M. R. Pearson[18], N. A. Robertson[18], M. Smizanska[18], O. van der Aa[19], C. Delaere[19,s], G. Leibenguth[19,v], V. Lemaitre[19,t], U. Blumenschein[20], F. Hölldorfer[20], K. Jakobs[20], F. Kayser[20], A.-S. Müller[20], B. Renk[20], H.-G. Sander[20], S. Schmeling[20], H. Wachsmuth[20], C. Zeitnitz[20], T. Ziegler[20], A. Bonissent[21], P. Coyle[21], C. Curtil[21], A. Ealet[21], D. Fouchez[21], P. Payre[21], A. Tilquin[21], F. Ragusa[22], A. David[23], H. Dietl[23,w] G. Ganis[23,r], K. Hüttmann[23], G. Lütjens[23], W. Männer[23,w], H.-G. Moser[23], R. Settles[23], M. Villegas[23], G. Wolf[23], J. Boucrot[24], O. Callot[24], M. Davier[24], L. Duflot[24], J.-F. Grivaz[24], Ph. Heusse[24], A. Jacholkowska[24,f], L. Serin[24], J.-J. Veillet[24], P. Azzurri[25], G. Bagliesi[25], T. Boccali[25], L. Foà[25], A. Giammanco[25], A. Giassi[25], F. Ligabue[25], A. Messineo[25], F. Palla[25], G. Sanguinetti[25], A. Sciabà[25], G. Sguazzoni[25], P. Spagnolo[25], R. Tenchini[25], A. Venturi[25], P. G. Verdini[25], O. Awunor[26], G. A. Blair[26], G. Cowan[26], A. Garcia-Bellido[26], M. G. Green[26], T. Medcalf[26,†], A. Misiejuk[26], J. A. Strong[26], P. Teixeira-Dias[26], R. W. Clifft[27], T. R. Edgecock[27], P. R. Norton[27], I. R. Tomalin[27], J. J. Ward[27], B. Bloch-Devaux[28], D. Boumediene[28], P. Colas[28], B. Fabbro[28], E. Lançon[28], M.-C. Lemaire[28], E. Locci[28], P. Perez[28], J. Rander[28], B. Tuchming[28], B. Vallage[28], A. M. Litke[29], G. Taylor[29], C. N. Booth[30], S. Cartwright[30], F. Combley[30,†] P. N. Hodgson[30], M. Lehto[30], L. F. Thompson[30], A. Böhrer[31], S. Brandt[31], C. Grupen[31], J. Hess[31], A. Ngac[31], G. Prange[31], C. Borean[32], G. Giannini[32], H. He[33], J. Putz[33], J. Rothberg[33], S. R. Armstrong[34], K. Berkelman[34], K. Cranmer[34], D. P. S. Ferguson[34], Y. Gao[34,h], S. González[34], O. J. Hayes[34], H. Hu[34], S. Jin[34], J. Kile[34], P. A. McNamara III[34], J. Nielsen[34], Y. B. Pan[34], J. H. von Wimmersperg-Toeller[34], W. Wiedenmann[34], J. Wu[34], Sau Lan Wu[34], X. Wu[34], G. Zobernig[34], G. Dissertori[35].

1 Physikalisches Institut das RWTH-Aachen, D-52056 Aachen, Germany

2 Laboratoire de Physique des Particules (LAPP), IN^2P^3-CNRS,
F-74019 Annecy-le-Vieux Cedex, France
3 Institut de Física d'Altes Energies, Universitat Autònoma de Barcelona,
E-08193 Bellaterra (Barcelona), Spain[α]
4 Dipartimento di Fisica, INFN Sezione di Bari, I-70126 Bari, Italy
5 Institute of High Energy Physics, Academia Sinica, Beijing, The People's Republic of China[β]
6 European Laboratory for Particle Physics (CERN), CH-1211 Geneva 23, Switzerland
7 Laboratoire de Physique Corpusculaire, Université Blaise Pascal, IN^2P^3-CNRS,
Clermont-Ferrand, F-63177 Aubière, France
8 Niels Bohr Institute, 2100 Copenhagen, DK-Denmark[γ]
9 Nuclear Research Center Demokritos (NRCD), GR-15310 Attiki, Greece
10 Laoratoire Leprince-Ringuet, Ecole Polytechnique, IN^2P^3-CNRS,
F-91128 Palaiseau Cedex, France
11 Dipartimento di Fisica, Università di Firenze, INFN Sezione di Firenze,
I-50125 Firenze, Italy
12 Laboratori Nazionali dell'INFN (LNF-INFN), I-00044 Frascati, Italy
13 Department of Physics and Astronomy, University of Glasgow,
Glasgow G128QQ,United Kingdom[δ]
14 Utah Valley State College, Orem, UT 84058, U.S.A.
15 Kirchhoff-Institut für Physik, Universität Heidelberg, D-69120 Heidelberg, Germany[ϵ]
16 Department of Physics, Imperial College, London SW7 2BZ, United Kingdom[δ]
17 Institut für Experimentalphysik, Universität Innsbruck, A-6020 Innsbruck, Austria[ν]
18 Department of Physics, University of Lancaster, Lancaster LA1 4YB, United Kingdom[δ]
19 Institut de Physique Nucléaire, Département de Physique,
Université Catholique de Louvain, 1348 Louvain-la-Neuve, Belgium
20 Institut für Physik, Universität Mainz, D-55099 Mainz, Germany[λ]
21 Centre de Physique des Particules de Marseille, Univ Méditerranée, IN^2P^3-CNRS,
F-13288 Marseille, France
22 Dipartimento di Fisica, Università di Milano e INFN Sezione di Milano,
I-20133 Milano, Italy
23 Max-Planck-Institut für Physik, Werner-Heisenberg-Institut, D-80805 München, Germany[λ]
24 Laboratoire de l'Accélérateur Linéaire, Université de Paris-Sud, IN^2P^3-CNRS,
F-91898 Orsay Cedex, France
25 Dipartimento di Fisica dell'Università, INFN Sezione di Pisa, e Scuola Normale Superiore,
I-56010 Pisa, Italy
26 Department of Physics, Royal Holloway & Bedford New College, University of London,
Egham, Surrey TW20 OEX, United Kingdom[δ]
27 Particle Physics Dept., Rutherford Appleton Laboratory, Chilton, Didcot,
Oxon OX11 OQX, United Kingdom[δ]
28 CEA, DAPNIA/Service de Physique des Particules, CE-Saclay,
F-91191 Gif-sur-Yvette Cedex, France[μ]
29 Institute for Particle Physics, University of California at Santa Cruz, Santa Cruz,
CA 95064, USA[π]
30 Department of Physics, University of Sheffield, Sheffield S3 7RH, United Kingdom[δ]
31 Fachbereich Physik, Universität Siegen, D-57068 Siegen, Germany[λ]

32 Dipartimento di Fisica, Università di Trieste e INFN Sezione di Trieste,
I-34127 Trieste, Italy
33 Experimental Elementary Particle Physics, University of Washington,
Seattle, WA 98195 U.S.A.
34 Department of Physics, University of Wisconsin, Madison, WI 53706, USA[ϵ]
35 Institute for Particle Physics, ETH Hönggerberg, 8093 Zürich, Switzerland.

a Also at CERN, 1211 Geneva 23, Switzerland
b Now at Fermilab, PO Box 500, MS 352, Batavia, IL 60510, USA
c Also at Dipartimento di Fisica di Catania and INFN Sezione di Catania,
95129 Catania, Italy.
d Now at University of Florida, Department of Physics, Gainesville, Florida 32611-8440, USA
e Also IFSI sezione di Torino, INAF, Italy.
f Also at Groupe d'Astroparticules de Montpellier, Université de Montpellier II,
34095 Montpellier, France.
g Now at Departement de Physique Corpusculaire, Université de Genève,
1211 Genève 4, Switzerland.
h Also at Department of Physics, Tsinghua University, Beijing,
The People's Republic of China.
i Supported by the Leverhulme Trust.
j Permanent address: Universitat de Barcelona, 08208 Barcelona, Spain.
k Now at SAP AG, 69185 Walldorf, Germany
l Now at Groupe d' Astroparticules de Montpellier, Université de Montpellier II,
34095 Montpellier, France.
m Now at BNP Paribas, 60325 Frankfurt am Mainz, Germany
n Now at Institut Inter-universitaire des hautes Energies (IIHE), CP 230,
Université Libre de Bruxelles, 1050 Bruxelles, Belgique
o Now at Dipartimento di Fisica e Tecnologie Relative, Università di Palermo,
Palermo, Italy.
q Now at SLAC, Stanford, CA 94309, U.S.A
r Now at CERN, 1211 Geneva 23, Switzerland
s Research Fellow of the Belgium FNRS
t Research Associate of the Belgium FNRS
u Now at Liverpool University, Liverpool L69 7ZE, United Kingdom
v Supported by the Federal Office for Scientific, Technical and Cultural Affairs
through the Interuniversity Attraction Pole P5/27
w Now at Henryk Niewodniczanski Institute of Nuclear Physics, Polish Academy of Sciences,
Cracow, Poland
† Deceased

α Supported by CICYT, Spain.
β Supported by the National Science Foundation of China.
γ Supported by the Danish Natural Science Research Council.

δ Supported by the UK Particle Physics and Astronomy Research Council.
ϵ Supported by the US Department of Energy, grant DE-FG0295-ER40896.
λ Supported by Bundesministerium für Bildung und Forschung, Germany.
μ Supported by the Direction des Sciences de la Matière, C.E.A.
ν Supported by the Austrian Ministry for Science and Transport.
π Supported by the US Department of Energy, grant DE-FG03-92ER40689.

Appendix C2: The DELPHI Collaboration

J. Abdallah[25], P. Abreu[22], W. Adam[51], P. Adzic[11], T. Albrecht[17], T. Alderweireld[2], R. Alemany-Fernandez[8], T. Allmendinger[17], P. P. Allport[23], U. Amaldi[29], N. Amapane[45], S. Amato[48], E. Anashkin[36], A. Andreazza[28], S. Andringa[22], N. Anjos[22], P. Antilogus[25], W.- D. Apel[17], Y. Arnoud[14], S. Ask[26], B. Asman[44], J. E. Augustin[25], A. Augustinus[8], P. Baillon[8], A. Ballestrero[46], P. Bambade[20], R. Barbier[27], D. Bardin[16], G. J. Barker[17], A. Baroncelli[39], M. Battaglia[8], M. Baubillier[25], K.- H. Becks[53], M. Begalli[6], A. Behrmann[53], E. Ben-Haim[20], N. Benekos[32], A. Benvenuti[5], C. Berat[14], M. Berggren[25], L. Berntzon[44], D. Bertrand[2], M. Besancon[40], N. Besson[40], D. Bloch[9], M. Blom[31], M. Bluj[52], M. Bonesini[29], M. Boonekamp[40], P. S. L. Booth[†23], G. Borisov[21], O. Botner[49], B. Bouquet[20], T. J. V. Bowcock[23], I. Boyko[16], M. Bracko[43], R. Brenner[49], E. Brodet[35], P. Bruckman[18], J. M. Brunet[7], B. Buschbeck[51], P. Buschmann[53], M. Calvi[29], T. Camporesi[8], V. Canale[38], F. Carena[8], N. Castro[22], F. Cavallo[5], M. Chapkin[42], Ph. Charpentier[8], P. Checchia[36], R. Chierici[8], P. Chliapnikov[42], J. Chudoba[8], S. U. Chung[8], K. Cieslik[18], P. Collins[8], R. Contri[13], G. Cosme[20], F. Cossutti[47], M. J. Costa[50], D. Crennell[37], J. Cuevas[34], J. D'Hondt[2], J. Dalmau[44], T. da Silva[48], W. Da Silva[25], G. Della Ricca[47], A. De Angelis[47], W. De Boer[17], C. De Clercq[2], B. De Lotto[47], N. De Maria[45], A. De Min[36], L. de Paula[48], L. Di Ciaccio[38], A. Di Simone[39], K. Doroba[52], J. Drees[53,8], G. Eigen[4], T. Ekelof[49], M. Ellert[49], M. Elsing[8], M. C. Espirito Santo[22], G. Fanourakis[11], D. Fassouliotis[11,3], M. Feindt[17], J. Fernandez[41], A. Ferrer[50], F. Ferro[13], U. Flagmeyer[53], H. Foeth[8], E. Fokitis[32], F. Fulda-Quenzer[20], J. Fuster[50], M. Gandelman[48], C. Garcia[50], Ph. Gavillet[8], E. Gazis[32], R. Gokieli[8],[52], B. Golob[43], G. Gomez-Ceballos[41], P. Goncalves[22], E. Graziani[39], G. Grosdidier[20], K. Grzelak[52], J. Guy[37], C. Haag[17], A. Hallgren[49], K. Hamacher[53], K. Hamilton[35], S. Haug[33], F. Hauler[17], V. Hedberg[26], M. Hennecke[17], H. Herr[†8], J. Hoffman[52], S.- O. Holmgren[44], P. J. Holt[8], M. A. Houlden[23], K. Hultqvist[44], J. N. Jackson[23], G. Jarlskog[26], P. Jarry[40], D. Jeans[35], E. K. Johansson[44], P. D. Johansson[44], P. Jonsson[27], C. Joram[8], L. Jungermann[17], F. Kapusta[25], S. Katsanevas[27], E. Katsoufis[32], G. Kernel[43], B. P. Kersevan[8,43], U. Kerzel[17], B. T. King[23], N. J. Kjaer[8], P. Kluit[31], P. Kokkinias[11], C. Kourkoumelis[3], O. Kouznetsov[16], Z. Krumstein[16], M. Kucharczyk[18], J. Lamsa[1], G. Leder[51], F. Ledroit[14], L. Leinonen[44], R. Leitner[30], J. Lemonne[2], V. Lepeltier[20], T. Lesiak[18], W. Liebig[53], D. Liko[51], A. Lipniacka[44], J. H. Lopes[48], J. M. Lopez[34], D. Loukas[11], P. Lutz[40], L. Lyons[35], J. MacNaughton[51], A. Malek[53], S. Maltezos[32], F. Mandl[51], J. Marco[41], R. Marco[41], B. Marechal[48], M. Margoni[36], J.- C. Marin[8], C. Mariotti[8], A. Markou[11], C. Martinez-Rivero[41], J. Masik[12], N. Mastroyiannopoulos[11], F. Matorras[41], C. Matteuzzi[29], F. Mazzucato[36], M. Mazzucato[36], R. Mc Nulty[23], C. Meroni[28], E. Migliore[45], W. Mitaroff[51], U. Mjoernmark[26], T. Moa[44], M. Moch[17], K. Moenig[8,10], R. Monge[13], J. Montenegro[31], D. Moraes[48], S. Moreno[22], P. Morettini[13], U. Mueller[53], K. Muenich[53], M. Mulders[31], L. Mundim[6], W. Murray[37], B. Muryn[19], G. Myatt[35], T. Myklebust[33], M. Nassiakou[11], F. Navarria[5], K. Nawrocki[52], R. Nicolaidou[40], M. Nikolenko[16,9], A. Oblakowska-Mucha[19], V. Obraztsov[42], A. Olshevski[16], A. Onofre[22], R. Orava[15], K. Osterberg[15], A. Ouraou[40], A. Oyanguren[50], M. Paganoni[29], S. Paiano[5], J. P. Palacios[23], H. Palka[18], Th. D. Papadopoulou[32], L. Pape[8], C. Parkes[24], F. Parodi[13], U. Parzefall[8], A. Passeri[39], O. Passon[53], L. Peralta[22], V. Perepelitsa[50], A. Perrotta[5], A. Petrolini[13], J. Piedra[41], L. Pieri[39], F. Pierre[40], M. Pimenta[22], E. Piotto[8], T. Podobnik[43], V. Poireau[8], M. E. Pol[6], G. Polok[18], V. Pozdniakov[16], N. Pukhaeva[2,16], A. Pullia[29], J. Rames[12], A. Read[33], P. Rebecchi[8], J. Rehn[17], D. Reid[31], R. Reinhardt[53], P. Renton[35], F. Richard[20], J. Ridky[12], M. Rivero[41], D. Rodriguez[41], A. Romero[45], P. Ronchese[36], P. Roudeau[20], T. Rovelli[5], V. Ruhlmann-Kleider[40], D. Ryabtchikov[42], A. Sadovsky[16], L. Salmi[15], J. Salt[50], C. Sander[17], A. Savoy-Navarro[25], U. Schwickerath[8], A. Segar[†35], R. Sekulin[37], M. Siebel[53], A. Sisakian[16], G. Smadja[27], O. Smirnova[26], A. Sokolov[42], A. Sopczak[21], R. Sosnowski[52], T. Spassov[8], M. Stanitzki[17], A. Stocchi[20], J. Strauss[51], B. Stugu[4], M. Szczekowski[52],

M. Szeptycka[52], T. Szumlak[19], T. Tabarelli[29], A. C. Taffard[23], F. Tegenfeldt[49], J. Timmermans[31], L. Tkatchev[16], M. Tobin[23], S. Todorovova[12], B. Tome[22], A. Tonazzo[29], P. Tortosa[50], P. Travnicek[12], D. Treille[8], G. Tristram[7], M. Trochimczuk[52], C. Troncon[28], M.- L. Turluer[40], I. A. Tyapkin[16], P. Tyapkin[16], S. Tzamarias[11], V. Uvarov[42], G. Valenti[5], P. Van Dam[31], J. Van Eldik[8], N. van Remortel[15], I. Van Vulpen[8], G. Vegni[28], F. Veloso[22], W. Venus[37], P. Verdier[27], V. Verzi[38], D. Vilanova[40], L. Vitale[47], V. Vrba[12], H. Wahlen[53], A. J. Washbrook[23], C. Weiser[17], D. Wicke[8], J. Wickens[2], G. Wilkinson[35], M. Winter[9], M. Witek[18], O. Yushchenko[42], A. Zalewska[18], P. Zalewski[52], D. Zavrtanik[43], V. Zhuravlov[16], N. I. Zimin[16], A. Zintchenko[16], M. Zupan[11].

1 Department of Physics and Astronomy, Iowa State University, Ames IA 50011-3160, USA
2 Physics Department, Universiteit Antwerpen, Universiteitsplein 1, B-2610 Antwerpen, Belgium
and IIHE, ULB-VUB, Pleinlaan 2, B-1050 Brussels, Belgium
and Faculté des Sciences, Univ. de l'Etat Mons, Av. Maistriau 19, B-7000 Mons, Belgium
3 Physics Laboratory, University of Athens, Solonos Str. 104, GR-10680 Athens, Greece
4 Department of Physics, University of Bergen, Allégaten 55, NO-5007 Bergen, Norway
5 Dipartimento di Fisica, Università di Bologna and INFN, Via Irnerio 46, IT-40126 Bologna, Italy
6 Centro Brasileiro de Pesquisas Físicas, rua Xavier Sigaud 150, BR-22290 Rio de Janeiro, Brazil
and Depto. de Física, Pont. Univ. Católica, C.P. 38071, BR-22453 Rio de Janeiro, Brazil
and Inst. de Física, Univ. Estadual do Rio de Janeiro, rua São Francisco Xavier 524, Rio de Janeiro, Brazil
7 Collège de France, Lab. de Physique Corpusculaire, IN2P3-CNRS, FR-75231 Paris Cedex 05, France
8 CERN, CH-1211 Geneva 23, Switzerland
9 Institut de Recherches Subatomiques, IN2P3 - CNRS/ULP - BP20, FR-67037 Strasbourg Cedex, France
10 Now at DESY-Zeuthen, Platanenallee 6, D-15735 Zeuthen, Germany
11 Institute of Nuclear Physics, N.C.S.R. Demokritos, P.O. Box 60228, GR-15310 Athens, Greece
12 FZU, Inst. of Phys. of the C.A.S. High Energy Physics Division, Na Slovance 2, CZ-180 40 Praha 8, Czech Republic
13 Dipartimento di Fisica, Università di Genova and INFN, Via Dodecaneso 33, IT-16146 Genova, Italy
14 Institut des Sciences Nucléaires, IN2P3-CNRS, Université de Grenoble 1, FR-38026 Grenoble Cedex, France
15 Helsinki Institute of Physics and Department of Physical Sciences, P.O. Box 64, FIN-00014 University of Helsinki, Finland
16 Joint Institute for Nuclear Research, Dubna, Head Post Office, P.O. Box 79, RU-101 000 Moscow, Russian Federation
17 Institut für Experimentelle Kernphysik, Universität Karlsruhe, Postfach 6980, DE-76128 Karlsruhe, Germany
18 Institute of Nuclear Physics PAN,Ul. Radzikowskiego 152, PL-31142 Krakow, Poland
19 Faculty of Physics and Nuclear Techniques, University of Mining and Metallurgy, PL-30055 Krakow, Poland
20 Université de Paris-Sud, Lab. de l'Accélérateur Linéaire, IN2P3-CNRS, Bât. 200, FR-91405 Orsay Cedex, France

21 School of Physics and Chemistry, University of Lancaster, Lancaster LA1 4YB, UK
22 LIP, IST, FCUL - Av. Elias Garcia, 14-1^o, PT-1000 Lisboa Codex, Portugal
23 Department of Physics, University of Liverpool, P.O. Box 147, Liverpool L69 3BX, UK
24 Dept. of Physics and Astronomy, Kelvin Building, University of Glasgow, Glasgow G12 8QQ
25 LPNHE, IN2P3-CNRS, Univ. Paris VI et VII, Tour 33 (RdC), 4 place Jussieu, FR-75252 Paris Cedex 05, France
26 Department of Physics, University of Lund, Sölvegatan 14, SE-223 63 Lund, Sweden
27 Université Claude Bernard de Lyon, IPNL, IN2P3-CNRS, FR-69622 Villeurbanne Cedex, France
28 Dipartimento di Fisica, Università di Milano and INFN-MILANO, Via Celoria 16, IT-20133 Milan, Italy
29 Dipartimento di Fisica, Univ. di Milano-Bicocca and INFN-MILANO, Piazza della Scienza 2, IT-20126 Milan, Italy
30 IPNP of MFF, Charles Univ., Areal MFF, V Holesovickach 2, CZ-180 00, Praha 8, Czech Republic
31 NIKHEF, Postbus 41882, NL-1009 DB Amsterdam, The Netherlands
32 National Technical University, Physics Department, Zografou Campus, GR-15773 Athens, Greece
33 Physics Department, University of Oslo, Blindern, NO-0316 Oslo, Norway
34 Dpto. Fisica, Univ. Oviedo, Avda. Calvo Sotelo s/n, ES-33007 Oviedo, Spain
35 Department of Physics, University of Oxford, Keble Road, Oxford OX1 3RH, UK
36 Dipartimento di Fisica, Università di Padova and INFN, Via Marzolo 8, IT-35131 Padua, Italy
37 Rutherford Appleton Laboratory, Chilton, Didcot OX11 OQX, UK
38 Dipartimento di Fisica, Università di Roma II and INFN, Tor Vergata, IT-00173 Rome, Italy
39 Dipartimento di Fisica, Università di Roma III and INFN, Via della Vasca Navale 84, IT-00146 Rome, Italy
40 DAPNIA/Service de Physique des Particules, CEA-Saclay, FR-91191 Gif-sur-Yvette Cedex, France
41 Instituto de Fisica de Cantabria (CSIC-UC), Avda. los Castros s/n, ES-39006 Santander, Spain
42 Inst. for High Energy Physics, Serpukov P.O. Box 35, Protvino, (Moscow Region), Russian Federation
43 J. Stefan Institute, Jamova 39, SI-1000 Ljubljana, Slovenia and Laboratory for Astroparticle Physics, Nova Gorica Polytechnic, Kostanjeviska 16a, SI-5000 Nova Gorica, Slovenia, and Department of Physics, University of Ljubljana, SI-1000 Ljubljana, Slovenia
44 Fysikum, Stockholm University, Box 6730, SE-113 85 Stockholm, Sweden
45 Dipartimento di Fisica Sperimentale, Università di Torino and INFN, Via P. Giuria 1, IT-10125 Turin, Italy
46 INFN,Sezione di Torino and Dipartimento di Fisica Teorica, Università di Torino, Via Giuria 1, IT-10125 Turin, Italy
47 Dipartimento di Fisica, Università di Trieste and INFN, Via A. Valerio 2, IT-34127 Trieste, Italy and Istituto di Fisica, Università di Udine, IT-33100 Udine, Italy
48 Univ. Federal do Rio de Janeiro, C.P. 68528 Cidade Univ., Ilha do Fundão BR-21945-970 Rio de Janeiro, Brazil
49 Department of Radiation Sciences, University of Uppsala, P.O. Box 535, SE-751 21 Uppsala, Sweden
50 IFIC, Valencia-CSIC, and D.F.A.M.N., U. de Valencia, Avda. Dr. Moliner 50, ES-46100 Burjassot (Valencia), Spain
51 Institut für Hochenergiephysik, Österr. Akad. d. Wissensch., Nikolsdorfergasse 18, AT-1050 Vienna, Austria

52 Inst. Nuclear Studies and University of Warsaw, Ul. Hoza 69, PL-00681 Warsaw, Poland
53 Fachbereich Physik, University of Wuppertal, Postfach 100 127, DE-42097 Wuppertal, Germany
† Deceased

Appendix C3: The L3 Collaboration

P. Achard[20], O. Adriani[17], M. Aguilar-Benitez[25], J. Alcaraz[25], G. Alemanni[23], J. Allaby[18], A. Aloisio[29], M. G. Alviggi[29], H. Anderhub[49], V. P. Andreev[6,34], F. Anselmo[8], A. Arefiev[28], T. Azemoon[3], T. Aziz[9], P. Bagnaia[39], A. Bajo[25], G. Baksay[26], L. Baksay[26], S. V. Baldew[2], S. Banerjee[9], Sw. Banerjee[4], A. Barczyk[49,47], R. Barillère[18], P. Bartalini[23], M. Basile[8], N. Batalova[46], R. Battiston[33], A. Bay[23], F. Becattini[17], U. Becker[13], F. Behner[49], L. Bellucci[17], R. Berbeco[3], J. Berdugo[25], P. Berges[13], B. Bertucci[33], B. L. Betev[49], M. Biasini[33], M. Biglietti[29], A. Biland[49], J. J. Blaising[4], S. C. Blyth[35], G. J. Bobbink[2], A. Böhm[1], L. Boldizsar[12], B. Borgia[39], S. Bottai[17], D. Bourilkov[49], M. Bourquin[20], S. Braccini[20], J. G. Branson[41], F. Brochu[4], J. D. Burger[13], W. J. Burger[33], X. D. Cai[13], M. Capell[13], G. Cara Romeo[8], G. Carlino[29], A. Cartacci[17], J. Casaus[25], F. Cavallari[39], N. Cavallo[36], C. Cecchi[33], M. Cerrada[25], M. Chamizo[20], Y. H. Chang[44], M. Chemarin[24], A. Chen[44], G. Chen[7], G. M. Chen[7], H. F. Chen[22], H. S. Chen[7], G. Chiefari[29], L. Cifarelli[40], F. Cindolo[8], I. Clare[13], R. Clare[38], G. Coignet[4], N. Colino[25], S. Costantini[39], B. de la Cruz[25], S. Cucciarelli[33], R. de Asmundis[29], P. Déglon[20], J. Debreczeni[12], A. Degré[4], K. Dehmelt[26], K. Deiters[47], D. della Volpe[29], E. Delmeire[20], P. Denes[37], F. DeNotaristefani[39], A. De Salvo[49], M. Diemoz[39], M. Dierckxsens[2], C. Dionisi[39], M. Dittmar[49], A. Doria[29], M. T. Dova[10,♯], D. Duchesneau[4], M. Duda[1], B. Echenard[20], A. Eline[18], A. El Hage[1], H. El Mamouni[24], A. Engler[35], F. J. Eppling[13], P. Extermann[20], M. A. Falagan[25], S. Falciano[39], A. Favara[32], J. Fay[24], O. Fedin[34], M. Felcini[49], T. Ferguson[35], H. Fesefeldt[1], E. Fiandrini[33], J. H. Field[20], F. Filthaut[31], P. H. Fisher[13], W. Fisher[37], G. Forconi[13], K. Freudenreich[49], C. Furetta[27], Yu. Galaktionov[28,13], S. N. Ganguli[9], P. Garcia-Abia[25], M. Gataullin[32], S. Gentile[39], S. Giagu[39], Z. F. Gong[22], G. Grenier[24], O. Grimm[49], M. W. Gruenewald[16], M. Guida[40], V. K. Gupta[37], A. Gurtu[9], L. J. Gutay[46], D. Haas[5], D. Hatzifotiadou[8], T. Hebbeker[1], A. Hervé[18], J. Hirschfelder[35], H. Hofer[49], M. Hohlmann[26], G. Holzner[49], S. R. Hou[44], J. Hu[31], B. N. Jin[7], P. Jindal[14], L. W. Jones[3], P. de Jong[2], I. Josa-Mutuberría[25], M. Kaur[14], M. N. Kienzle-Focacci[20], J. K. Kim[43], J. Kirkby[18], W. Kittel[31], A. Klimentov[13,28], A. C. König[31], M. Kopal[46], V. Koutsenko[13,28], M. Kräber[49], R. W. Kraemer[35], A. Krüger[48], A. Kunin[13], P. Ladron de Guevara[25], I. Laktineh[24], G. Landi[17], M. Lebeau[18], A. Lebedev[13], P. Lebrun[24], P. Lecomte[49], P. Lecoq[18], P. Le Coultre[49], J. M. Le Goff[18], R. Leiste[48], M. Levtchenko[27], P. Levtchenko[34], C. Li[22], S. Likhoded[48], C. H. Lin[44], W. T. Lin[44], F. L. Linde[2], L. Lista[29], Z. A. Liu[7], W. Lohmann[48], E. Longo[39], Y. S. Lu[7], C. Luci[39], L. Luminari[39], W. Lustermann[49], W. G. Ma[22], L. Malgeri[18], A. Malinin[28], C. Maña[25], J. Mans[37], J. P. Martin[24], F. Marzano[39], K. Mazumdar[9], R. R. McNeil[6], S. Mele[18,29], L. Merola[29], M. Meschini[17], W. J. Metzger[31], A. Mihul[11], H. Milcent[18], G. Mirabelli[39], J. Mnich[1], G. B. Mohanty[9], G. S. Muanza[24], A. J. M. Muijs[2], B. Musicar[41], M. Musy[39], S. Nagy[15], S. Natale[20], M. Napolitano[29], F. Nessi-Tedaldi[49], H. Newman[32], A. Nisati[39], T. Novak[31], H. Nowak[48], R. Ofierzynski[49], G. Organtini[39], I. Pal[46], C. Palomares[25], P. Paolucci[29], R. Paramatti[39], G. Passaleva[17], S. Patricelli[29], T. Paul[10], M. Pauluzzi[33], C. Paus[13], F. Pauss[49], M. Pedace[39], S. Pensotti[27], D. Perret-Gallix[4], D. Piccolo[29], F. Pierella[8], M. Pieri[41], M. Pioppi[33], P. A. Piroué[37], E. Pistolesi[27], V. Plyaskin[28], M. Pohl[20], V. Pojidaev[17], J. Pothier[18], D. Prokofiev[34], G. Rahal-Callot[49], M. A. Rahaman[9], P. Raics[15], N. Raja[9], R. Ramelli[49], P. G. Rancoita[27], R. Ranieri[17], A. Raspereza[48], P. Razis[30], S. Rembeczki[26], D. Ren[49], M. Rescigno[39], S. Reucroft[10], S. Riemann[48], K. Riles[3], B. P. Roe[3], L. Romero[25], A. Rosca[48], C. Rosemann[1], C. Rosenbleck[1], S. Rosier-Lees[4], S. Roth[1], J. A. Rubio[18], G. Ruggiero[17], H. Rykaczewski[49], A. Sakharov[49], S. Saremi[6], S. Sarkar[39], J. Salicio[18], E. Sanchez[25], C. Schäfer[18], V. Schegelsky[34], H. Schopper[21], D. J. Schotanus[31], C. Sciacca[29], L. Servoli[33], S. Shevchenko[32], N. Shivarov[42], V. Shoutko[13], E. Shumilov[28], A. Shvorob[32], D. Son[43], C. Souga[24], P. Spillantini[17], M. Steuer[13], D. P. Stickland[37], B. Stoyanov[42], A. Straessner[20], K. Sudhakar[9], G. Sultanov[42], L. Z. Sun[22], S. Sushkov[1], H. Suter[49], J. D. Swain[10], Z. Szillasi[26,¶], X. W. Tang[7], P. Tarjan[15], L. Tauscher[5],

L. Taylor[10], B. Tellili[24], D. Teyssier[24], C. Timmermans[31], Samuel C. C. Ting[13], S. M. Ting[13], S. C. Tonwar[9], J. Tóth[12], C. Tully[37], K. L. Tung[7], J. Ulbricht[49], E. Valente[39], R. T. Van de Walle[31], R. Vasquez[46], G. Vesztergombi[12], I. Vetlitsky[28], G. Viertel[49], M. Vivargent[4], S. Vlachos[5], I. Vodopianov[26], H. Vogel[35], H. Vogt[48], I. Vorobiev[35,28], A. A. Vorobyov[34], M. Wadhwa[5], Q. Wang[31], X. L. Wang[22], Z. M. Wang[22], M. Weber[18], S. Wynhoff[37], L. Xia[32], Z. Z. Xu[22], J. Yamamoto[3], B. Z. Yang[22], C. G. Yang[7], H. J. Yang[3], M. Yang[7], S. C. Yeh[45], An. Zalite[34], Yu. Zalite[34], Z. P. Zhang[22], J. Zhao[22], G. Y. Zhu[7], R. Y. Zhu[32], H. L. Zhuang[7], A. Zichichi[8,18,19], B. Zimmermann[49], M. Zöller[1].

1 III. Physikalisches Institut, RWTH, D-52056 Aachen, Germany[§]
2 National Institute for High Energy Physics, NIKHEF, and University of Amsterdam, NL-1009 DB Amsterdam, The Netherlands
3 University of Michigan, Ann Arbor, MI 48109, USA
4 Laboratoire d'Annecy-le-Vieux de Physique des Particules, LAPP,IN2P3-CNRS, BP 110, F-74941 Annecy-le-Vieux CEDEX, France
5 Institute of Physics, University of Basel, CH-4056 Basel, Switzerland
6 Louisiana State University, Baton Rouge, LA 70803, USA
7 Institute of High Energy Physics, IHEP, 100039 Beijing, China[△]
8 University of Bologna and INFN-Sezione di Bologna, I-40126 Bologna, Italy
9 Tata Institute of Fundamental Research, Mumbai (Bombay) 400 005, India
10 Northeastern University, Boston, MA 02115, USA
11 Institute of Atomic Physics and University of Bucharest, R-76900 Bucharest, Romania
12 Central Research Institute for Physics of the Hungarian Academy of Sciences, H-1525 Budapest 114, Hungary[‡]
13 Massachusetts Institute of Technology, Cambridge, MA 02139, USA
14 Panjab University, Chandigarh 160 014, India
15 KLTE-ATOMKI, H-4010 Debrecen, Hungary[¶]
16 UCD School of Physics, University College Dublin, Belfield, Dublin 4, Ireland
17 INFN Sezione di Firenze and University of Florence, I-50125 Florence, Italy
18 European Laboratory for Particle Physics, CERN, CH-1211 Geneva 23, Switzerland
19 World Laboratory, FBLJA Project, CH-1211 Geneva 23, Switzerland
20 University of Geneva, CH-1211 Geneva 4, Switzerland
21 University of Hamburg, D-22761 Hamburg, Germany
22 Chinese University of Science and Technology, USTC, Hefei, Anhui 230 029, China[△]
23 University of Lausanne, CH-1015 Lausanne, Switzerland
24 Institut de Physique Nucléaire de Lyon, IN2P3-CNRS,Université Claude Bernard, F-69622 Villeurbanne, France
25 Centro de Investigaciones Energéticas, Medioambientales y Tecnológicas, CIEMAT, E-28040 Madrid, Spain♭
26 Florida Institute of Technology, Melbourne, FL 32901, USA
27 INFN-Sezione di Milano, I-20133 Milan, Italy
28 Institute of Theoretical and Experimental Physics, ITEP, Moscow, Russia
29 INFN-Sezione di Napoli and University of Naples, I-80125 Naples, Italy
30 Department of Physics, University of Cyprus, Nicosia, Cyprus
31 Radboud University and NIKHEF, NL-6525 ED Nijmegen, The Netherlands

32 California Institute of Technology, Pasadena, CA 91125, USA
33 INFN-Sezione di Perugia and Università Degli Studi di Perugia, I-06100 Perugia, Italy
34 Nuclear Physics Institute, St. Petersburg, Russia
35 Carnegie Mellon University, Pittsburgh, PA 15213, USA
36 INFN-Sezione di Napoli and University of Potenza, I-85100 Potenza, Italy
37 Princeton University, Princeton, NJ 08544, USA
38 University of Californa, Riverside, CA 92521, USA
39 INFN-Sezione di Roma and University of Rome, "La Sapienza", I-00185 Rome, Italy
40 University and INFN, Salerno, I-84100 Salerno, Italy
41 University of California, San Diego, CA 92093, USA
42 Bulgarian Academy of Sciences, Central Lab. of Mechatronics and Instrumentation, BU-1113 Sofia, Bulgaria
43 The Center for High Energy Physics, Kyungpook National University, 702-701 Taegu, Republic of Korea
44 National Central University, Chung-Li, Taiwan, China
45 Department of Physics, National Tsing Hua University, Taiwan, China
46 Purdue University, West Lafayette, IN 47907, USA
47 Paul Scherrer Institut, PSI, CH-5232 Villigen, Switzerland
48 DESY, D-15738 Zeuthen, Germany
49 Eidgenössische Technische Hochschule, ETH Zürich, CH-8093 Zürich, Switzerland

§ Supported by the German Bundesministerium für Bildung, Wissenschaft, Forschung und Technologie.
‡ Supported by the Hungarian OTKA fund under contract numbers T019181, F023259 and T037350.
¶ Also supported by the Hungarian OTKA fund under contract number T026178.
♭ Supported also by the Comisión Interministerial de Ciencia y Tecnología.
♯ Also supported by CONICET and Universidad Nacional de La Plata, CC 67, 1900 La Plata, Argentina.
△ Supported by the National Natural Science Foundation of China.

Appendix C4: The OPAL Collaboration

G. Abbiendi[2], C. Ainsley[5], P. F. Åkesson[3,y], G. Alexander[22], J. Allison[16], P. Amaral[9], G. Anagnostou[1], K. J. Anderson[9], S. Asai[23], D. Axen[27], G. Azuelos[18,a], I. Bailey[26], E. Barberio[8,p], T. Barillari[32], R. J. Barlow[16], R. J. Batley[5], P. Bechtle[25,b], T. Behnke[25], K. W. Bell[20], P. J. Bell[1], G. Bella[22], A. Bellerive[6], G. Benelli[4], S. Bethke[32], O. Biebel[31], O. Boeriu[10], P. Bock[11], M. Boutemeur[31], S. Braibant[8], L. Brigliadori[2], R. M. Brown[20], K. Buesser[25], H. J. Burckhart[8], S. Campana[4], R. K. Carnegie[6], A. A. Carter[13], J. R. Carter[5], C. Y. Chang[17], D. G. Charlton[1], C. Ciocca[2], A. Csilling[29], M. Cuffiani[2], S. Dado[21], S. de Jong[12,t], A. De Roeck[8], E.A. De Wolf[8,s], K. Desch[25], B. Dienes[30], M. Donkers[6], J. Dubbert[31], E. Duchovni[24], G. Duckeck[31], I. P. Duerdoth[16], E. Etzion[22], F. Fabbri[2], L. Feld[10], P. Ferrari[8], F. Fiedler[31], I. Fleck[10], M. Ford[5], A. Frey[8], P. Gagnon[12], J. W. Gary[4], S. M. Gascon-Shotkin[17], G. Gaycken[25], C. Geich-Gimbel[3], G. Giacomelli[2], P. Giacomelli[2], M. Giunta[4], J. Goldberg[21], E. Gross[24], J. Grunhaus[22], M. Gruwé[8], P. O. Günther[3], A. Gupta[9], C. Hajdu[29], M. Hamann[25], G. G. Hanson[4], A. Harel[21], M. Hauschild[8], C. M. Hawkes[1], R. Hawkings[8], R. J. Hemingway[6], G. Herten[10], R. D. Heuer[25], J. C. Hill[5], K. Hoffman[9], D. Horváth[29,c], P. Igo-Kemenes[11], K. Ishii[23], H. Jeremie[18], U. Jost[11], P. Jovanovic[1], T.R. Junk[6,i], N. Kanaya[26], J. Kanzaki[23,u], D. Karlen[26], K. Kawagoe[23], T. Kawamoto[23], R. K. Keeler[26], R. G. Kellogg[17], B. W. Kennedy[20], S. Kluth[32], T. Kobayashi[23], M. Kobel[3], S. Komamiya[23], T. Krämer[25], P. Krieger[6,l], J. von Krogh[11], K. Kruger[8], T. Kuhl[25], M. Kupper[24], G. D. Lafferty[16], H. Landsman[21], D. Lanske[14], J. G. Layter[4], D. Lellouch[24], J. Letts[o], L. Levinson[24], J. Lillich[10], S. L. Lloyd[13], F. K. Loebinger[16], J. Lu[27,w], A. Ludwig[3], J. Ludwig[10], W. Mader[3], S. Marcellini[2], A. J. Martin[13], G. Masetti[2], T. Mashimo[23], P. Mättig[m], J. McKenna[27], R. A. McPherson[26], F. Meijers[8], W. Menges[25], F. S. Merritt[9], H. Mes[6,a], N. Meyer[25], A. Michelini[2], S. Mihara[23], G. Mikenberg[24], D. J. Miller[15], S. Moed[21], W. Mohr[10], T. Mori[23], A. Mutter[10], K. Nagai[13], I. Nakamura[23,v], H. Nanjo[23], H. A. Neal[33], R. Nisius[32], S. W. O'Neale[1,†], A. Oh[8], M. J. Oreglia[9], S. Orito[23,†], C. Pahl[32], G. Pásztor[4,g], J. R. Pater[16], J. E. Pilcher[9], J. Pinfold[28], D. E. Plane[8], B. Poli[2], O. Pooth[14], M. Przybycień[8,n], A. Quadt[3], K. Rabbertz[8,r], C. Rembser[8], P. Renkel[24], J. M. Roney[26], Y. Rozen[21], K. Runge[10], K. Sachs[6], T. Saeki[23], E. K. G. Sarkisyan[8,j], A. D. Schaile[31], O. Schaile[31], P. Scharff-Hansen[8], J. Schieck[32], T. Schörner-Sadenius[8,z], M. Schröder[8], M. Schumacher[3], W. G. Scott[20], R. Seuster[14,f], T. G. Shears[8,h], B. C. Shen[4], P. Sherwood[15], A. Skuja[17], A. M. Smith[8], R. Sobie[26], S. Söldner-Rembold[15], F. Spano[9], A. Stahl[3,x], D. Strom[19], R. Ströhmer[31], S. Tarem[21], M. Tasevsky[8,s], R. Teuscher[9], M. A. Thomson[5], E. Torrence[19], D. Toya[23], P. Tran[4], I. Trigger[8], Z. Trócsányi[30,e], E. Tsur[22], M. F. Turner-Watson[1], I. Ueda[23], B. Ujvári[30,e], C. F. Vollmer[31], P. Vannerem[10], R. Vértesi[30,e], M. Verzocchi[17], H. Voss[8,q], J. Vossebeld[8,h], C. P. Ward[5], D. R. Ward[5], P. M. Watkins[1], A. T. Watson[1], N. K. Watson[1], P. S. Wells[8], T. Wengler[8], N. Wermes[3], G. W. Wilson[16,k], J. A. Wilson[1], G. Wolf[24], T. R. Wyatt[16], S. Yamashita[23], D. Zer-Zion[4], L. Zivkovic[24].

1 School of Physics and Astronomy, University of Birmingham, Birmingham B15 2TT, UK
2 Dipartimento di Fisica dell' Università di Bologna and INFN, I-40126 Bologna, Italy
3 Physikalisches Institut, Universität Bonn, D-53115 Bonn, Germany
4 Department of Physics, University of California, Riverside CA 92521, USA
5 Cavendish Laboratory, Cambridge CB3 0HE, UK
6 Ottawa-Carleton Institute for Physics, Department of Physics, Carleton University, Ottawa, Ontario K1S 5B6, Canada
8 CERN, European Organisation for Nuclear Research, CH-1211 Geneva 23, Switzerland

9 Enrico Fermi Institute and Department of Physics, University of Chicago, Chicago IL 60637, USA
10 Fakultät für Physik, Albert-Ludwigs-Universität Freiburg, D-79104 Freiburg, Germany
11 Physikalisches Institut, Universität Heidelberg, D-69120 Heidelberg, Germany
12 Indiana University, Department of Physics, Bloomington IN 47405, USA
13 Queen Mary and Westfield College, University of London, London E1 4NS, UK
14 Technische Hochschule Aachen, III Physikalisches Institut, Sommerfeldstrasse 26-28, D-52056 Aachen, Germany
15 University College London, London WC1E 6BT, UK
16 Department of Physics, Schuster Laboratory, The University, Manchester M13 9PL, UK
17 Department of Physics, University of Maryland, College Park, MD 20742, USA
18 Laboratoire de Physique Nucléaire, Université de Montréal, Montréal, Québec H3C 3J7, Canada
19 University of Oregon, Department of Physics, Eugene OR 97403, USA
20 CCLRC Rutherford Appleton Laboratory, Chilton, Didcot, Oxfordshire OX11 0QX, UK
21 Department of Physics, Technion-Israel Institute of Technology, Haifa 32000, Israel
22 Department of Physics and Astronomy, Tel Aviv University, Tel Aviv 69978, Israel
23 International Centre for Elementary Particle Physics and Department of Physics, University of Tokyo, Tokyo 113-0033, and Kobe University, Kobe 657-8501, Japan
24 Particle Physics Department, Weizmann Institute of Science, Rehovot 76100, Israel
25 Universität Hamburg/DESY, Institut für Experimentalphysik, Notkestrasse 85, D-22607 Hamburg, Germany
26 University of Victoria, Department of Physics, P O Box 3055, Victoria BC V8W 3P6, Canada
27 University of British Columbia, Department of Physics, Vancouver BC V6T 1Z1, Canada
28 University of Alberta, Department of Physics, Edmonton AB T6G 2J1, Canada
29 Research Institute for Particle and Nuclear Physics, H-1525 Budapest, P O Box 49, Hungary
30 Institute of Nuclear Research, H-4001 Debrecen, P O Box 51, Hungary
31 Ludwig-Maximilians-Universität München, Sektion Physik, Am Coulombwall 1, D-85748 Garching, Germany
32 Max-Planck-Institute für Physik, Föhringer Ring 6, D-80805 München, Germany
33 Yale University, Department of Physics, New Haven, CT 06520, USA

a and at TRIUMF, Vancouver, Canada V6T 2A3
b now at SLAC
c and Institute of Nuclear Research, Debrecen, Hungary
e and Department of Experimental Physics, University of Debrecen, Hungary
f and MPI München
g and Research Institute for Particle and Nuclear Physics, Budapest, Hungary
h now at University of Liverpool, Dept of Physics, Liverpool L69 3BX, U.K.
i now at Dept. Physics, University of Illinois at Urbana-Champaign, U.S.A.
j and Manchester University
k now at University of Kansas, Dept of Physics and Astronomy, Lawrence, KS 66045, U.S.A.
l now at University of Toronto, Dept of Physics, Toronto, Canada
m current address Bergische Universität, Wuppertal, Germany
n now at University of Mining and Metallurgy, Cracow, Poland
o now at University of California, San Diego, U.S.A.

p now at The University of Melbourne, Victoria, Australia
q now at IPHE Université de Lausanne, CH-1015 Lausanne, Switzerland
r now at IEKP Universität Karlsruhe, Germany
s now at University of Antwerpen, Physics Department, B-2610 Antwerpen, Belgium; supported by Interuniversity Attraction Poles Programme – Belgian Science Policy
t now at University of Nijmegen, Nijmegen, The Netherlands
u and High Energy Accelerator Research Organisation (KEK), Tsukuba, Ibaraki, Japan
v now at University of Pennsylvania, Philadelphia, Pennsylvania, USA
w now at TRIUMF, Vancouver, Canada
x now at DESY Zeuthen
y now at CERN
z now at DESY
† Deceased

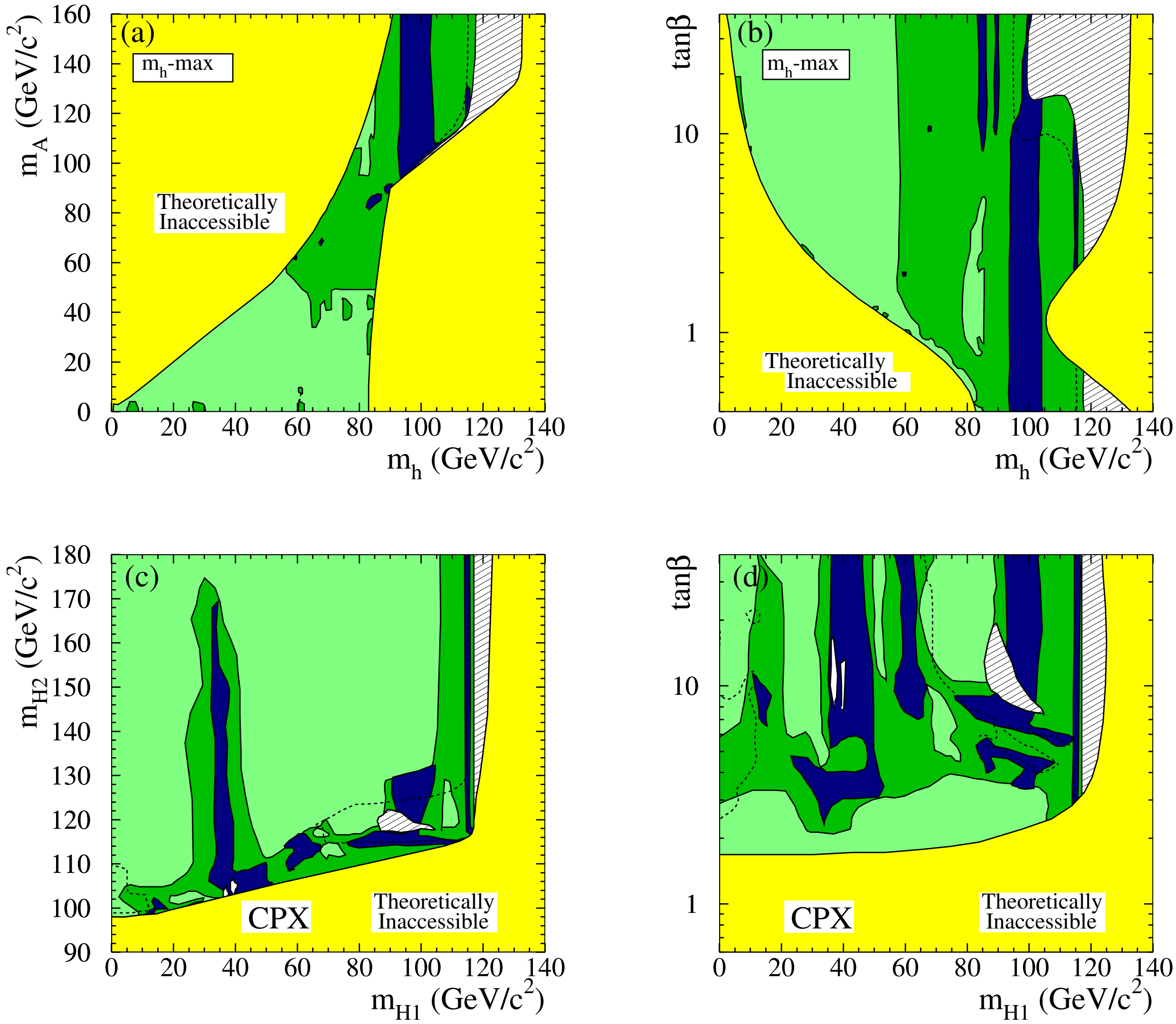

Figure 1: *Contours of the observed p-values, $1 - CL_b$, indicating the statistical significances of local excesses in the data. Plots (a) and (b) refer to the CP-conserving MSSM benchmark scenario m_{h}-max and plots (c) and (d) to the CP-violating scenario CPX. For each scenario, the parameter space is shown in two projections. Regions which are not part of the parameter space (labelled "Theoretically Inaccessible") are shown in light-grey or yellow. In the medium-grey or light-green regions the data show an excess of less than one standard deviation above the expected background. Similarly, in the dark-grey or dark-green regions the excess is between one and two standard deviations while in the darkest-grey or blue regions it is between two and three standard deviations. In plots (c) and (d), two small regions with excesses larger than three standard deviations are shown in white. The dashed lines show the expected exclusion limit at 95% CL. The hatched areas represent regions where the median expected value of CL_s in the background hypothesis is larger than 0.4; apparent excesses in these regions would not be significant.*

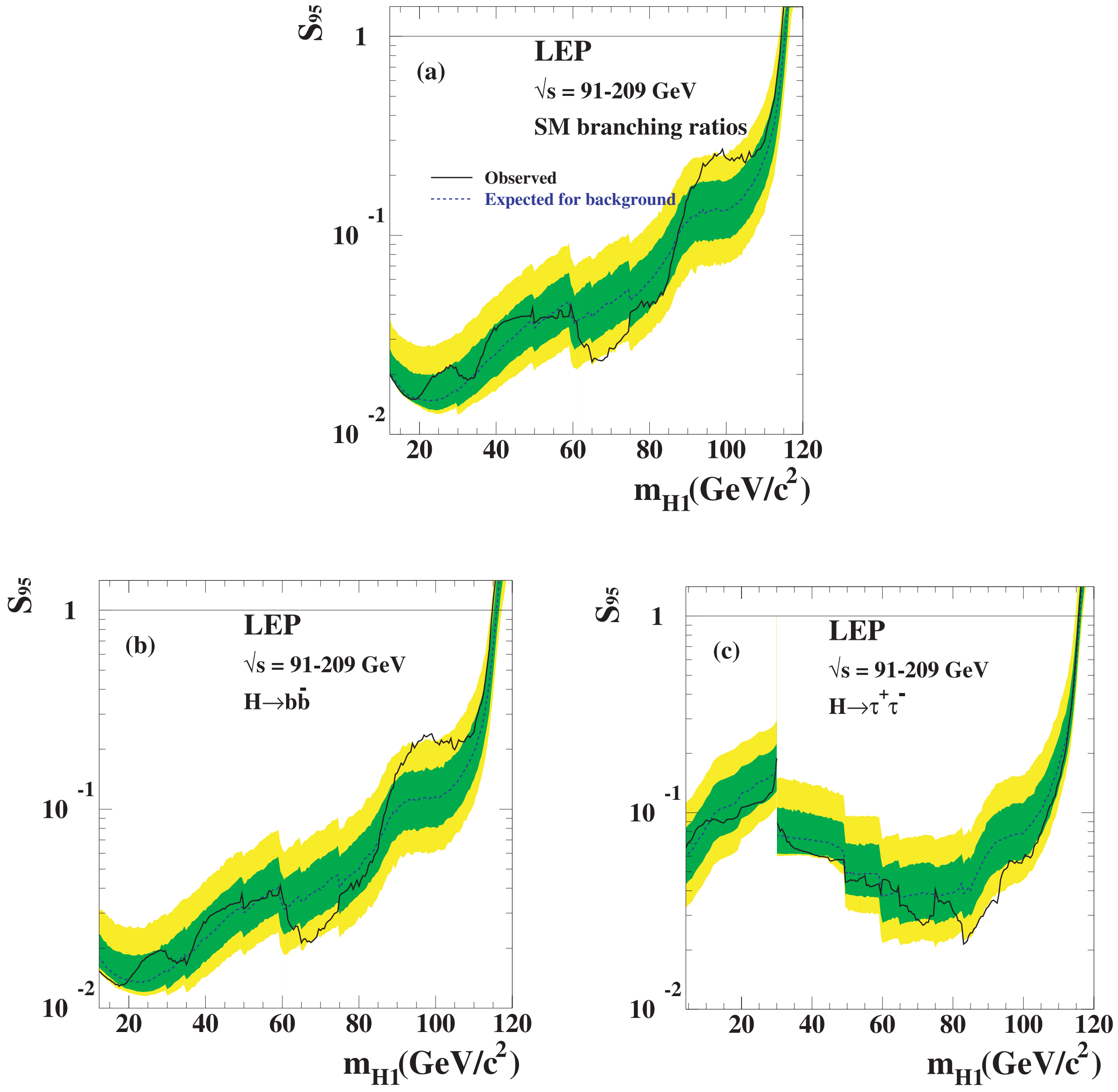

Figure 2: *The 95% CL upper bounds, S_{95} (see text), for various topological cross-sections motivated by the Higgsstrahlung process* $e^+e^- \to \mathcal{H}_1Z$*, as a function of the Higgs boson mass (the figure is reproduced from Ref. [3]). The full lines represent the observed limits. The dark (green) and light (yellow) shaded bands around the median expectations (dashed lines) correspond to the 68% and 95% probability bands. The horizontal lines correspond to the Standard Model cross-sections. In part (a) the Higgs boson decay branching ratios are assumed to be those predicted by the Standard Model; in part (b) the Higgs boson is assumed to decay exclusively to* $b\bar{b}$ *and in part (c) exclusively to* $\tau^+\tau^-$*. In part (c), the discontinuity at about 30* GeV/c^2 *arises because at lower masses only one of the LEP experiments is contributing to the cross-section limit.*

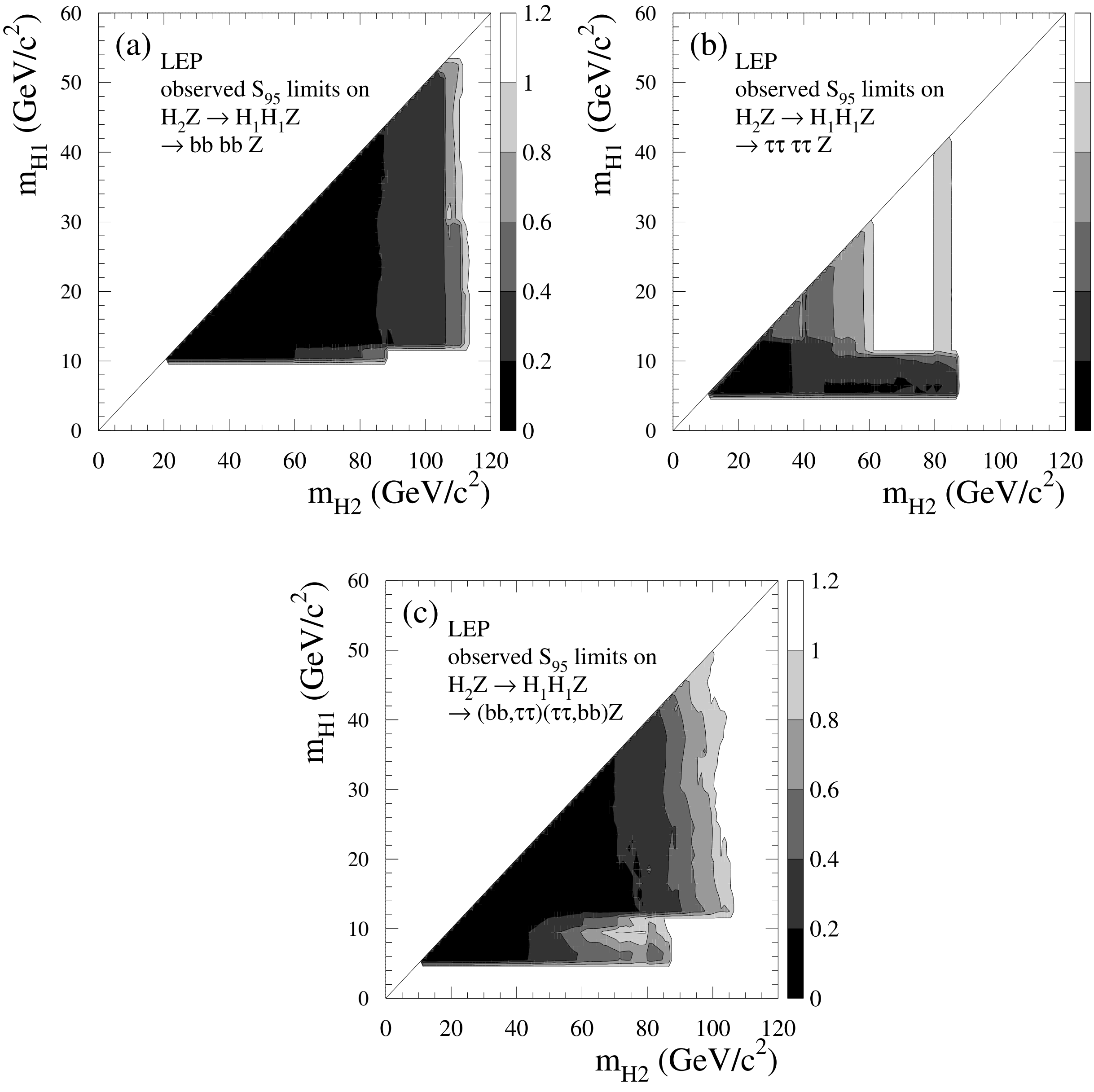

Figure 3: *Contours of the 95% CL upper bound, S_{95} (see text), for various topological cross-sections motivated by the Higgsstrahlung cascade process* $e^+e^- \to$ *($\mathcal{H}_2 \to \mathcal{H}_1\mathcal{H}_1$)Z, projected onto the ($m_{\mathcal{H}_2}$, $m_{\mathcal{H}_1}$) plane. The scales for the shadings are given on the right-hand side of each plot. In plot (a) the $\mathcal{H}_1$ boson is assumed to decay exclusively to* $b\bar{b}$ *and in plot (b) exclusively to $\tau^+\tau^-$; in plot (c) it is assumed to decay with equal probabilities to* $b\bar{b}$ *and to $\tau^+\tau^-$.*

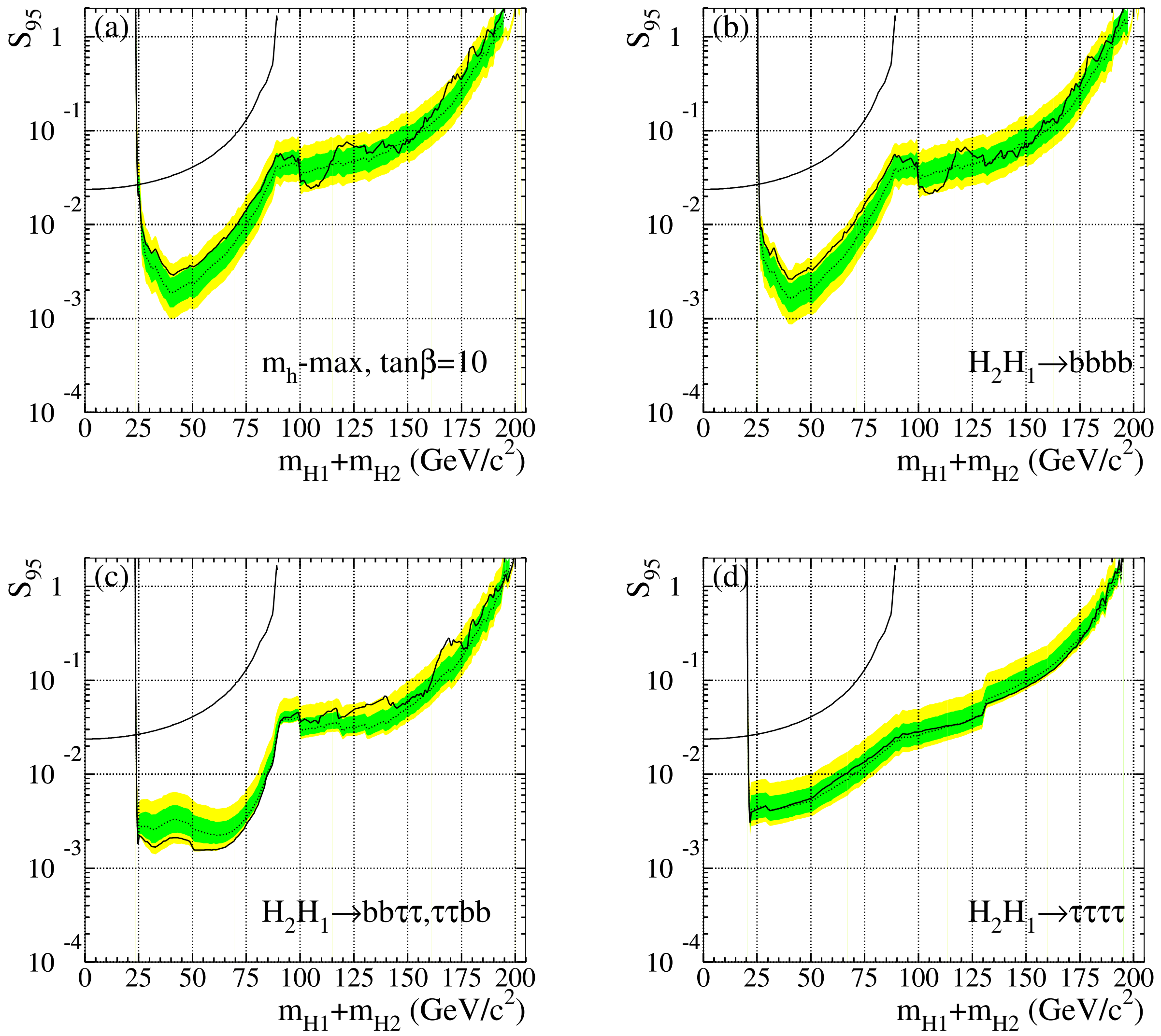

Figure 4: *The 95% CL upper bounds, S_{95} (see text), for various topological cross-sections motivated by the pair production process* $e^+e^- \rightarrow \mathcal{H}_2\mathcal{H}_1$. *The bounds are obtained for the particular case where $m_{\mathcal{H}_2}$ and $m_{\mathcal{H}_1}$ are approximately equal. Such is the case, for example, in the CP-conserving MSSM scenario m_h-max for* $\tan\beta$ *greater than 10 and small $m_{\mathcal{H}_2}$ ($\equiv m_A$). The abscissa is the sum of the two Higgs boson masses. The full lines represent the observed limits. The dark (green) and light (yellow) shaded bands around the median expectations (dashed lines) correspond to the 68% and 95% probability bands. The curves which complete the exclusions at low masses are obtained using the constraint from the measured decay width of the Z boson, see Section 3.2. Plot (a): the Higgs boson decay branching ratios correspond to the m_h-max benchmark scenario with* $\tan\beta$*=10, namely 94% $\mathcal{H}_1 \rightarrow$* $b\bar{b}$, *6% $\mathcal{H}_1 \rightarrow \tau^+\tau^-$, 92% $\mathcal{H}_2 \rightarrow$* $b\bar{b}$ *and 8% $\mathcal{H}_2 \rightarrow \tau^+\tau^-$; plot (b): both Higgs bosons are assumed to decay exclusively to* $b\bar{b}$*; plot (c): one of the Higgs bosons is assumed to decay exclusively to* $b\bar{b}$ *and the other exclusively to $\tau^+\tau^-$; plot (d): both Higgs bosons are assumed to decay exclusively to $\tau^+\tau^-$.*

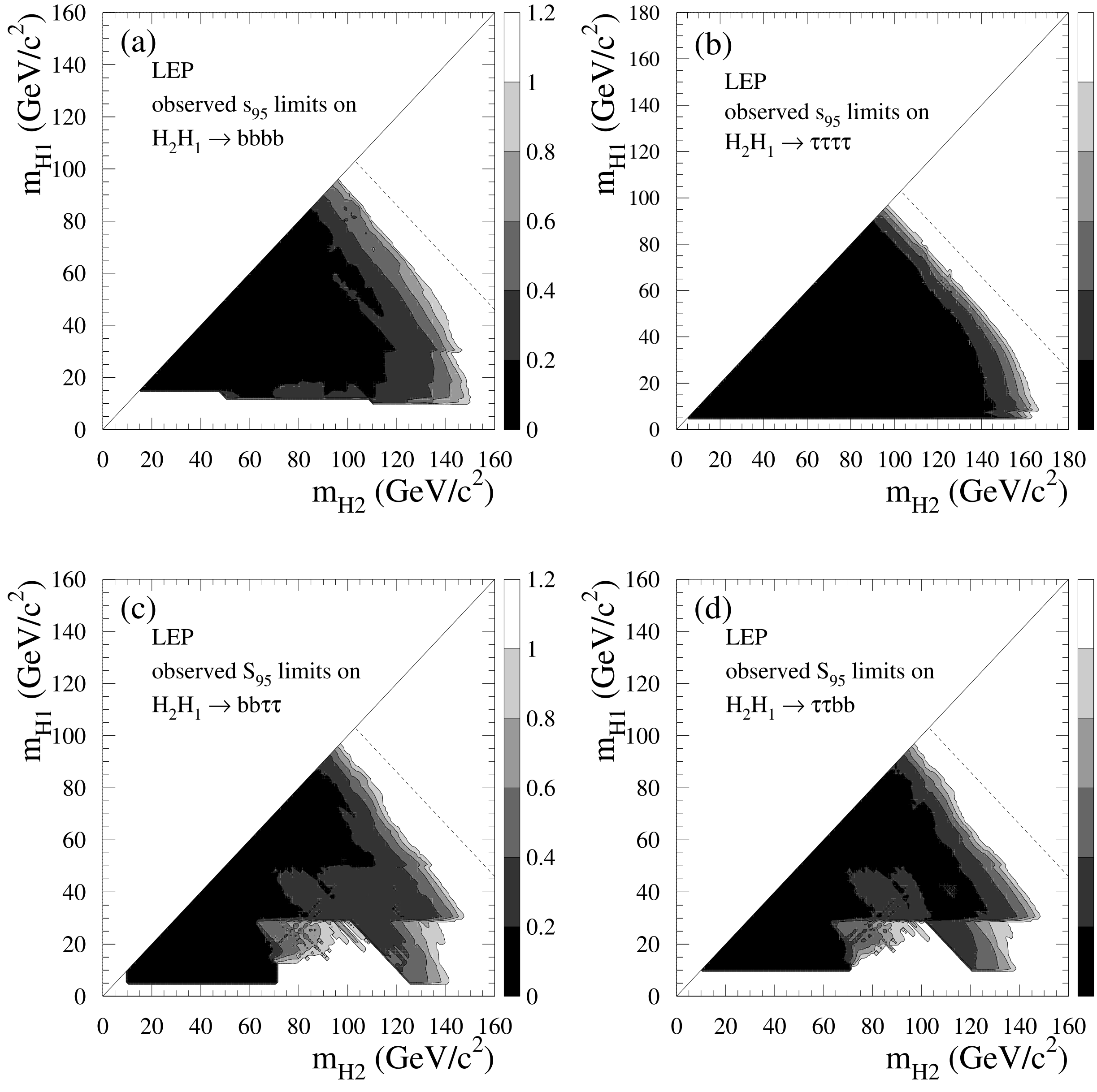

Figure 5: *Contours of the 95% CL upper bound, S_{95} (see text), for various topological cross-sections motivated by the pair production process* $\mathrm{e^+e^-} \rightarrow \mathcal{H}_2\mathcal{H}_1$, *projected onto the* ($m_{\mathcal{H}_2}$, $m_{\mathcal{H}_1}$) *plane. The scales in terms of the shadings are given on the right-hand side of each plot. In plot (a) both Higgs bosons are assumed to decay exclusively to* $\mathrm{b\bar{b}}$ *and in plot (b) exclusively to* $\tau^+\tau^-$. *In plot (c) the* $\mathcal{H}_2$ *boson is assumed to decay exclusively to* $\mathrm{b\bar{b}}$ *and the* $\mathcal{H}_1$ *boson exclusively to* $\tau^+\tau^-$ *and in plot (d) the* $\mathcal{H}_1$ *boson is assumed to decay exclusively to* $\mathrm{b\bar{b}}$ *and the* $\mathcal{H}_2$ *boson exclusively to* $\tau^+\tau^-$. *The dashed lines represent the approximate kinematic limits of the processes.*

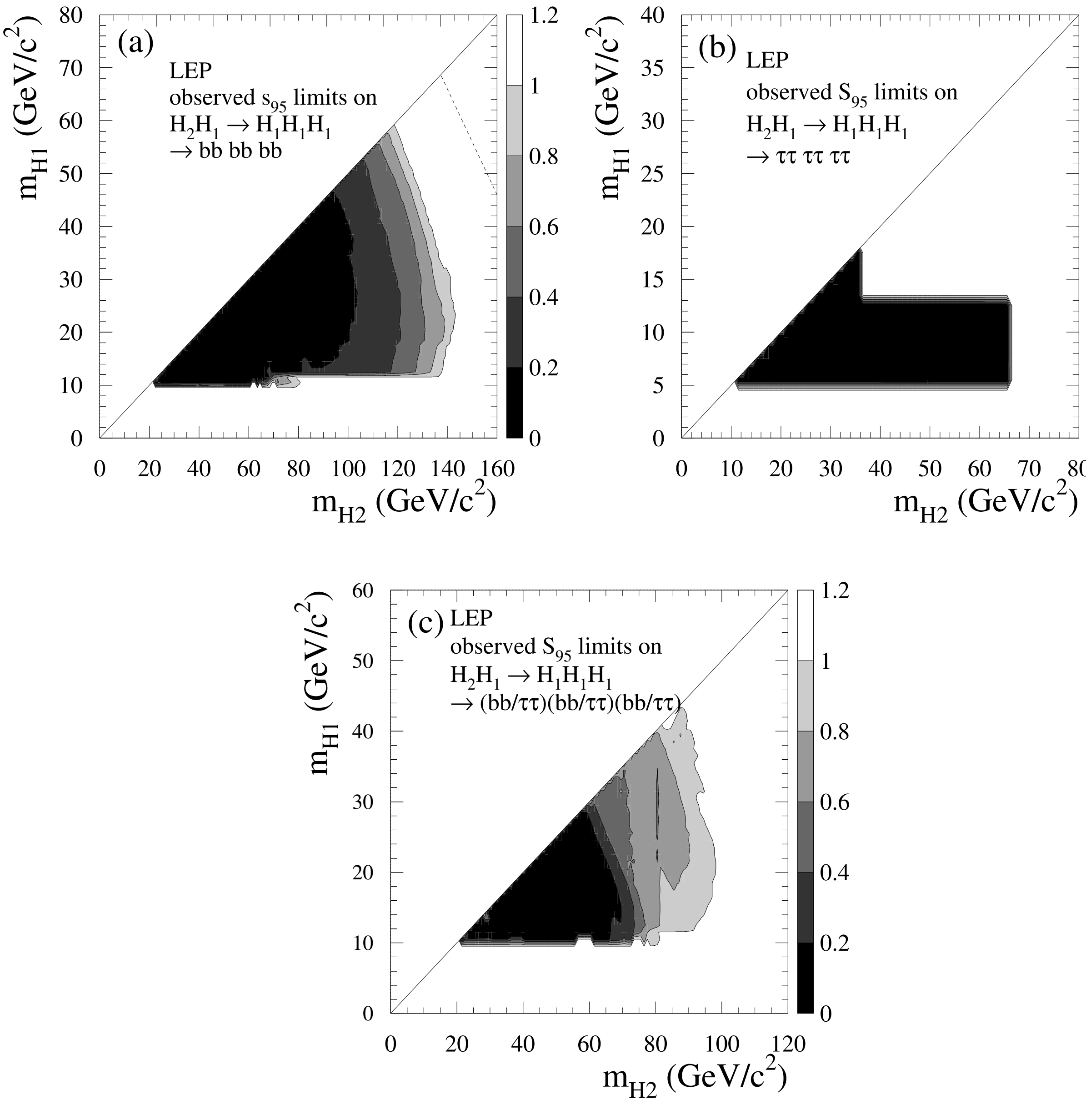

Figure 6: *Contours of the 95% CL upper bound, S_{95} (see text), for various topological cross-sections motivated by the pair production cascade process* $e^+e^- \rightarrow (\mathcal{H}_2 \rightarrow \mathcal{H}_1\mathcal{H}_1)\mathcal{H}_1$*, projected onto the* $(m_{\mathcal{H}_2}, m_{\mathcal{H}_1})$ *plane. The scales in terms of the shadings are given on the right-hand side of each plot. In plot (a) the* $\mathcal{H}_1$ *boson is assumed to decay exclusively to* $b\bar{b}$ *and in plot (b) exclusively to* $\tau^+\tau^-$*. In plot (c) the* $\mathcal{H}_1$ *boson is assumed to decay with equal probability to* $b\bar{b}$ *and to* $\tau^+\tau^-$*. The dashed line in part (a) represents the approximate kinematic limit of the process.*

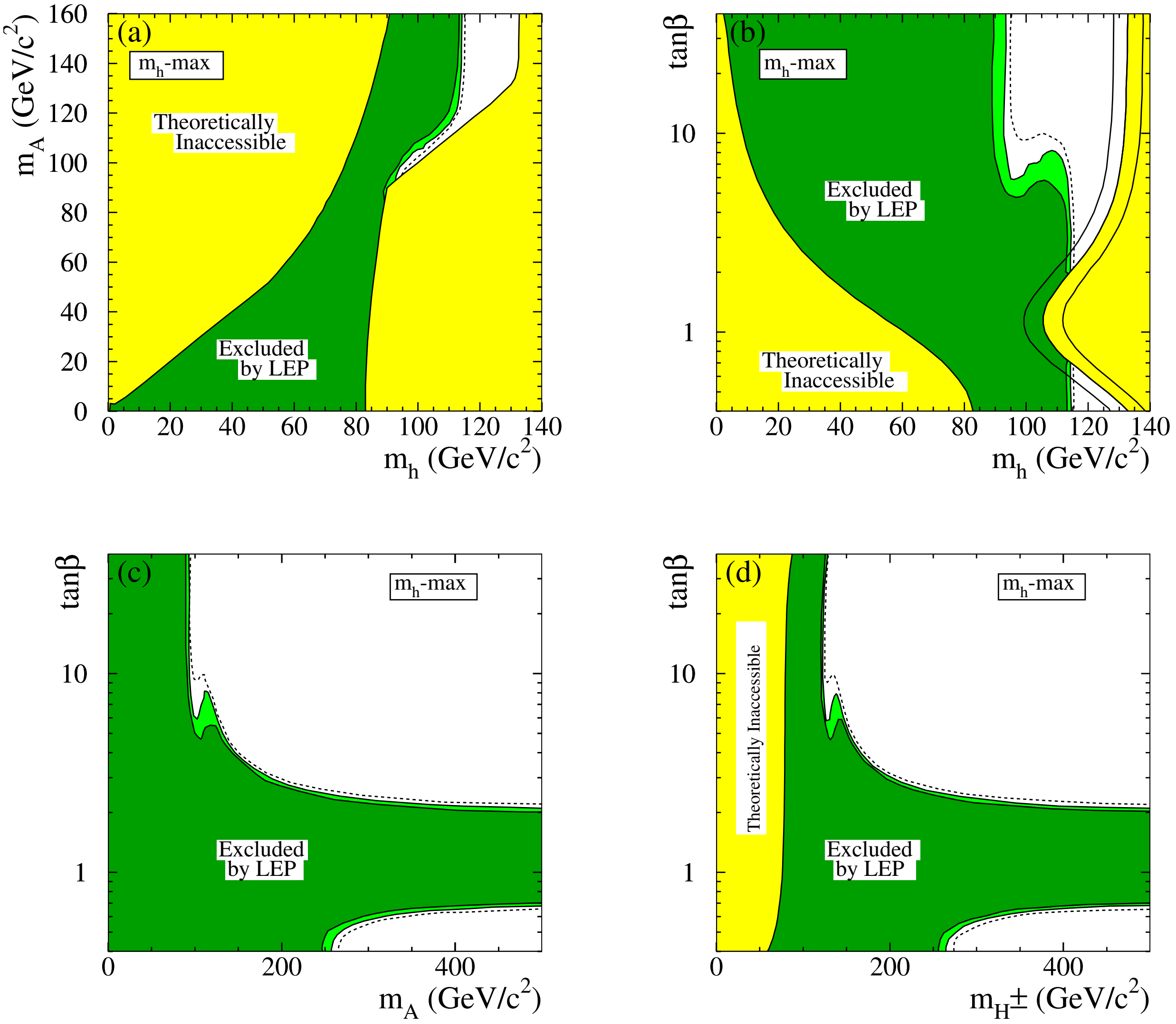

Figure 7: *Exclusions, at 95% CL (medium-grey or light-green) and the 99.7% CL (dark-grey or dark-green), in the case of the CP-conserving m_{h}-max benchmark scenario, for* $m_{\mathrm{t}} = 174.3$ GeV/c^2. *The figure shows the theoretically inaccessible domains (light-grey or yellow) and the regions excluded by this search, in four projections of the MSSM parameters: (a): (m_{h}, m_{A}); (b): (m_{h}, $\tan\beta$); (c): (m_{A}, $\tan\beta$); (d): ($m_{\mathrm{H}^\pm}$, $\tan\beta$). The dashed lines indicate the boundaries of the regions which are expected to be excluded, at 95% CL, on the basis of Monte Carlo simulations with no signal. In the (m_{h}, $\tan\beta$) projection (plot (b)), the upper boundary of the parameter space is indicated for three values of the top quark mass; from left to right: m_{t} = 169.3, 174.3 and 179.3* GeV/c^2.

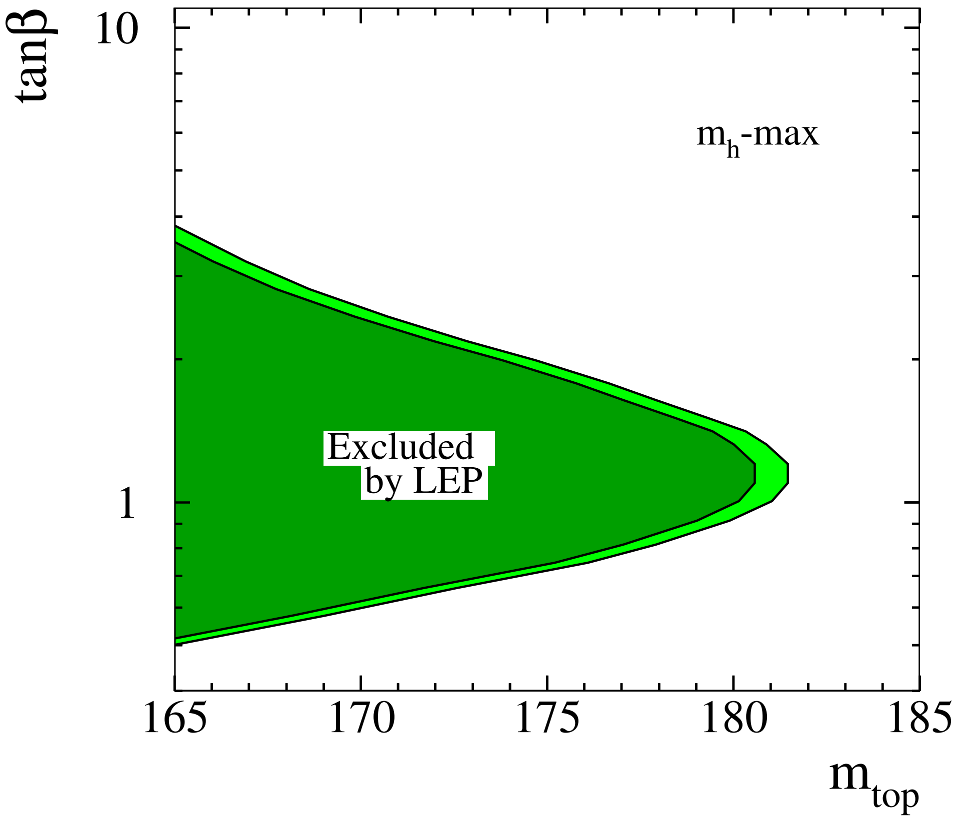

Figure 8: *Domains of* $\tan\beta$ *which are excluded at the 95% CL (light-grey or light-green) and the 99.7% CL (dark-grey or dark-green), in the case of the CP-conserving* $m_{\rm h}$*-max benchmark scenario, as a function of the assumed top quark mass.*

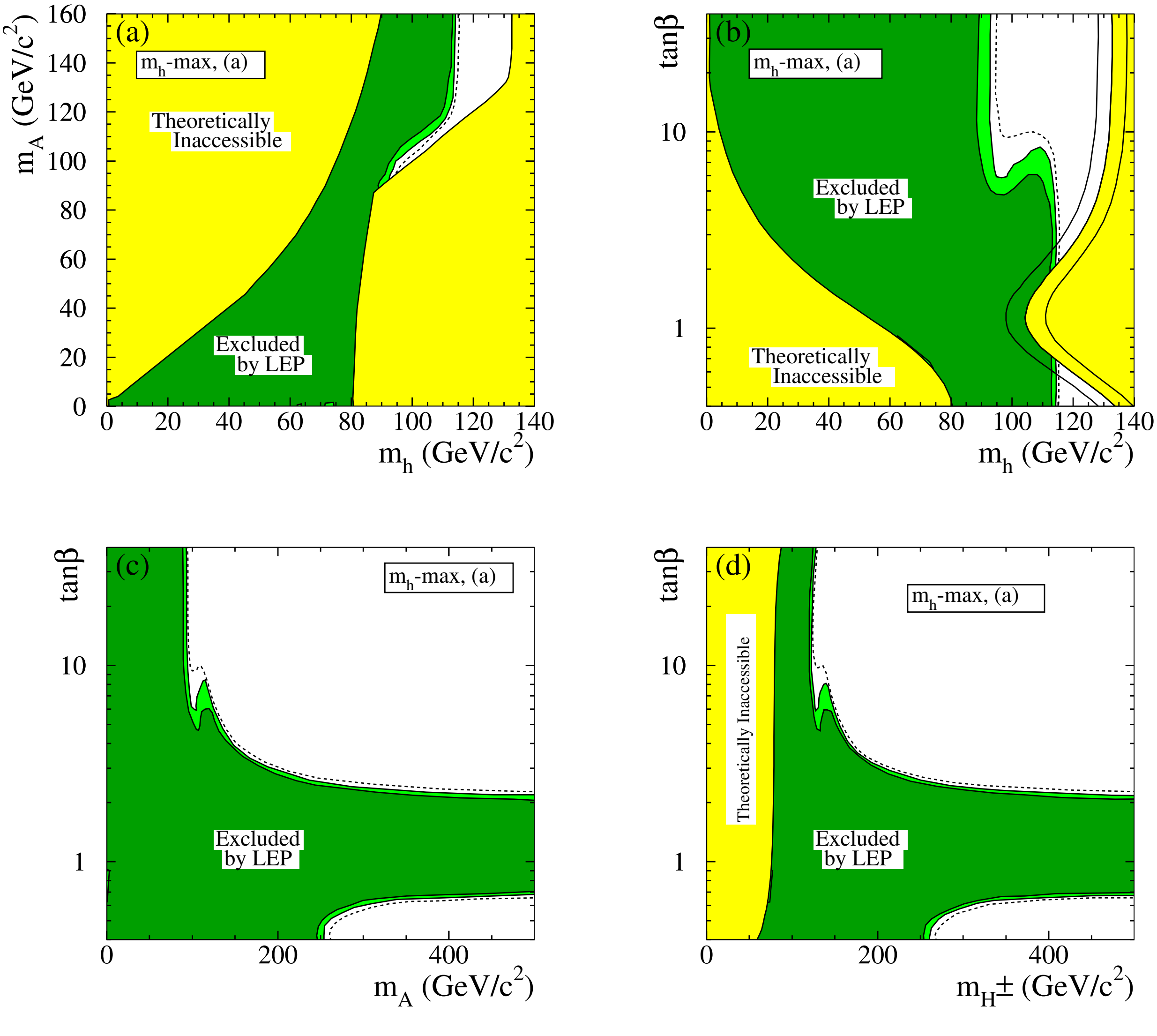

Figure 9: *Exclusions in the case of the CP-conserving m_{h}-max benchmark scenario, variant (a) (see Section 2.1.1.). See the caption of Figure 7 for the legend. Note the small domains at m_{h} between 60 and 75* GeV$/c^2$, *small m_{A} and $\tan\beta < 0.9$ which, although excluded at the 95% CL, are not excluded at the 99.7% CL.*

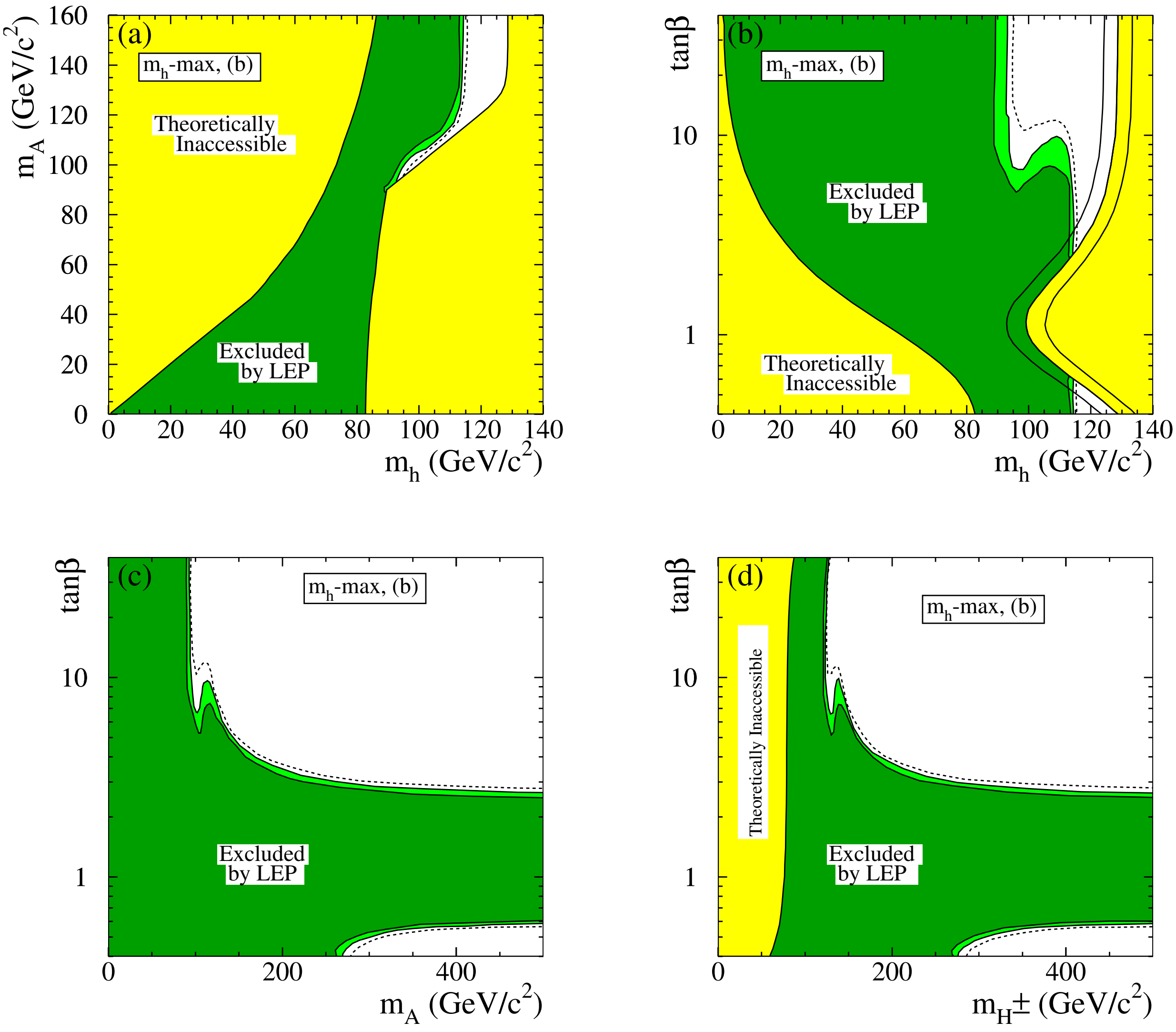

Figure 10: *Exclusions in the case of the CP-conserving m_h-max benchmark scenario, variant (b) (see Section 2.1.1.). See the caption of Figure 7 for the legend.*

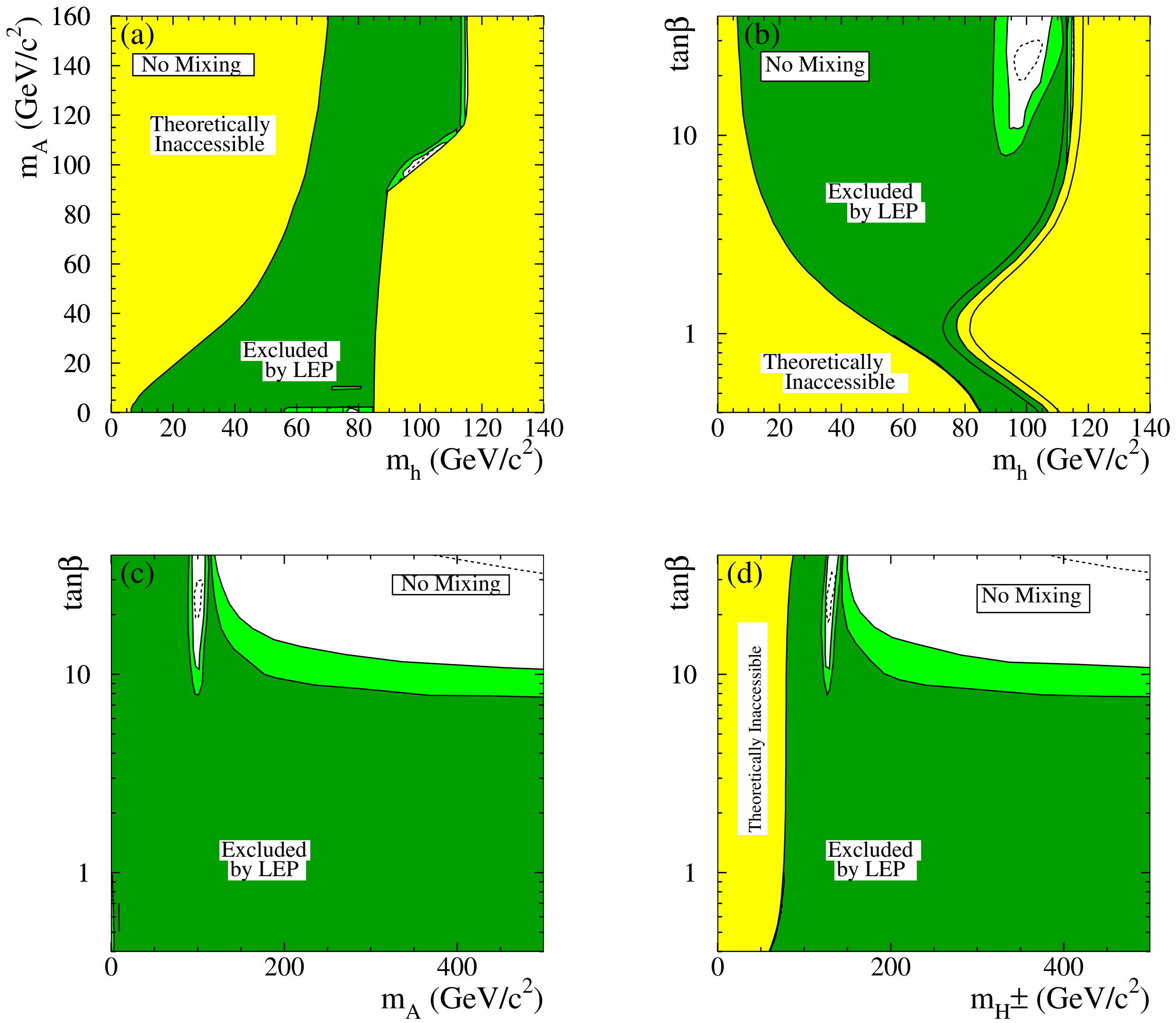

Figure 11: *Exclusions in the case of the CP-conserving* no-mixing *benchmark scenario. See the caption of Figure 7 for the legend. Note the small domain at m_h between 75 and 80* GeV/c^2*, small m_A and $\tan\beta < 0.7$ which is not excluded at the 95% CL.*

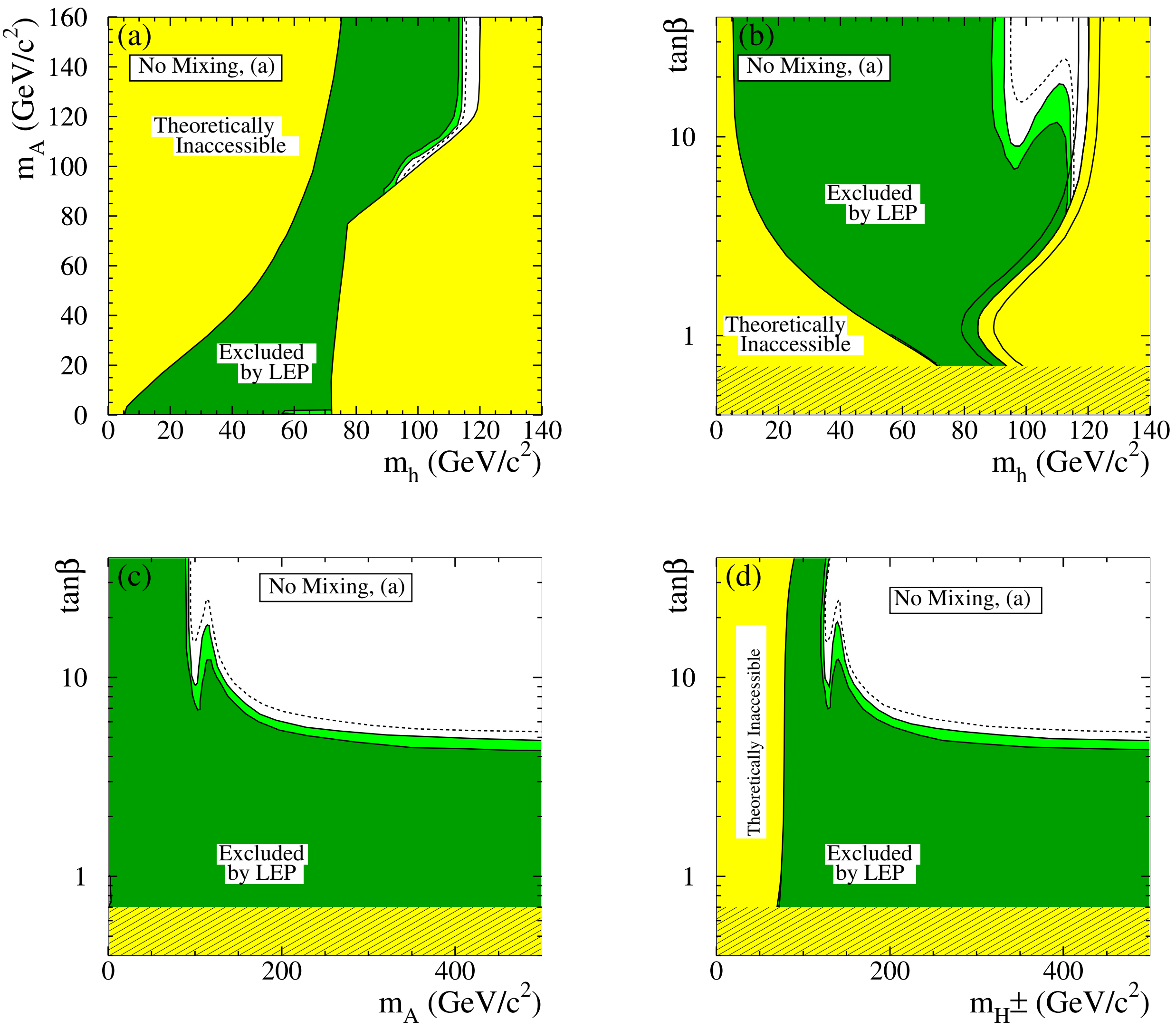

Figure 12: *Exclusions in the case of the CP-conserving* no-mixing *benchmark scenario, variant (a) (see Section 2.1.2). See the caption of Figure 7 for the legend. In the hatched domain* ($\tan\beta$ < *0.7), the contributions from top and stop quark loops to the radiative corrections are large and uncertain. Note the small domain at* $m_{\rm h}$ *between 56 and 72* GeV/c^2*, small* $m_{\rm A}$ *and* $\tan\beta < 1$ *which, although excluded at the 95% CL, is not excluded at the 99.7% CL.*

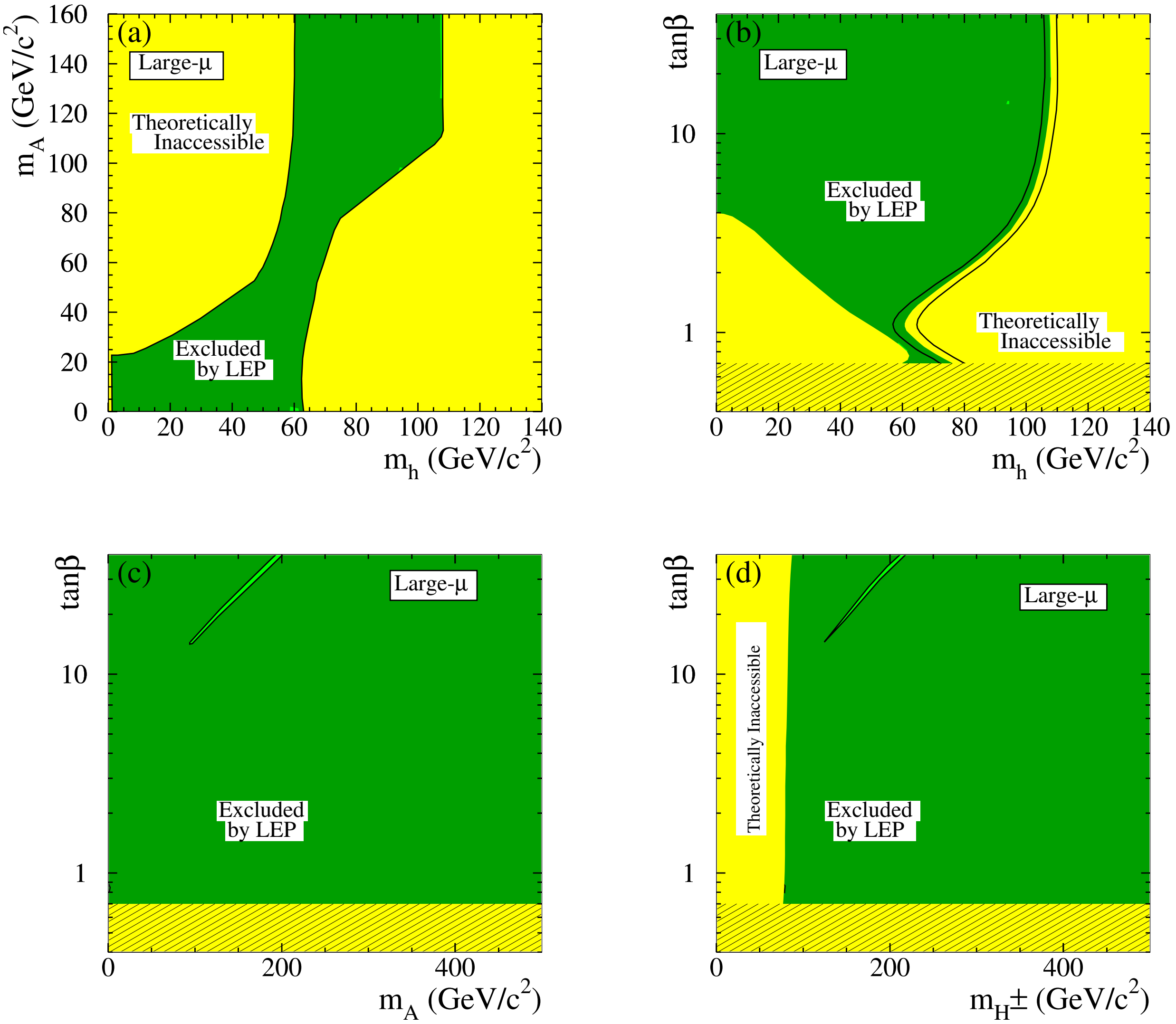

Figure 13: *Exclusions in the case of the CP-conserving large-μ benchmark scenario (see Section 2.1.3). See the caption of Figure 7 for the legend. In the hatched domain ($\tan\beta$ < 0.7), the contributions from top and stop quark loops to the radiative corrections become large and uncertain; hence, no exclusions can be claimed there.*

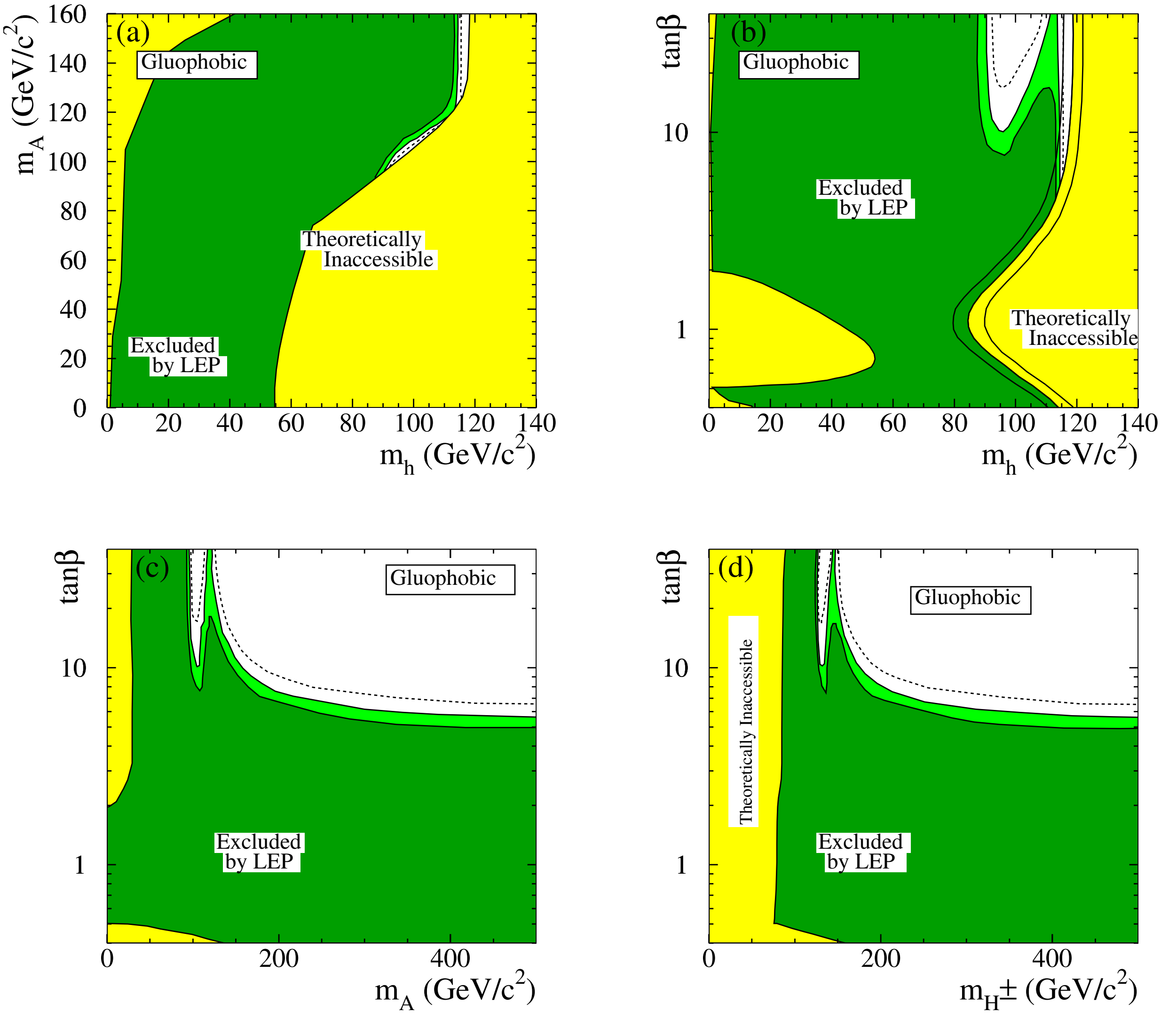

Figure 14: *Exclusions in the case of the gluophobic benchmark scenario (see Section 2.1.3). See the caption of Figure 7 for the legend.*

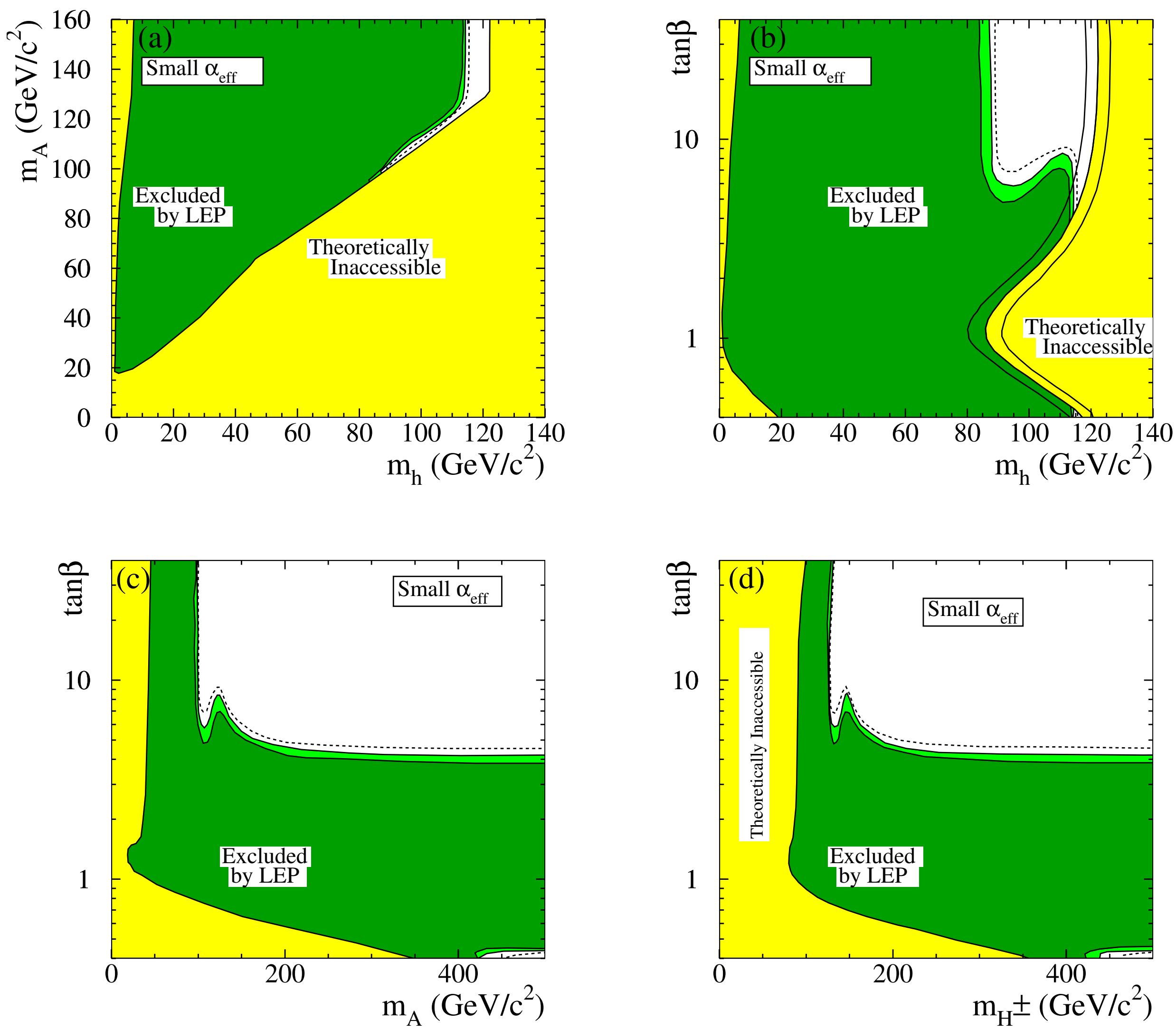

Figure 15: *Exclusions in the case of the CP-conserving small-α_{eff} benchmark scenario (see Section 2.1.3). See the caption of Figure 7 for the legend.*

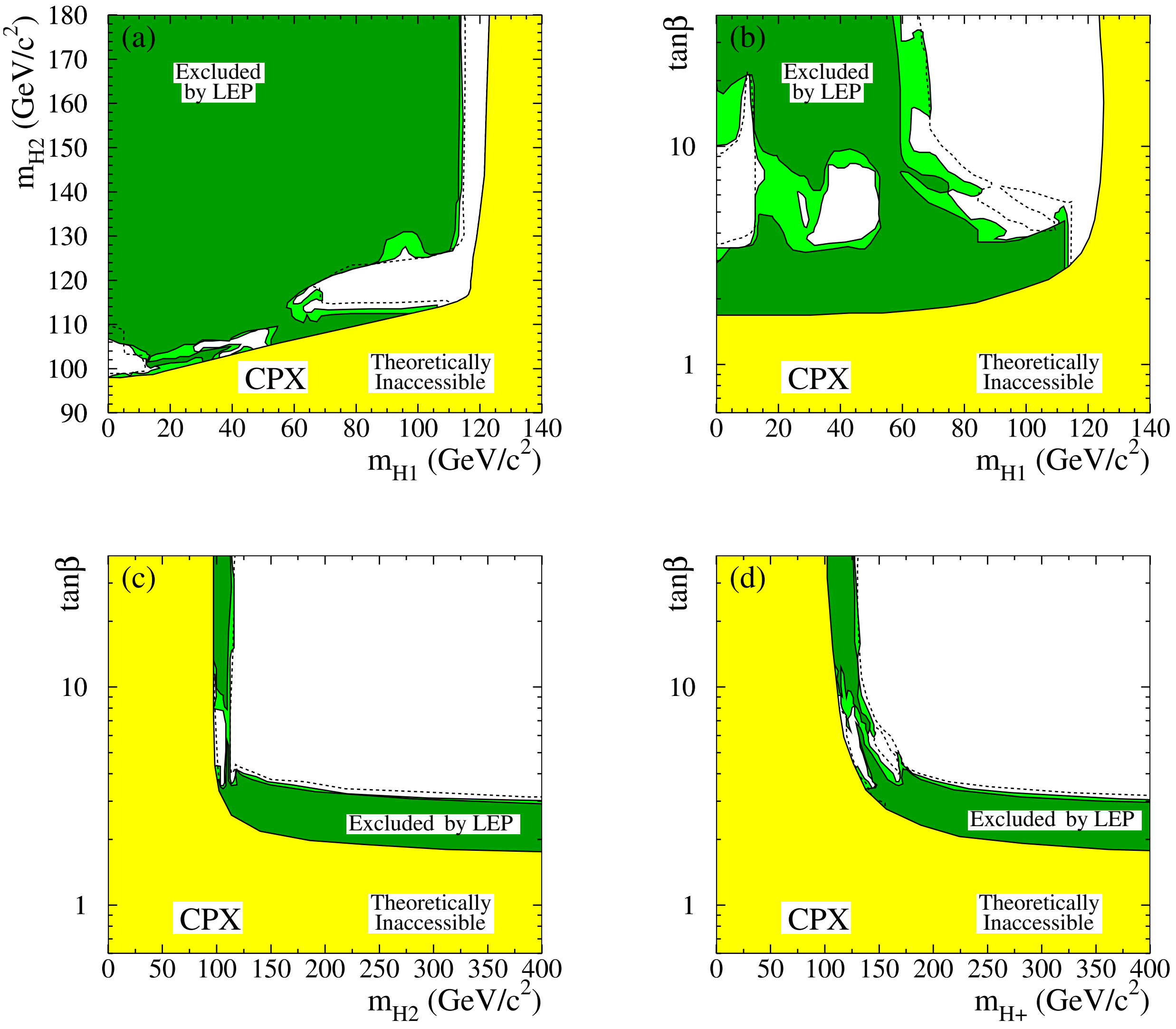

Figure 16: *Exclusions, at 95% CL (medium-grey or light-green) and the 99.7% CL (dark-grey or dark-green), for the CP-violating CPX scenario with* $m_{\rm t} = 174.3$ GeV/c^2. *The figure shows the theoretically inaccessible domains (light-grey or yellow) and the regions excluded by the present search, in four projections of the MSSM parameter space:* $(m_{\mathcal{H}_1}, m_{\mathcal{H}_2})$, $(m_{\mathcal{H}_1}, \tan\beta)$, $(m_{\mathcal{H}_2}, \tan\beta)$ *and* $(m_{\rm H+}, \tan\beta)$. *The dashed lines indicate the boundaries of the regions expected to be excluded, at the 95% CL, on the basis of Monte Carlo simulations with no signal. In each scan point, the more conservative of the two theoretical calculations,* `FeynHiggs` *or* `CPH`, *is used.*

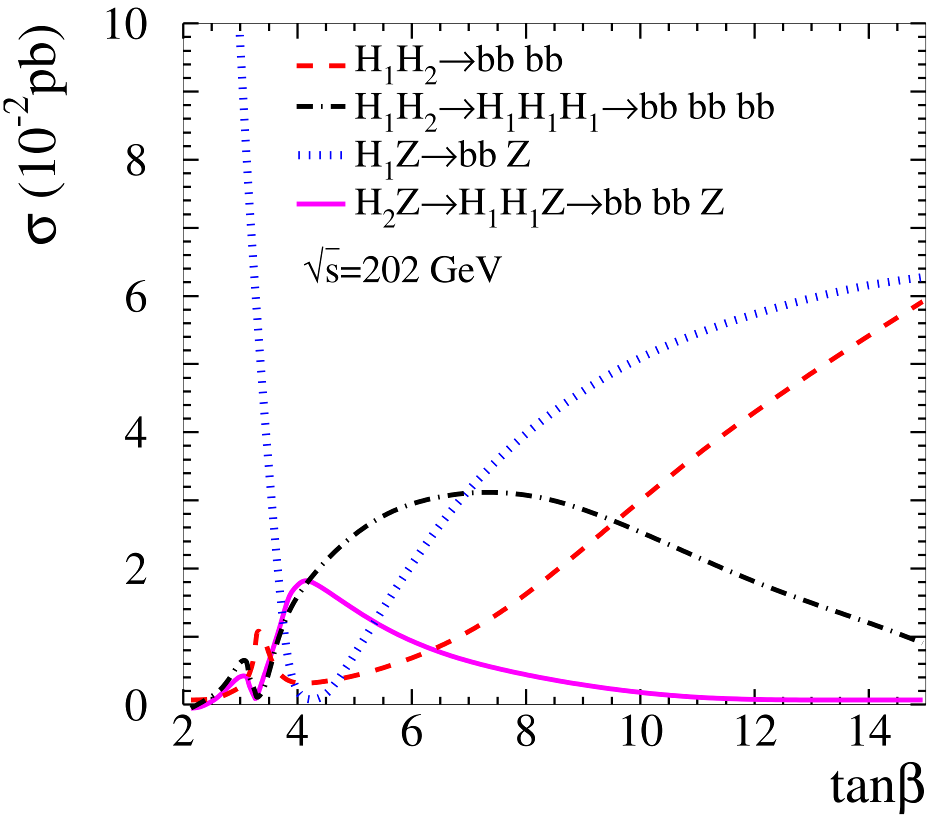

Figure 17: *Cross-sections, as a function of* $\tan\beta$*, for some of the dominant signal processes, in the CP-violating scenario CPX, using the* `FeynHiggs` *calculation, with a centre-of-mass energy of 202* GeV, $m_{\mathrm{t}} = 175$ GeV/c^2*, and* $m_{\mathcal{H}_1}$ *between 35 and 45* GeV/c^2.

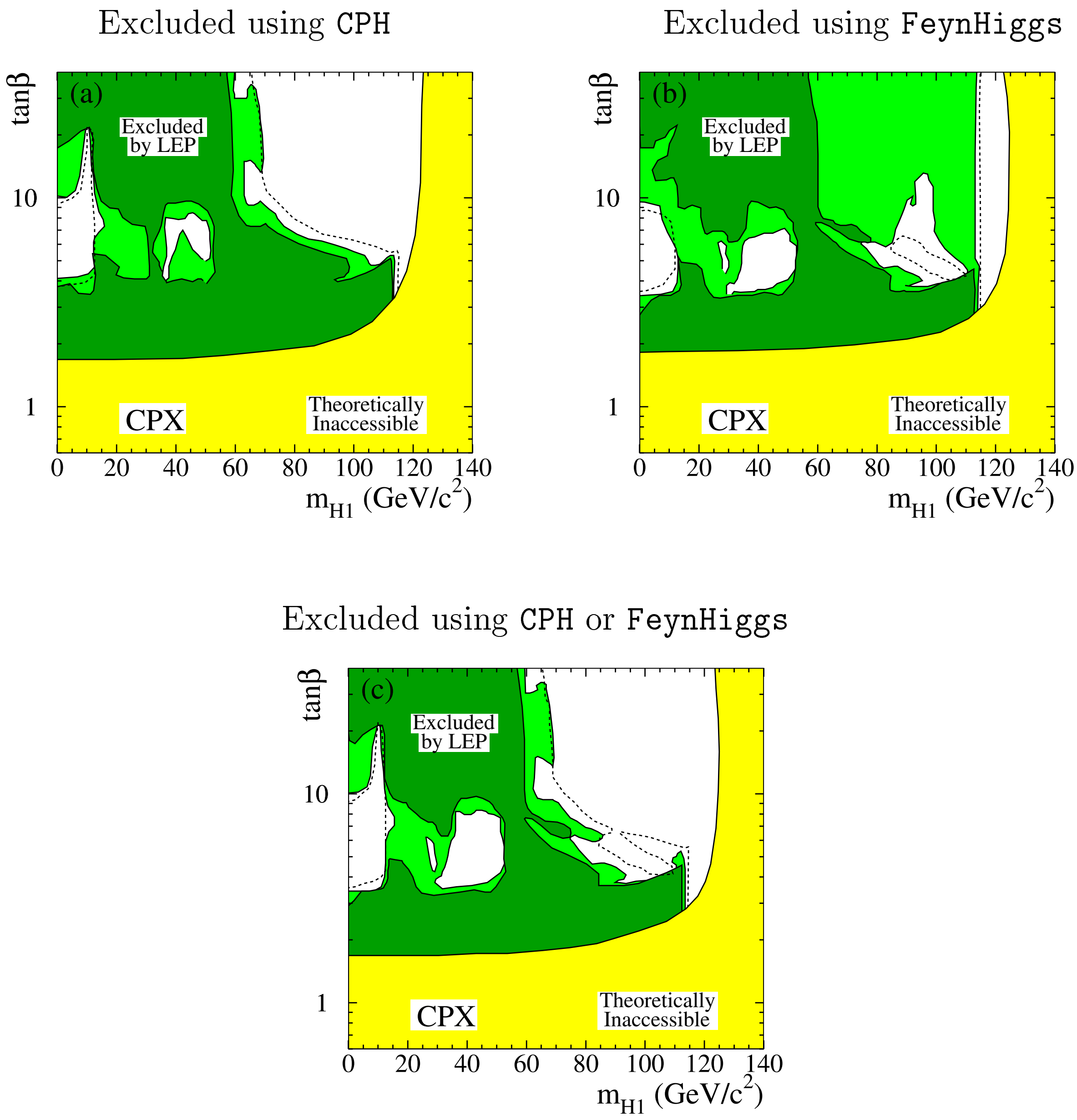

Figure 18: *Exclusions, in the case of the CP-violating CPX scenario, for the two theoretical approaches,* `CPH` *and* `FeynHiggs`*. See the caption of Figure 16 for the legend. In part (a) the* `CPH` *calculation is used and in part (b) the* `FeynHiggs` *calculation. In part (c) the procedure is adopted where, in each scan point of the parameter space, the more conservative of the two calculations is used.*

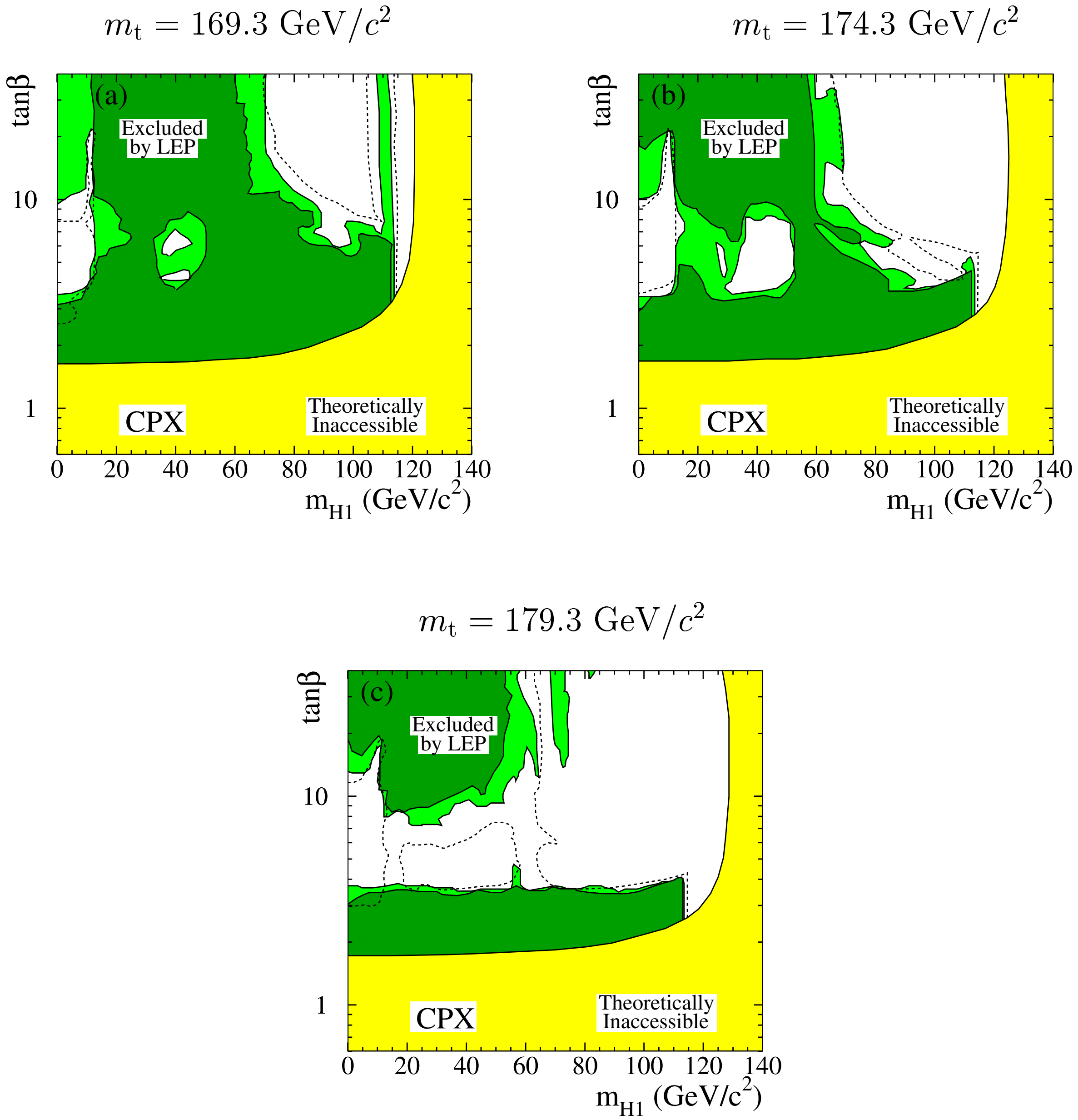

Figure 19: *Exclusions, in the case of the CP-violating CPX scenario, for three top quark masses:* m_t *= 169.3, 174.3 and 179.3* GeV/c^2. *See the caption of Figure 16 for the legend.*

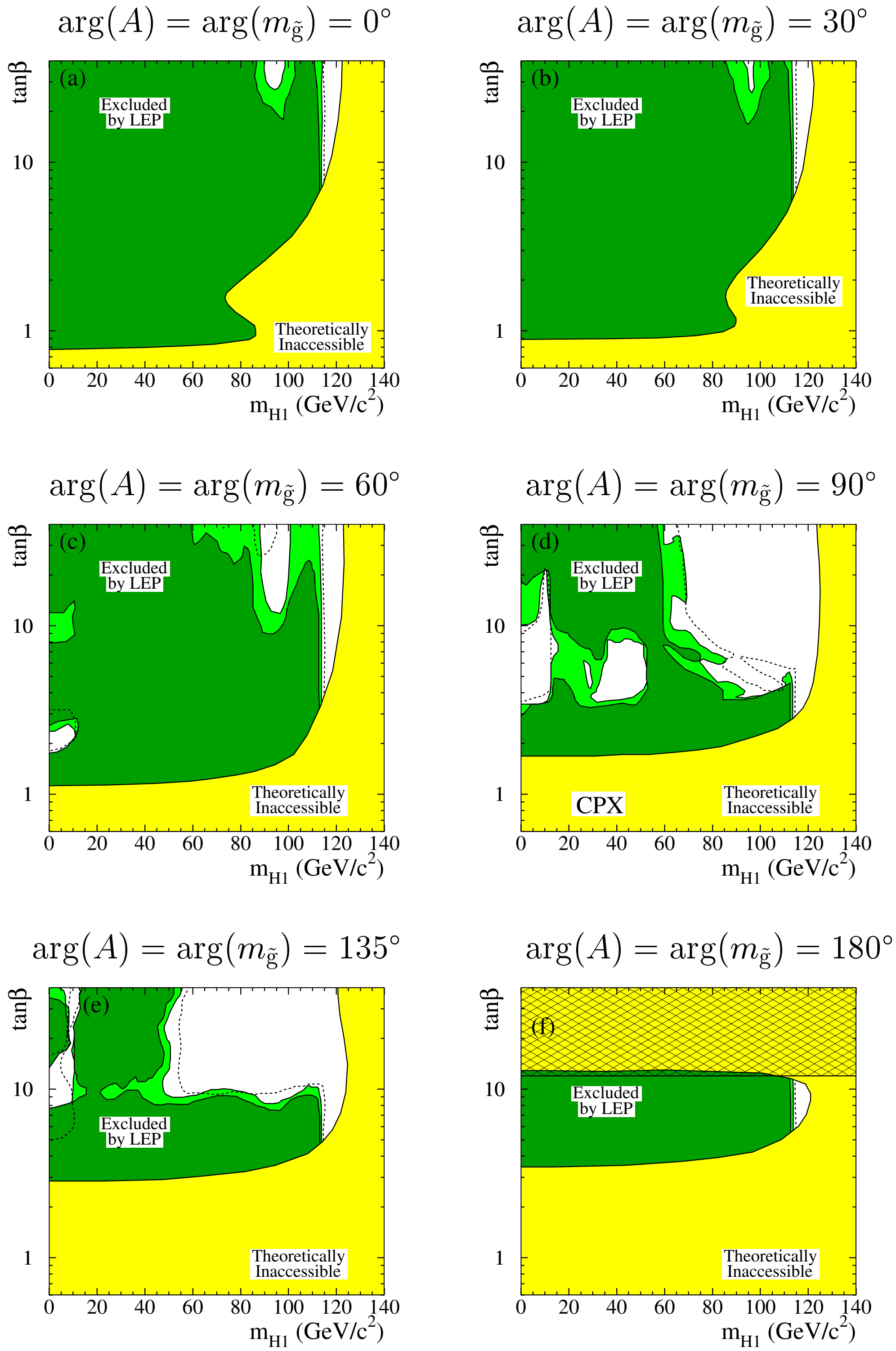

Figure 20: *Exclusions, in the case of the CPX scenario with various CP-violating phases,* $\arg(A) = \arg(m_{\tilde{g}})$*:* 0°, 30°, 60°, 90° *(the CPX value),* 135° *and* 180°*. See the caption of Figure 16 for the legend. In the hatched region in part (f) the calculations are uncertain (see text).*

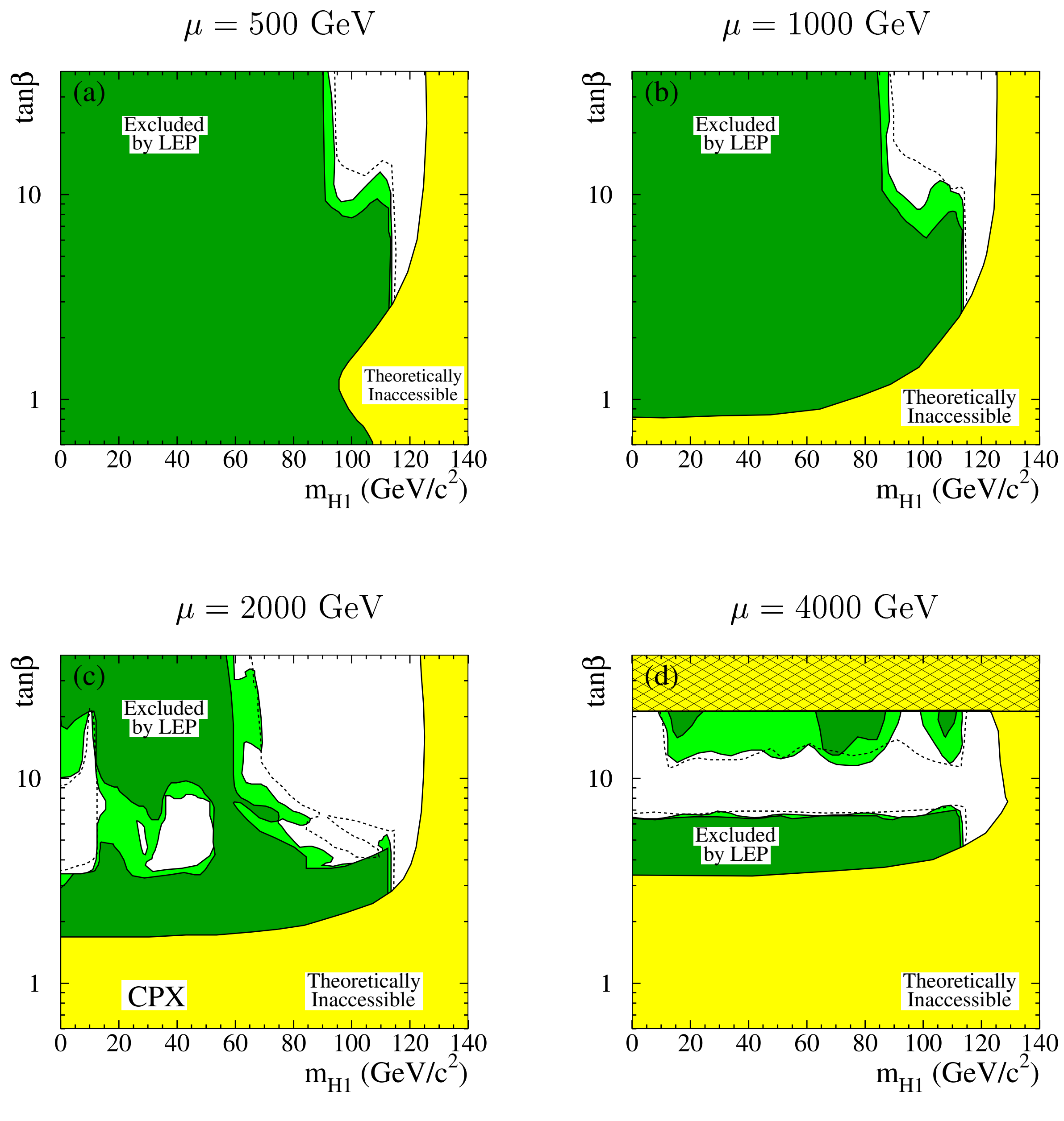

Figure 21: *Exclusions, for the CP-violating CPX scenario with various values of the Higgs mass parameter* μ*: 500 GeV, 1000 GeV, 2000 GeV (the standard CPX value) and 4000 GeV. See the caption of Figure 16 for the legend. In the hatched region in part (d) the calculations are uncertain (see text).*

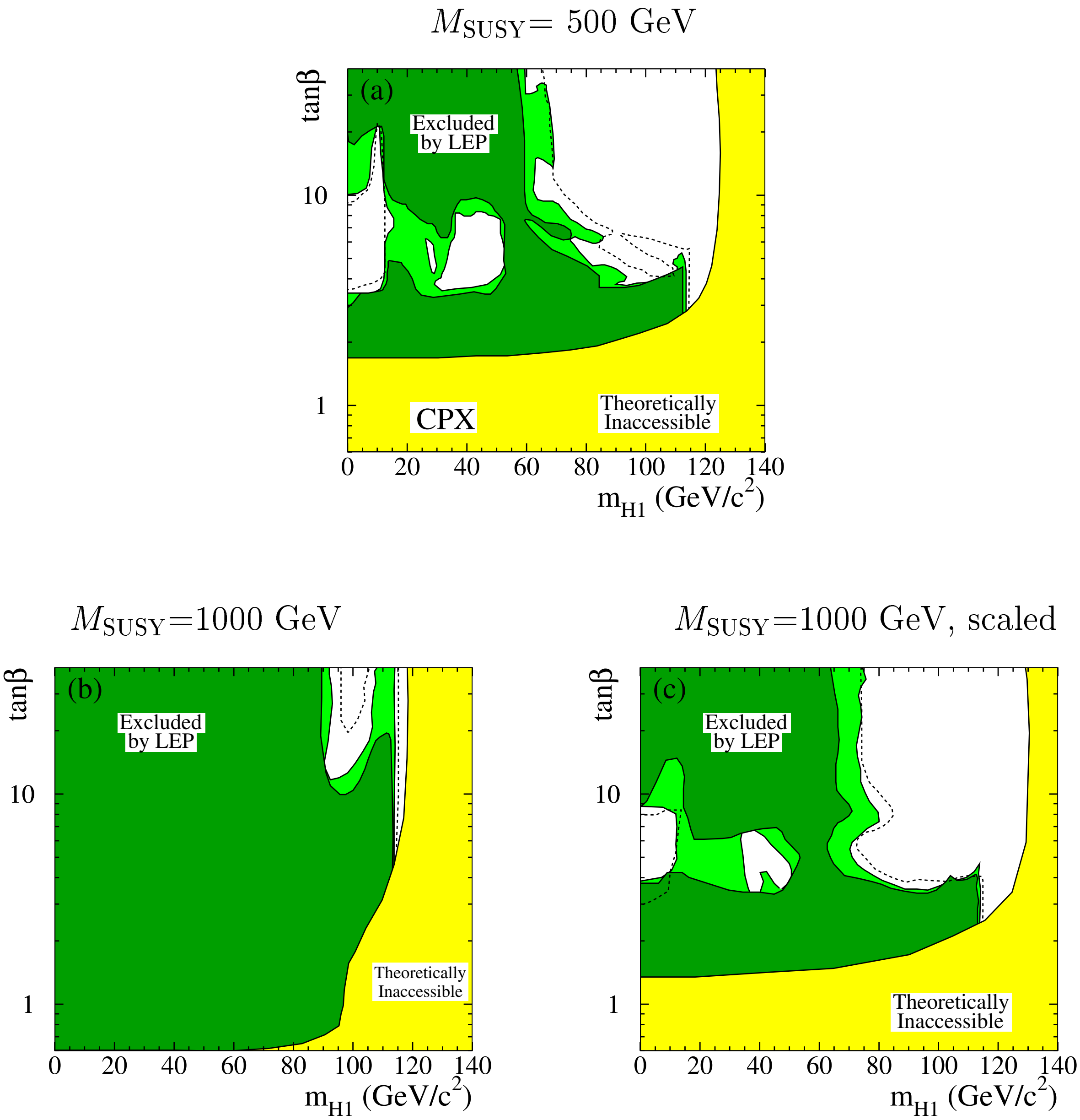

Figure 22: *Exclusions, for the CP-violating CPX scenario with various values of the soft SUSY-breaking scale $M_{\rm SUSY}$. (a): $M_{\rm SUSY}$=500 GeV (the standard CPX value); (b): $M_{\rm SUSY}$=1000 GeV while all other parameters are kept at their standard CPX values; (c): $M_{\rm SUSY}$=1000 GeV while A, $m_{\tilde{g}}$ and μ are "scaled" to 2000 GeV, 2000 GeV and 4000 GeV, respectively. See the caption of Figure 16 for the legend.*